VILNIUS UNIVERSITY
CENTER FOR PHYSICAL SCIENCES AND TECHNOLOGY

ANTON POPOV

INVESTIGATION OF COLLOID SOLUTIONS CONSISTING OF POLYMERIC AND METALLIC NANOPARTICLES

Doctoral dissertation
Physical sciences, Chemistry (03P)

Vilnius, 2018

The dissertation was prepared at Vilnius University Faculty of Chemistry and Geosciences and J. Haber Institute of Catalysis and Surface Chemistry in the period of 2013 – 2017.

Supervisor: prof. dr. Almira Ramanavičienė (Vilnius University, Physical Sciences, Chemistry – 03P).

VILNIAUS UNIVERSITETAS
FIZINIŲ IR TECHNOLOGIJOS MOKSLŲ CENTRAS

ANTON POPOV

KOLOIDINIŲ TIRPALŲ SUDARYTŲ IŠ POLIMERINIŲ IR METALINIŲ NANODALELIŲ TYRIMAI

Daktaro disertacija
Fiziniai mokslai, chemija (03P)

Vilnius, 2018 metai

Disertacija rengta 2013 – 2017 metais Vilniaus universitete, Chemijos ir geomokslų fakultete, Chemijos institute ir Lenkijos mokslo akademijos J. Haber katalizės ir paviršių chemijos institute.

Mokslinė vadovė: prof. dr. Almira Ramanavičienė (Vilniaus universitetas, fiziniai mokslai, chemija – 03P).

Table of Contents

List of abbreviations and definitions

1,6-HDT - 1,6-hexanedithiol

σ - two-dimensional electrokinetic charge densities

ε - permittivity

ζ - zeta potential

η - viscosity

θ - coverage

μ_e - electrophoretic mobility

ρ - density

λ - wavelength

A - Hamaker constant

AFM - atomic force microscopy

AgNPs - silver nanoparticles

ANI - aniline

AuNPs - gold nanoparticles

Au SD - sensor disc with a planar Au layer

A_v - Avogadro's constant

B. C. E. - before Common Era

c - bulk concentration

CPs - conducting polymers

D - diffusion coefficient

DLS - dynamic light scattering

EB - emeraldine base

GOx - glucose oxidase

I - number concentration of cations in the bulk

k_B - Boltzmann's constant

LB - leucoemeraldine base

N - surface concentration

N_c - number of elementary charge

NMNPs - nobel metal nanoparticles

NPs - nanoparticles

PAH - poly(allylamine hydrochloride)

PANI - polyaniline

PB - pernigraniline base

PBS - phosphate buffered saline

R_h - hydrodynamic radius

RSA - random sequential model

t_{ch} - adsorption time

SA - sodium acetate

SAM - self-assembled monolayer

SEM - scanning electron microscopy

SERS - surface-enhanced Raman spectroscopy

S_g - geometrical cross-section area

SPR - surface plasmon resonance

T - absolute temperature

UV - ultraviolet

v - molecular volume

V_a - attractive energy

Vis - visible

w - bulk concentration of colloidal solution

Introduction

Nanotechnology has been a well-known field of science since the 20th century. This swiftly developing scientific field unites broad range of areas that are connected to synthesis, investigation and application of various materials at nanoscale level. High level of interest and development of nanoscience is driven by differences in materials' properties in nanoscale and in bulk scale. This opens new innovative range of materials' applications. Furthermore, particles in nanoscopic scale are characterized by large surface area to volume ratio.

Synthesis of various nanoparticles (NPs) is frequently performed by preparation of their colloidal solution. Choice of colloids manufacturing method depends largely on which desired properties prepared NPs should possess. Size, shape and surface modification can affect NPs optical, electronic and many other properties. Therefore, it is essential to design new ways of NPs' synthesis for their novel application. It is equally important to control and optimize preparation of NPs to ensure stability, purity and uniformity of shape and size distribution for their future use.

Nanostructures of conductive polymers (CPs) such as nanoparticles, nanowires and nanocomposites are attractive for broad application due to possibility to combine their conductive properties with other characteristics attributable to CPs. Polyaniline (PANI) is one of the most extensively studied CPs. The level of PANI conductivity can be changed in the range from insulator to conductor by altering PANI doping level and synthesis condition. Moreover, PANI possesses sufficiently good thermal and chemical stability, flexibility and mechanical properties, wherein it is problematic to prepare PANI nanostructures with high-level biocompatibility. Usage of enzymatic polymerization and additional cleaning procedures can be beneficial for improvement of biocompatibility and solubility in water of PANI nanoparticles and allows to avoid employment of toxic and non-biodegradable compounds.

Silver nanoparticles (AgNPs) and gold nanoparticles (AuNPs) are widely used in wide range of scientific areas. Unique optical properties of AgNPs and

AuNPs are related to phenomenon of surface plasmon resonance, and therefore these metallic nanoparticles are widely used in sensors design, surface-enhanced Raman spectroscopy and other research fields.

AgNPs are commonly used in medicine due to their antimicrobial properties. For instance, formation of AgNPs monolayers allows to prevent bacterial growth, wherein various factors such as ionic strength, pH value and presence of additional compounds can affect monolayer stability and prevent achievement of higher AgNPs coverage. Therefore, investigation of AgNPs monolayer formation process is especially important.

Enlargement of AuNPs seeds due to formation of H_2O_2 during enzymatic reaction and enhancement of analytical signal are highly promising application areas. Different oxidases, such as glucose oxidase (GOx), are suitable for this purpose. AuNPs enlargement can be performed equally well when AuNPs are in colloidal solution or adsorbed onto the surface of a self-assembled monolayer. Process of AuNPs enlargement can be monitored spectrofotometrically or by dynamic light scattering method (DLS), atomic force microscopy (AFM) or scanning electron microscopy (SEM).

The aim of the study:

To investigate chemically and enzymatically synthetized or biocatalytically enlarged polymeric and metallic nanoparticles colloidal solutions by different methods for further biomedical and bioanalytical application.

The objectives of the study:

1. To determine optimal conditions of polyaniline nanoparticles synthesis carried out by polymerization/oligomerization of aniline in the presence of hydrogen peroxide formed during glucose oxidase catalyzed enzymatic reaction.

2. To characterize polyaniline nanoparticles synthesized at optimal conditions using dynamic light scattering and cyclic voltammetry methods.
3. To determine the physicochemical properties and stability of tannic acid solution and silver nanoparticles colloidal solution.
4. To study the deposition kinetics of charge-stabilized silver nanoparticles from colloidal solution containing tannic acid on mica covered by the poly(allylamine hydrochloride).
5. To investigate biocatalytic enlargement of AuNPs in colloidal solution and immobilized on the surface by UV-Vis spectroscopy, atomic force microscopy and dynamic light scattering methods.
6. To study the dependence of biocatalytically enlarged AuNPs size on concentration of glucose.

Statements for defense:

1. PANI nanoparticles formation depends on concentrations of aniline and glucose oxidase and on duration of polymerization.
2. The size of PANI nanoparticles increases with increasing duration of polymerization.
3. The formation of AgNPs monolayer on PAH-covered mica depends on concentration of tannic acid in colloidal solution.
4. Hydrodynamic diameter of biocatalytically enlarged AuNPs in the solution and the height of nanoparticles immobilized on the surface depends on the glucose concentration and on the duration of reaction.
5. The enlargement of AuNPs seeds could be applied for the glucose concentration determination by analytical systems based on dynamic light scattering and atomic force microscopy.

1. Literature review

1.1. Colloids

A colloid is a mixture of at least two phases. Length scale of dispersed phase is ranging from a few nanometers to a few tens of micrometers. In most cases the size of dispersed phase particles is lower than 1 μm [1]. Different and extraordinary examples of the colloid systems are found in nature (e.g. clouds, smoke, soil and cell fluids). Additionally, a lot of agricultural and industrial products, especially foodstuffs, consist of colloidal structures that define their rheological properties and textures. Clay and soil, whose constituents are of a colloidal nature, are the object of explore of environmental science. As a result, a colloid science is an interdisciplinary field where chemists, physics, biologists, engineers and other scientists are working in collaboration [2].

Although the term "colloid" was used for the first time only in 19th century, colloidal solutions made use thousands of years earlier. In Egypt stones were lubricated with a greasy substance by slaves for moving to building places of pyramids. Manufacturing of bricks of clay, a classic colloid, and effect of oil pouring on storm-tossed waters to damp the waves are known from ancient times. Colloidal phenomena was also used in manufacturing of paints and pigments, bread, cheeses, butter and other products [3].

It is considered that Benjamin Franklin started scientific research of interfacial phenomena. In his reports (1765) it was described what amount of oil should be used for covering of pond surface with the thinnest possible layer. Furthermore, Francesco Selmi in the 1840s performed aggregation studies of sulfur and silver iodide in water (*pseudo-solutions*). Meanwhile in 1861 Thomas Graham based on Selmi's results of *pseudo-solutions* study developed the term "colloid" from the Greek word *κολλα* (glue). Well known scientists such as Faraday, Laplace, Poisson, Landau were involved in further research of colloidal solutions [4, 5].

As it was mentioned above colloidal systems are composed of at least two phases. Dispersed phase and another phase (the medium) can be in different states of matter. Various examples of colloidal systems are given in Table 1.

Table 1. Classification of colloidal dispersions [2].

	Dispersed material		
Medium	Solid (S)	Liquid (L)	Gas (G)
Solid (S)	Solid suspension (*bone, wood, various composite materials*)	Solid emulsion (*opals, pearls*)	Solid foam (*loofah, bread, pumice, styrofoam*)
Liquid (L)	Sol, Suspension *(blood, polymer latex, paint, ink*)	Emulsion (*milk, rubber, crude oil, shampoo, mayonnaise*)	Foam (*detergent foam, beer foam*)
Gas (G)	Aerosol (*smokes, dust*)	Aerosol (*fog, sprays*)	-

The colloids can be classified based on nature of interaction between dispersed phase and medium. Colloidal solutions in which dispersed phase has a high affinity for the medium are called as lyophilic. If, in contrast, there is a little interaction between dispersed phase and medium such colloid solutions are termed as lyophobic. If medium is water, lyophilic colloids are called hydrophilic and lyophobic are respectively called hydrophobic. In association colloids (micelles) one part of dispersed molecules interacts with medium, opposite part is lyophobic and have little interaction with medium. Lastly, network colloids (gels) are sometimes considered as a separate category [6, 7].

Significance of particles' shape is difficult to overestimate. Shape of particles is one of parameters on which their optical and electronic properties, employment possibilities and stability of colloidal system depend. Solid particles in liquid medium can be of different shapes. The geometrically simplest shape is the sphere. A variety of spherical particles are commercially available

and extensively spread in nature, for instance, vesicles, liposomes and some globular proteins. Also a lot of various non-spherical particles were found in nature or synthesized. Ellipses, cylinders, discs, rod-like particles are only a small part of existing diversity of particles shapes. Furthermore, various particle systems that are anisotropic by shape were created in laboratories [2, 8-11].

1.2. Stability of colloidal system

Due to giant surface area of particles, colloidal system possesses high levels of free energy. Therefore, colloidal system will prone to minimize surface area, thereby colloid will tend to aggregate. Stability of colloid is a property of system to resist the tendency to particles aggregation [3].

Stability of system is one of the key problems of colloid chemistry. In colloidal solution stability depends on balance of repulsive and attractive forces between particles. Derjaguin, Landau, Verwey, and Overbeek (DLVO) theory is most commonly used theory for description of colloidal system stability. According to this theory the total interaction of two colloidal particles consist of two forces: the repulsive interaction of particles' double layers and attractive Van der Waals interaction [12, 13]. The Van der Waals interaction of two spheres can be modeled as:

$$V_a = -\frac{Ar}{12y} \quad (1)$$

where V_a is the attractive energy, r is the radius of spheres, y is the distance between spheres and A is the Hamaker constant, which characterizes interaction strength. In most cases Hamaker constant is positive, meaning that particles attract each other [14, 15]. Hamaker constant depends on the nature of particles and on the medium. In the work of K. Jiang *et al.* it was shown that Hamaker constant of metal nanoparticles depends on temperature and size of particles [16].

Repulsive double layers attraction consists of an electrostatic and osmotic force components. When distance between colloidal particles decreases, the ions of double layer become clenched to the smaller volume. Since then, increase of osmotic pressure, which is proportional to concentration of ions, is observed. Electrostatic repulsion is the result of interaction between the double layers of colloidal particles. When colloidal particles become separated by the distance less than twice double layer, repulsion occurs [17, 18].

DLVO theory is not enough for describing of interaction between particles which are closer than few nanometers. In this distance solvation and structural forces arise and affect the interaction. Solvation forces define how solvent interacts with surface of colloidal particles. These forces depend on properties of solvent and particles surface. For example, such characteristics as smoothness, hydrophilicity or homogeneity of particles surface affect this type of interaction. Solvation forces can be divided into three subcategories: oscillatory, hydration and hydrophobic forces. Molecules of the medium that are getting into the space between particles begin to oscillate. This oscillation process can be the cause of repulsive or attraction forces depending on distance between particles [19, 20].

Hydrophobic forces arise when particles that have a hydrophobic surface are dissolved in water medium. When nonpolar groups on surface of particles interact with water molecules, changes in structure of water are observed. As a result layer of water molecules varies between particles [21]. Hydrophobic forces are implicated in various biochemical processes such as receptor – ligand or enzyme – subtract interactions. These forces are also significant in formation of proteins tertiary and quaternary structure [22].

There are few theories that describe a mechanism of hydration forces. Underlying of hydration process is interaction between water molecules and hydrophilic surface of particles. The first theory builds upon abnormal polarization of water molecules, which interact with particles. According to this conception, hydration forces are electrostatic by nature. In other sources it is expected that hydration forces are the result of entropic repulsion of thermally

excited polar groups that bulge from the surface [23]. The term “structural forces” is used for describing all other types of interaction.

The value of zeta potential is a parameter, which is often used for describing of colloidal system stability. Zeta potential provides guidance on repulsion interaction between particles. It is recognized that if value of zeta potential is between -30 and +30 mV then the colloidal solution is unstable. Meanwhile, zeta potential of stable colloid should be lower than -30 mV or higher than +30 mV.

Particles concentration, pH and ionic strength are parameters influencing zeta potential. pH is probably the most important factor for zeta potential value. Change in pH value may cause increasing or decreasing zeta potential value. Dependency between concentration of particles and zeta potential is complicated. Generally, in strongly diluted solution zeta potential increases with increasing concentration of particles. In solutions with high concentration perverse effect is noticed. With the increase of ionic strength the electric double layer becomes thicker [24, 25]. Ionic strength can be controlled by changing salt concentration in colloidal solution. The valence of counter-ions also affects stability of colloidal solution (zeta potential). The electric double layer becomes thicker if counter-ions with higher valence are used. It is important to choose suitable background electrolyte and its concentration if high concentration of colloidal particles is used. In such cases spacing between particles becomes almost equal to the diffuse layer and employment of electrolyte with high valence may be the reason of particles aggregation [26, 27].

As was mentioned previously the value of zeta potential is important for stability of colloids. One more option to control zeta potential is to use surfactants or molecules such as polymers or even proteins. As a result of deposition of such compounds the change in zeta potential of particles is observed [28]. Besides it can affect hydrophobic, hydration and structural interaction between particles [29].

Surfactants play a vital role in manufacturing of different products such as cosmetics and detergents [30]. Surfactants are the amphiphilic molecules. In

these compounds polar and non-polar groups are presented simultaneously. Such chemical structure stipulates possibility for surfactants to adsorb on colloidal particles/medium interface. This kind of interaction helps to reduce surface and interfacial tensions. There are few types of surfactants: anionic, cationic, nonionic and amphoteric. The choice of surfactant type depends on application area of colloidal particles. For instance, cationic surfactants, which are positively charged, can interact with cells membranes. Therefore, they are used as germicides. It is also necessary to pay attention to such parameters as particles charge and hydrophilicity in order to choose the best surfactant [31-33].

By structural analogy of surfactants various macromolecules or polymers containing hydrophilic and hydrophobic groups are often used for increasing of colloids stability. If hydrophilic and hydrophobic parts are repeated in polymer structure, such surfactants are called “Polysoaps”. In contrast macrosurfactants have hydrophobic and hydrophilic parts separated from each other. Narrow classification of polymeric surfactants is based on differences of surfactants polymerization (Fig. 1) [34].

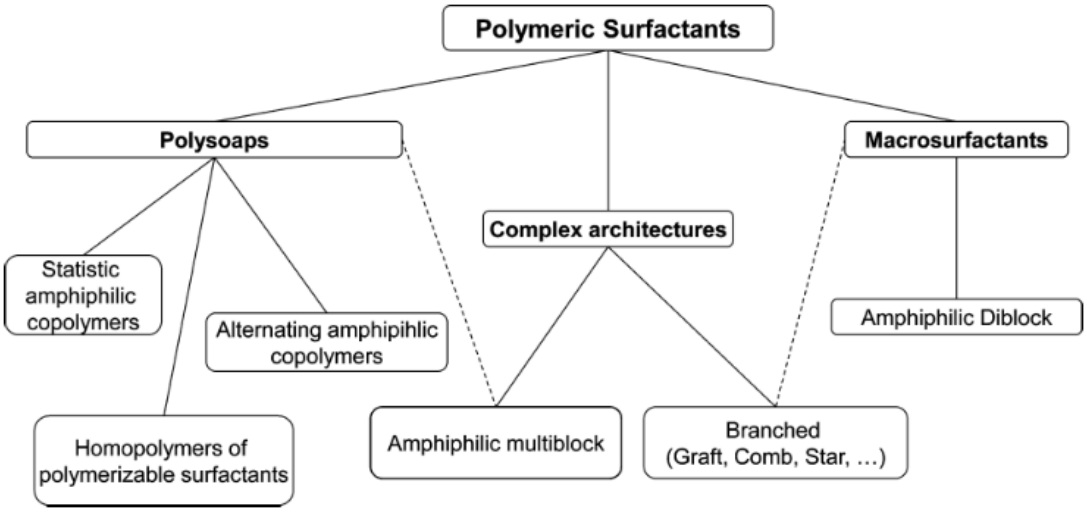

Fig. 1. Classification of polymeric surfactants. Adapted from [34].

There are two types of colloidal particles stabilization by polymeric surfactants. When polymers are adsorbed on surface and form particles coating, it is called steric stabilization. Repulsive forces, which emerged due to adsorption of polymers, prevent aggregation of colloids. Another kind of

stabilization is based on unattached interaction between polymers molecules and particles. Molecules of unanchored polymer can induce interaction. Mechanism of such interaction can be depletion repulsion or depletion attraction [35].

Application of proteins (natural polymers) is another method for stabilization of colloidal solution. Presence of protein casein in milk is an example of usage of proteins for colloidal solution stabilization in nature. Proteins are biomolecules consisting of chains of amino acids residues. Depending on pH proteins can be negatively or positively charged or be neutral. Thereby when proteins adsorb on surface of particles effectiveness of stabilizing layer is increasing [36]. In the work of M. Ocwieja *et al*. cysteamine was used for postmodification of gold nanoparticles. As a result negatively charged synthesized gold nanoparticles became positively charged after adsorption of cysteamine molecules [37].

Proteins can also affect hydration forces in colloids. In the work of J. A. Molina-Bolivar *et al*. different proteins for stabilization of the latex particles were used. It was observed that stabilization efficiency depends on hydrophilicity of proteins. Such type of stabilization arises in solution with high salt concentration [38]. Naturally this effect of stabilization also depends on composition of colloidal particles [39].

1.3. Polymer colloids

A polymer colloid is mostly a heterogeneous system of submicron polymer particles dispersed in medium. Polymer-based colloids are used in different areas such as medicine, electronics, paper coating, rubbers, paints and many others. Such wide scope of polymers usage is based on their variety. Depending on research purpose polymer with set of necessary properties can be selected [40].

Sometimes various applications of polymer colloidal particles require surface modification. Such functionalization is normally used for addition of specific properties to colloidal particles or for protection of polymers that are not stable under the chosen conditions. Diverse methods from chemical oxidation

and reduction to employment of plasma can be used for surface modification [41].

Many of polymer-based colloids are biocompatible and well suited for drug delivery. Wide variety of polymers nanostructures including liposomes, micelles and particles are used in the drug delivery systems. Biodegradable nanoparticles can be used for encapsulation and delivery of protein-based drugs [42]. Among wide range of biocompatible polymers, conducting polymers can be distinguished separately [43].

Due to their unique optical and electrical properties conducting polymers (CPs) are attractive for scientific investigation [44]. The history of these polymers started from the discovery of polyacetylene's good conductivity [45]. After a while it was observed that various CPs such as polypyrrole, polythiophene and poly (ethylenedioxythiophene) also possess good conductivity. Nowadays one of the developing directions in science of conducting polymers is controlling of CPs morphology and structure. Different CPs nanostructures such as nanoparticles, nanowires and nanorods were developed in the last ten years. Various nanostructures of CPs were employed in sensors fabrication, electrochromic devices manufacturing, electronics and other industrial areas. In this context, nowadays, the search for new synthesis methods of CPs nanostructures is especially relevant and sought after [44, 46-48].

1.4. Polyaniline

Polyaniline is an organic conducting polymer. In some scientific works it is claimed that PANI is the earliest known synthetically obtained organic polymer [49]. PANI is produced by the oxidation of aniline (ANI) molecules (Fig. 2). According to value of conductivity PANI is referred to as an organic semiconductor. The main reason for wide range of PANI and other CPs applications is not conductive properties but the opportunity to combine them with other CPs characteristics. PANI as well as many other CPs possesses such properties as partial biodegradability [50], flexibility [51], biocompatibility to

several cell lines [52] and processability as well as low cost [53] and good mechanical properties [54]. It is worth noting that aniline polymerization is inexpensive and easily performed [55]. Generally, for synthesis of PANI electrochemical [56] or chemical polymerization [57] is used. Alteration of PANI polymerization conditions and strict control over them makes it possible to produce PANI with prefered structure and morphology. Differences in synthesis procedure bring not only distinction in structure and morphology, but in polymer physical properties as well [57-60]. Another advantage of using PANI is opportunity to change its physical properties by copolymerization [61] or by forming PANI nanocomposites with ions of metals [62] or other inorganic compounds [63].

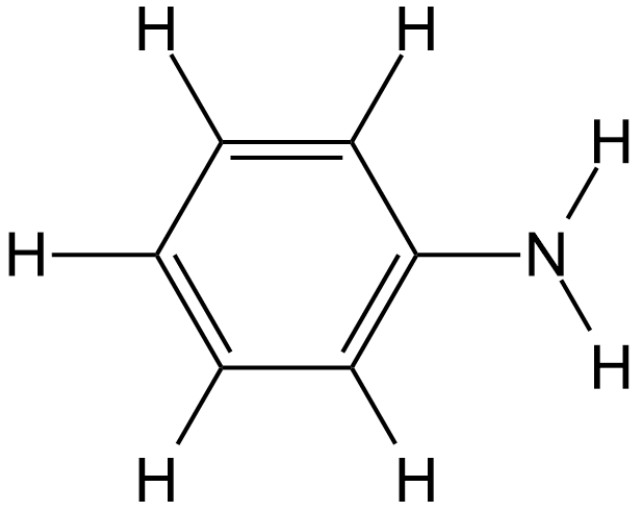

Fig. 2. Aniline molecule.

The history of aniline started in 1834 from F. F. Runge works of investigation of coal-tar distillates. During this work F. F. Runge isolated colorless salt. Thereafter, it was proved that this salt was so-called “aniline black” [64]. Later in 1840 C. J. Fritzsche pursue to determine the molecule structure of indigo, also separated “aniline black” [65]. Subsequently, based on F. F. Runge and C. J. Fritzsche works F. Crase-Carvet, S. Clift and C. Lowe found a method for commercial dyes manufacturing applying aniline [49]. H. Letheby in 1862 for the first time performed PANI synthesis by the anodic oxidation and shown electrochromic behavior and conductive properties of PANI [66].

The new story of conducting polymers, including PANI, began in 1970s. A. J. Heeger, A. G. MacDiarmid and H. Shirakawa working in collaboration studied conductivity of CPs. For their pioneer research they got the Nobel Prize in Chemistry in 2000 “for the discovery and development of conductive polymers” [66]. These developments encouraged worldwide interest to CPs investigations.

As previously noted, range of PANI application is very wide. In literature one can find a lot of examples of possible practical use of PANI. Thus, PANI is one of mostly studied organic conducting polymers that have been developed over the past 30 years [67-69]. PANI has a great promise for applications in supercapacitors [70], rechargeable batteries, light-emitting diodes, electrochromic display devices, corrosion inhibitors [71] and detecting material for sensors [72-75]. PANI could contribute to the development of portable, sensitive biosensors. PANI-based various microfabricated electrochemical biosensors, such as enzymatic, DNA sensors or immunosensors offer many advantages and new possibilities for the determination of biologically important compounds [76-78]. Conducting polymers including PANI are good alternative to paints, which are more harmful to environment [79]. Among possible applications of PANI there is such creatively different usage as smart conductive textiles [80].

Over the last decade, special interest was concentrated in searching of new application fields of PANI nanostructures. Physical properties of such materials differ from PANI properties. Carbon nanotube-polyaniline composites [63] and PANI nanofibers [81] are case in point of PANI nanostructure which have many of possible applications [82]. PANI nanofibers can be used in design of gas vapor sensors, printable electronics, filtration membranes and many other devices [83]. Also worth noting is that PANI nanoparticles can be used as electrocatalysts, immobilization matrixes for biomolecules [67, 72-74] and in many other biomedical fields [83].

1.4.1. Properties of polyaniline

In general, there are three possible oxidation states of PANI: leucoemeraldine base (LB), emeraldine base (EB) and pernigraniline base (PB). For emeraldine and pernigraniline base or salt forms are possible (Fig. 3). PANI as electrochromic polymer possesses various optical and electrochemical properties at different oxidation states. Characteristics of PANI such as stability and mechanical properties differ depending on the degree of oxidation [84]. Additionally conductivity of PANI can greatly vary (from 10^{-10} to 10^{3} S cm^{-1} [85]). In protonate state conductivity of PANI is on the same level as conductivity of semiconductors (100 S cm^{-1}) [86]. On the other hand PANI is insulating material in LB form [87].

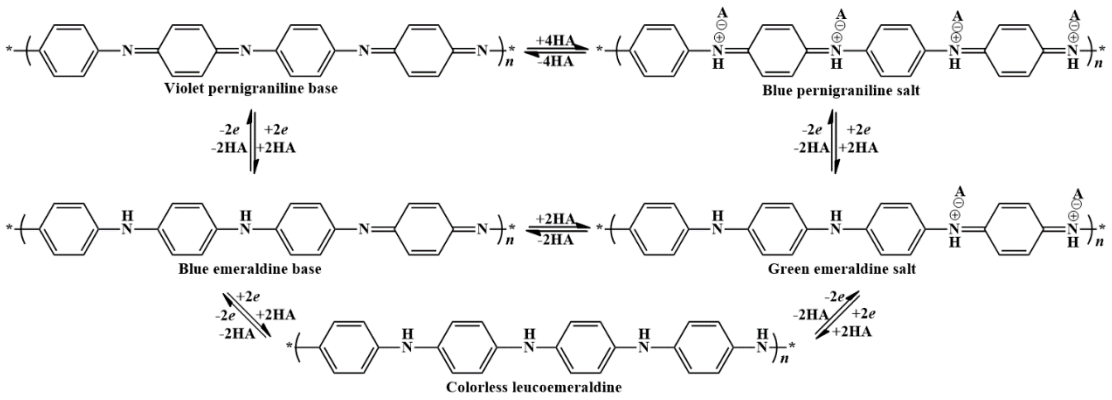

Fig. 3. Different forms of polyaniline. Adapted from [108].

Conductivity of PANI depends on molecular weight, percentage of crystallinity and inter-chain separation, oxidation level, molecular arrangement, percentage of doping and type of dopant. Therewith, oxidation level is the most important parameter for conductivity. In order to achieve high conducting level PANI should be in half-oxidized form. Doping level is the second most affecting factor. Doping of PANI allows to form a polaron structure. In this structure a current is carried by the holes [88]. Conductivity also depends on the nature of dopant. Synthesis of PANI is typically performed in acid solution, so mostly doping anions are incorporated in PANI originate from the acid [89].

Conductivity of PANI can be easily reduced by changing oxidation level or by dedoping process. Typically dedoping process is performed by placement of sample in basic solution [90]. Surely, there are also other methods for dedoping of PANI. For example, emeraldine salt can be transformed to EB form by the irradiation of ultraviolet (UV) light [91].

In LB form PANI contains only amino groups and benzene rings. As mentioned before, this fully reduced form of PANI is non-conducting. In all possible forms in spectra of PANI two absorption bands are presented around 6.89 eV (180 nm) and 6.20 eV (200 nm). This two bands correspond to π–π* transition in benzene ring. Another absorption maximum at 3.94 eV (315 nm) for LB form corresponds to π–π* transition connected with delocalization of benzene ring electrons on nitrogen atoms [92, 93]. Transparent yellow is specific color for PANI in LB form. In reduced form PANI is not stable in air atmosphere. Slightest oxidation of LB leads to shift of absorption peak 3.94 eV (315 nm) to 3.79 eV (327 nm) and change of PANI color to light green-yellow.

Continuing of oxidation process PANI passes into half-oxidized form. In this EB form PANI is comprised of both benzene and quinoidal rings. Conductivity of blue EB form is around 10^{-5} S cm^{-1}. Usage of doping assists to improve conductivity of PANI layer. During doping process EB is passed into emeraldine salt and color of polymer is changing from blue to green [94, 95]. Electrical conductivity of emeraldine salt can reach 10^{3} S cm^{-1} [85]. High electrical conductivity of emeraldine salt can be explained by formation of low-energy hole levels [96]. The absorption at 3.19 eV (388 nm) due to benzenoid rings and at 1.47 eV (843 nm) due to quinoid rings is specific for EB form [97].

Completely oxidized form of PANI is called pernigraniline base. In this oxidation state PANI is insulating violet polymer. Two absorption maximums at 2.35 eV (528 nm) and 3.88 eV (320 nm) are specific for PB [98]. Pernigraniline salt is fully oxidized form of PANI in acidic medium which has bipolarons in its structure. In this form PANI can be conductive. During doping process of EB shift of the band at 2.35 eV (528 nm) to 2.14 eV (580 nm) is observed. Such shift

of absorption peak is specific for EB protonation in acidic medium and pernigraniline salt formation [99, 100].

PANI is a relatively stable polymer with low manufacturing cost. PANI shows good mechanical properties. Depending on preparation conditions changes in stiffness and elasticity of PANI are possible. Young's modulus of PANI pellets is comparable with other frequently used polymers such as polystyrene [101]. P. Peikertova *et al.* investigated stability of protonation form of PANI in various storage condition after different time of oxidation. It was observed that in course of time PANI films drop into a deprotonation state. Furthermore, stability of PANI in time depends on relative humidity of environment [102]. Storage temperature and pH can also affect stability of PANI [103, 104]. EB is thermally stable polymer (up to 420 °C). It was observed that thermal stability of emeraldine salt depends on type of dopant [105]. Even in aggressive chemical environments, PANI is characterized by high thermal stability and by slight loss of conductivity at relatively high temperature (100 °C) [106, 107].

Bulk PANI possesses lower biocompatibility in comparison with PANI nanofibers [109]. Purification of PANI allows to reduce cytotoxicity of PANI to the minimum. Washing procedure allows to eliminate ANI and reaction intermediates (aniline dimers and oligomers) from mixture. Cytotoxic effect of such low-molecular-weight compounds, which are aromatic amines and can be physiologically active or even harmful, is much higher than PANI is alone [110]. Actual studies of PANI biocompatibility can be separated into two groups. The first one is working on *in vivo* testing of PANI implantability [111]. The second one is focused on *in vivo* investigations of cells proliferation in presence of PANI [112], its copolymers [113] or composites [114]. Prevalently PANI is used as a matrix for decreasing of cytotoxicity of employed materials [115]. On the other hand, employment of compounds such as dopamine and cysteine can improve biocompatibility of PANI [116, 117].

An important aspect of biocompatibility is biodegradation of materials. Although PANI is non-biodegradable in all oxidation states, there are some

technologies allowing to synthesize copolymers, which are conducting and biodegradable, containing oligomers of PANI [118].

1.4.2. Synthesis of polyaniline

Generally, chemical or electrochemical polymerization in presence of dopant are used for preparation of PANI. Choice of polymerization method depends on the aim of synthesis. Chemical polymerization is more favorable when large quantity of PANI is needed. Further, for direct deposition of PANI on substrate, especially for formation of thin polymer film, electrochemical synthesis is more suitable. Whereas, chemical polymerization allows to form conducting PANI layer on the non-conducting substrate [89]. The oxidation process of ANI is exothermic, thereby can be tracked by observing the temperature [119].

Mechanism of PANI formation consists of three main steps: initiation step, dimerization and oligomerization/polymerization. Initiation step is the limiting step of polymerization reaction. This can be explained by differences in oxidizability of ANI and its protonated form, as well as variations in redox properties of its reactive species [120]. In this phase rate of reaction strongly depends on type of oxidant or on anodic potential and acidity of the medium. At higher pH oligomers with low molecular weight are formed [121]. It is widely thought that first step of ANI polymerization reaction is formation of its radical (Fig. 4) [122]. pKa value of aniline cation radical is 7.05. Therefore, in medium, whose pH value is lower than 7, aniline cation radical prevails. It denotes that at lower pH the rate of polymerization should be higher [123].

In following steps further formation of oligomers and polymer is more probable due to higher oxidation potential of ANI in comparison to its dimers. However, it should be noted that dimerization process also depends on pH of medium. Different dimeric products are formed depending on acidity of solution. These dimers, due to differences in reactibility, are not equally involved in polymerization process [120]. In oligomerization/polymerization

step propagation of polymer chain occurs in acidic media due to redox reaction. In this reaction pernigraniline form of PANI is involved as oxidant and aniline is applied as reductant. Oxidation potential of polymer chain depends on degree of oxidation, length of the chain and degree of protonation [69].

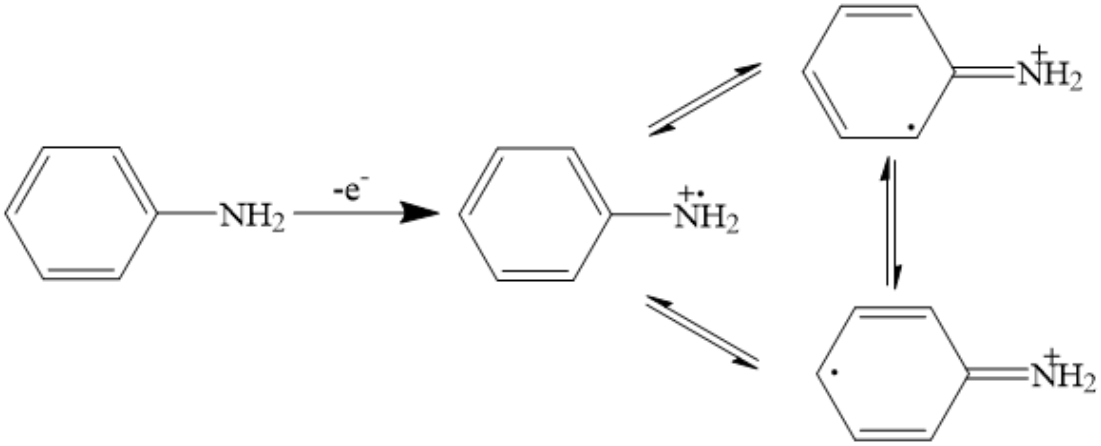

Fig. 4. Oxidation of monomer during polymerization of aniline.

Chemical polymerization of ANI is typically performed by oxidation with various oxidants in acidic aqueous medium. Thereat, more often than other oxidants ammonium persulfate is used. More rarely oxidants with high oxidation potential such as salts of iron, cerium, silver, or dichromates are employed [124]. The highest yield (~ 90%) of PANI is achieved in presence of $(NH_4)_2S_2O_8$ as oxidant. Usage of acidic medium ($1 < pH \leq 3$) is necessary for synthesis of conducting PANI form [108]. Electrochemical polymerization is carried out by oxidation of ANI in electrolyte solution by applying electric potential. For electrochemical synthesis, typically galvanostatic, potentiostatic and potentiodynamic (e.g. cyclic voltammetry) methods are used in two- or three-electrode systems [125].

Many other methods of PANI synthesis are described in the literature. PANI can be obtained by photopolymerization [126], various heterophase polymerization methods [88], self-assembling polymerization [127], sonochemical synthesis [128] and plasma polymerization [129]. Enzymatic synthesis stand out among all other methods, which are suitable for PANI preparation. In this method, contrary to others, macromolecular biological

catalysts – enzymes are used. Also in majority of methods, including electrochemical [72, 130] and chemical [73, 107] oxidation of ANI, different chemical compounds, even toxic, are employed. Such chemicals should be removed after synthesis and utilized. Contrary to such compounds enzymes are biodegradable and non-toxic. Low or very low pH is necessary for electrochemical or chemical PANI synthesis [68]. PANI formed during such synthesis mostly is conductive and is characterized by poor solubility in water [77, 131]. The enzymatic polymerization of PANI can be carried out in aqueous solutions [132-134]. This synthesis can be done at almost neutral pH value. Additional advantages of enzymatic polymerization are (i) possible control of the reaction kinetics and (ii) simple, one-step procedure based process [133]. Different enzymes such as horseradish peroxidase [135, 136], laccase [137], bilirubin oxidase [138], chloroperoxidase [139] and glucose oxidase [140] can be employed for PANI synthesis. Usage of various enzymes, stabilization agents ant templates allows to obtain PANI nanostructures with required properties [141].

1.5. Noble metal nanoparticles

Noble metals were known and used in our daily life for a long time. In the past noble metals were used as a material for making of jewellery and currencies, while in our times, possibilities of their application are very wide. Breadth of potential application areas is attributable to their unique properties [142]. Also it must be noted that the majority of noble metals except for gold and silver were discovered in the eighteenth century or later. Gradually studying their properties even more possible application fields were found. Furthermore, the development of nanoparticles synthesis and fabrication gave a strong impulse to utilization and research of noble metals.

Noble metal nanoparticles (NMNPs) possess unique photonic, electric, electronic and catalytic properties. Few kinds of noble metal NPs have interesting optical properties such as fluorescence, absorption, scattering and

surface plasmons. Those properties allow to use NMNPs in biolabeling and bioimaging, for instance, in X-ray computed tomography, magnetic resonance imaging and optical imaging [143]. Referring to medicine, it is also worth mentioning that catalysis, drug delivery, sensing and therapy are also possible application areas for NMNPs [144]. NMNPs can be used for treatment and diagnostic of cancer. Among the possible options of NMNPs usage may be noted catalysis, electronics, optoelectronics and antimicrobial applications [145-148]. Silver and gold nanoparticles are the most frequently used NMNPs.

1.6. Silver nanoparticles

Silver is the third known metal after gold and copper, which were used by humans. Chaldeans have learned how to purify silver as early as 4.000 B. C. E. Ever since, coins, jewellery, utensils, vessels and many other things were made from silver. Also, silver was very actively used in medicine. For water purification silver was employed as early as in ancient Egypt, Greece and Rome [149]. Macedonians applied silver plates for achieving better wound healing. Ancient Greeks used silver preparations as a cure for ulcers and for stimulation of wound healing. It can be appreciated that silver and its compounds were the most significant antimicrobial preparations until discovering of antibiotics. Nowadays, silver is used due to its antibacterial properties in a wide range of medical applications: as a topical cream in the treatment of burn wounds, in bone prostheses, cardiac implants, surgical sutures and needles, dentistry, catheters, wound therapy and surgical textiles. Contemporary application of silver includes photographic use, electronics, photovoltaic devices, mirrors and glasses, as well as brazing and soldering [150-153].

First recorded utilization of colloidal silver is dated IV century of our era. Lycurgus cup, which was made in ancient Rome, consists of mixed silver nanoparticles (AgNPs) and gold nanoparticles (AuNPs). The size of nanoparticles which was found in the cup is about 70 nm. Besides, it has long been known that colloidal solution is the most effective form among possible

silver preparations and possesses good activity at sufficiently low concentrations [154].

The modern history of AgNPs extends back more than 120 years. In 1889, M. C. Lea reported the method of AgNPs synthesis through reduction of $AgNO_3$ using ferrous sulfate. As stabilization agent of AgNPs citrate ions were employed. Already since 1897 this colloidal solution under the name "Collargol" has been produced commercially for medical purpose. Different colloidal solutions of AgNPs were manufactured commercially and used for medical applications. According to data, from 2011, worldwide manufacturing of AgNPs has reached 320 tons/year and these nanoparticles are one of the most commercially produced nanomaterials in the world having applications in over 200 products [155, 156].

1.6.1. Synthesis of AgNPs

Chemical reduction is the most common approach for synthesis of AgNPs. During this reaction Ag^+ ions are reduced to Ag^0. The standard reduction potential of this reaction in water is relatively high and equal to +0.799 V. It allows to use several reducing agent such as sodium citrate, sodium borohydride, hydrazine and some others [157]. Synthesis of metallic nanoparticles consist of two stages: nucleation and growth. For this reaction there are three essential elements: metal precursor, reducing agent and stabilization agent [158]. Scheme of such reaction using the example of AgNPs formation is showen in Fig. 5.

In 1982, Lee and Meisel carried out modified Turkevich method for the synthesis of AuNPs using $AgNO_3$ instead of $HAuCl_4$ and sodium citrate as the reducing agent synthesized AgNPs [159]. In this case, citrate also acts as stabilization agent. Growth of AgNPs is influenced by citrate ions by complexing with Ag_2^+ dimers. Generally, mechanism of growth depends on the type of reduction method [160, 161].

Creighton and his co-workers [162] performed synthesis of AgNPs in which $NaBH_4$ was used as reducing agent. Recent researches have shown that

possibly process of AgNPs growth during reduction of Ag^+ ions by $NaBH_4$ consist of four steps (Fig. 6). In first step (< 200 ms) rapid reduction of $Ag^+ \rightarrow Ag^0$ takes place. In the second step (< 5 s) reduced Ag atoms form dimers, trimers, *etc*. These clusters further coalesce to nanoparticles with radius of around 2-3 nm. During the third step (around 5-10 min) particles with size higher than 1 nm are not growing anymore. Further comes a point when stability of AgNPs dramatically decreases. Such drop of stability leads to further coalescence and formation of 5-8 nm AgNPs during the final stage. Eventually, colloidal solution stabilizes, stirring is not required anymore and AgNPs solution can be stored during long periods of time [163].

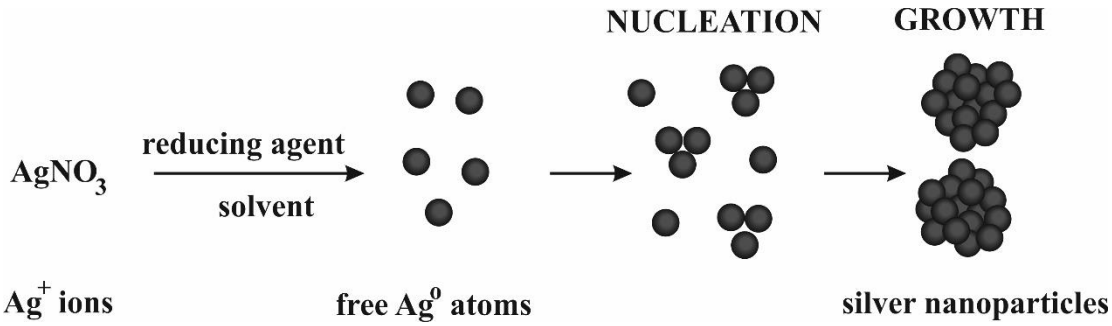

Fig. 5. Mechanism of AgNPs formation by the reduction of the $AgNO_3$ salt.

Size, shape, polydispersity index and other parameters of AgNPs can be controlled by choosing synthesis conditions such as concentration, temperature, pH, stabilization agent, *etc*. [158].

Synthesis of AgNPs can be performed in organic solvents, which can act as a reduction agents. It can be difficult to control aggregation process in organic solvent. On the other hand, advantages of this method are high yield and low polydispersity index [157, 164]. Photochemical synthesis of AgNPs is a process of Ag precursor solution irradiation. Reduction agent is not needed for performing of synthesis. As an irradiation source it is possible to use, for instance, laser or microwave or sunlight irradiation, ionizing radiation and UV light [165]. Also such methods as electrolysis, pyrolysis, sonoelectrochemistry, physical vapor condensation and arc-discharge method are suitable for AgNPs synthesis [166].

Additionally, biogenic methods are suitable for synthesis of AgNPs. Plants, fungi and bacteria are used for production of AgNPs. Biogenically produced AgNPs possess lower toxicity in comparison with AgNPs synthesized by chemical reduction or physical methods [165, 167, 168].

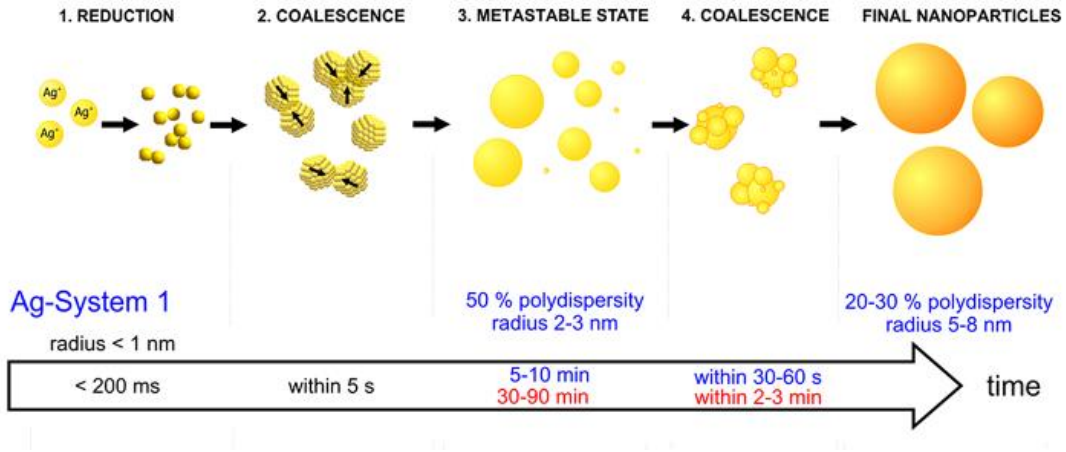

Fig. 6. Scheme of growing mechanism of AgNPs when $NaBH_4$ is used as reducing agent. Adapted from [163].

In plants reduction rate of metal ions is higher than in microorganisms. Mostly extracts of plants are used for synthesis purposes. Procedure of AgNPs solution filtration is needed before application of nanoparticles. Besides, exact mechanism of AgNPs synthesis as well as enzymes, which are involved in this process, are not known yet [169].

1.6.2. Properties and applications of AgNPs

AgNPs possess unique physical, electrical, catalytic and chemical properties. Exclusive optical properties of AgNPs are connected to such quantum electromagnetic phenomenon as surface plasmon resonance (SPR), which is the result of interaction between the light and metal surface. Electrons on surface of AgNPs collectively oscillate when nanoparticles are irradiated by electromagnetic wave with specific wavelength [170]. AgNPs have shown impressive light trapping potential among metal nanoparticles. Furthermore, SPR absorption spectra of AgNPs can be controlled from 300 to 1200 nm [171]

and depend on AgNPs size, shape and surrounding matrix [172]. The forementioned parameters affect light scattering of AgNPs as well as absorption [173]. Such optical properties allow to employ AgNPs in different plasmonic applications including surface-enhanced Raman spectroscopy (SERS) [174], near-field optical microscopy [175], surface-enhanced fluorescence [175], localized surface plasmon resonance spectroscopy [176] and plasmonic circuitry [177]. Employment of AgNPs in SERS allow to detect single molecules, enhancing signal by as much as $10^{14} – 10^{15}$ fold [178]. Due to possible toxicity of Ag^+ ions, which can come from the nanoparticles, AgNPs mostly are used in *in vitro* plasmonic applications [179].

Due to good electrical and thermal conductivity of silver, AgNPs are used in electronics. In addition, silver possesses fairly low resistance [180]. Nanosilver is applied in electronic equipment as solder, single-electron transistors, nanoelectrodes and nanoconectors [181-183]. Also, AgNPs are used in manufacturing of silver pastes [184, 185].

AgNPs are perfect candidate for catalysis. Large surface area of AgNPs provides them more possible reactive sites and high surface energy. High catalytic activities and longer lifetime can be achieved by imparting them with functional groups or supporting materials [180, 186]. AgNPs are suitable catalyst for CO or benzene oxidation [186], 4-nitrophenol to 4-aminophenol [187] and many others [188].

AgNPs are well suited for application as antimicrobial agents in medicine. As mentioned previously silver was used for wound healing and for water purification since ancient times. Silver is comparatively cheap and commercially available. Also silver can be used as antimicrobial agent in different forms such as salts, immobilized ions and nanoparticles [189]. As antimicrobial agents nanosilver has few benefits. Silver has relatively low toxicity towards human cells. Toxicity of AgNPs in comparison with toxicity of silver ions for human mesenchymal stem cells is 10 – 29 times lower [190]. AgNPs typically possess high antimicrobial activity against wide range of microorganisms. Furthermore,

relatively low concentrations of AgNPs are enough for ultimate growth inhibition of microbes [189].

The crucial role in antimicrobial activity of AgNPs play silver atoms (Ag^0). There are two main speculation about antimicrobial actions of AgNPs. Firstly, due to accumulation and aggregation of nanoparticles at the bacteria's membranes, preservation of membrane integrity became no longer possible, which in turn leads to death of bacteria [191]. Secondly, the oxidative stress of cells, which is the result of reactive oxygen species generation by AgNPs, leads to cell death [189].

In presence of an oxidizer, Ag^0 atoms on the surface of AgNPs can dissolve and oxidize to Ag^+ ions. In this case antibacterial actions fall within few mechanisms. Often, as in the case of Ag^0 atoms, formation of reactive oxygen species is possible. For Ag^+ ions it is also typical to have high affinity for thiols, phosphates and amines. Thus, targets of silver ions can be different molecules such as DNA, peptides and enzymes. Binding of Ag^+ ions can affect processes occurring in cells and, consequently, causes death of cell [192-194].

Chemical and physical properties of AgNPs such as size, shape, morphology, coating and many others define AgNPs cytotoxicity. Furthermore, cytotoxic effect of AgNPs mostly depend on types of molecules, which are on their surface. Depending on goal of application it's possible to select condition of synthesis and thus obtain AgNPs with higher toxicity to chosen microorganisms or cells type [195]. Presence of some anions such as S^{2-} can reduce or completely stop antibacterial action of AgNPs, which is related to Ag^+ ions activity. In such case produced silver salts are poorly soluble or insoluble and antibacterial activity of Ag^+ is suppressed [196].

Besides traditional areas of silver medical application, which are well known for a long time, there are some more innovative scopes of AgNPs use. Infections are the most common cause of complications in orthopaedic surgery. Employment of AgNPs reduces the risk of infection sites emergence. Studies have shown that use of AgNPs in bone cement, trauma implants and in tumor prostheses have beneficial effect on the results of orthopedic surgical

procedures [197]. There are many different bacteria in the oral cavity. Chronic periodontitis is very frequently encountered disease worldwide [198, 199]. Any odonatological procedure can cause the infection in such circumstances. Use of AgNPs in dentistry allows to minimize possibility of the microbial colonization. Researches of AgNPs incorporation in composite resin, endodontic materials, acrylic resin and implants were performed in the last decade. Despite positive antimicrobial effect use of AgNPs in dentistry is not possible at this point. For routine use of AgNPs in the future it is necessary to prioritize further research and studies related to cytotoxicity and long term properties of silver nanoparticles [200].

Among possible future applications of AgNPs in medicine also may be noted application of nanoparticles as virucidal agents, photosensitizers or radiosensitizers, anti-angiogenesis agents and anticancer therapeutic agents [201]. AgNPs, similar to some other metal nanoparticles, are powerful tools for inhibition of enzymes involved in membrane synthesis of bacteria. Consequently, in future, it might be possible to replace more expensive antibiotics and enzyme inhibitors [202]. Also, in future AgNPs can be used in agroecosystems for plant disease management. Especially, biosynthesized AgNPs are suitable for this purpose [203].

1.7. Gold nanoparticles

History of gold usage began over 6000 years ago. Already in 4000 B. C. E. remarkable jewellery had been manufactured from gold sheets. Such early employment is the result of ease of gold processing [204]. Since then, gold as a material for jewellery manufacturing was used in ancient Egypt, Rome and other ancient civilizations. In ancient Egypt over 5000 years ago people swallowed pieces of gold for mental and body purification. In 700 B. C. E. gold was applied in prosthetic dentistry in Etruscan civilization [205]. The first use of gold as a material for coins dates back to 700 B. C. E. in Lydia, which was located on the territory of modern Turkey. In the 13th century gold Ducat, which was

manufactured in Venice, was the most commonly used coin in the world [206]. Alchemists were preparing an elixir "*aurum potabile*" in the middle ages. Solution of $NaAuCl_4$ had been used as drug for syphilis treatment in the 19th century. Employment of gold compounds in treatment of such disease as tuberculosis began in the 20th century. Nonetheless, afterwards and until now chrysotherapy (from Greek: *chrysos* – gold) has been more frequently used for treatment of arthritis and similar diseases [207].

Colloidal gold has a rich history. For the first time "soluble" gold was used for medical purposes in Egypt and China at around 4th century B. C. E. AuNPs had been used for treatment of various illnesses [208]. Due to its optical properties, colloidal gold has been widely used as a colorant in making ruby glass. The best known example of such AuNPs application is Lycurgus Cup dating back as far as 4th century B. C. E. Ruby glass can be often found in stained-glass windows of ancient churches [209]. AuNPs were also used in manufacturing of glaze decoration on ceramics. Color of so-called "lustre" can differ depending on the angle of observation. The earliest archaeological finds date back as far as 8th century B. C. E. and were manufactured in Mesopotamia [210].

The first mention of AuNPs was in book, which was published in 1618 by F. Antonii. J. Kunckels, H. H. Helcher, E. Fuhlame and J. B. Richters in their respective works also described some properties and medical applications of AuNPs [208]. The modern history of AuNPs started in 1857 when Michael Faraday observed differences in properties of bulk and colloidal gold [211]. In his works, it was shown that gold chloride can be reduced by various compounds. Faraday attracted attention to formation and optical properties of gold colloids. He was the first who optically monitored and described in a scientific work the plasmon resonance of AuNPs [212]. Gold colloids synthesized by Faraday were so stable that some of them are still stored in Royal Institution in London [213]. In their works, Zsigmondy, Svedberg and Ostwald detailed new synthesis methods such as electrochemical and preparing of AuNPs in organic solutions. Furthermore, they described physical properties of colloidal

gold solutions and methods, which are suitable for size, shape and other parameters determination [214]. In 1951 Turkevich [215] proposed AuNPs synthesis method in which citrate was used simultaneously as reducing and stabilizing agents. This method allows to obtain monodispersed AuNPs with size lower than 20 nm. Aforementioned synthesis method was reinvestigated by Frens [216] and already was suitable for preparation of colloidal solution of AuNPs with diameter ranging from 15 to 150 nm by changing ratio of citrate and gold precursor. Turkevich – Frens method subsequently was modified by different scientists, but remained possibly the most common and most cited AuNPs synthesis method [217, 218].

1.7.1. Synthesis of AuNPs

AuNPs synthesis methods can be divided into chemical and physical. Preparation of gold colloids in terms of media could be split into synthesis in aqueous and non-aqueous solutions. Since Faraday synthesized AuNPs using phosphorus vapor as reducing agent, tetrachloroauric acid ($HAuCl_4$) is still the most common used gold precursor. The most widely used synthesis method is reduction of $HAuCl_4$ with trisodium citrate (Na_3Ct) [219]. The size of nanoparticles depends on amount of citrate ions [220]. In this AuNPs synthesis method there must be at least 0.05% of citrate ions ($Na_3Ct : AuCl_4^- > 0.5$) in the mixture for reduction of all gold. Colloidal gold is stabilized by combination of citrate and chloride anions [213].

There are two mechanisms of $AuCl_4^-$ reduction by citrate ions described in the literature. According to earlier nucleation – grown mechanism system tends to reduce its Gibbs energy. Clusters of gold atoms (“nuclei”), which consist of few atoms, are formed in the solution. If diameter of gold clusters is lower than so called critical cluster size dissolution is more possible than growth process. For clusters, which reached critical size, growing becomes increasingly possible [221, 222]. The group of professor Peng [223] suggested that mechanism of AuNPs may vary depending on the pH. According to them, it is

connected with structural changes of Au complexes in solution (from $AuCl_3(OH)^-$ to $AuCl(OH)_3^-$).

Technological advancement allows to employ new analytical methods for investigation of AuNPs synthesis process. As a result another mechanism was proposed. In seed-mediated growth mechanism (Fig. 7), formation of gold seeds that consist of more than hundred atoms is observed during the first stage. In the next step, due to coalescence process, formation of particles with diameter larger than 3 nm is occurring. Particles size is further changing to 8 – 10 nm during the third step due to diffusional growth. Gold ions are attached in the electronic double layer of the seed particles. This explains shift of plasmon band from 530 to 520 nm in the synthesis beginning. The last step of AuNPs formation is quite quick. Within this stage nanoparticles are formed [224-226].

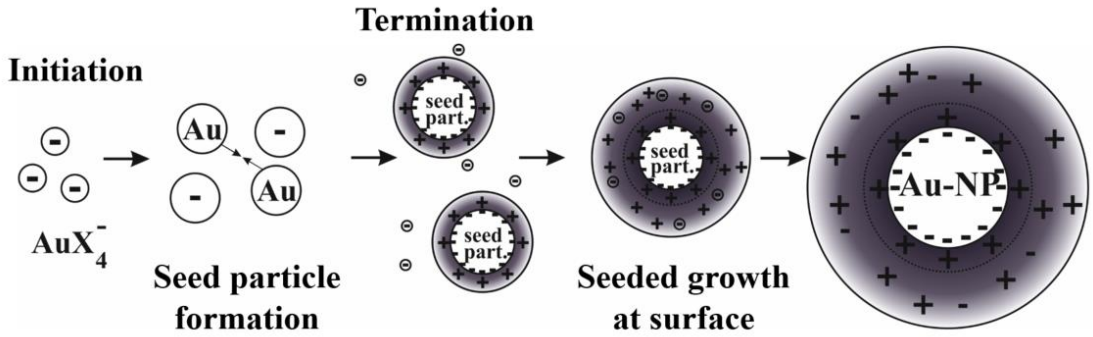

Fig. 7. Scheme of the seed-mediated growth mechanism of AuNPs. Adapted from [224].

The final diameter of AuNPs significantly depend on $AuCl_4^-$ ions concentration in solution. Initial concentration of $HAuCl_4$ define pH value and ratio of Au complexes at the beginning of synthesis. Increasing of $HAuCl_4$ concentration allows to obtain smaller AuNPs. More AuNPs are formed due to higher available $AuCl_4^-$ ions amount during the seed particle formation. Conversely, concentration of Na_3Ct is practically unimportant for the size of AuNPs until pH changes are not observed [219, 224]. Interaction between citrate ions and AuNPs surface were investigated by J. Park and J. Shumaker-Parry [227]. Citrate anions stabilize AuNPs by adsorption on their surface through central carboxylate group. Moreover, citrate anions that are

coordinated on AuNPs surface interact with one another and other anions through terminal carboxyl group by forming hydrogen bonds. Citrate anions on surface are joined to 1-D chains, which interact between themselves by Van der Waals interaction [228].

Chemical AuNPs synthesis in aqueous solution can be performed using various methods. As a reducing agent it is possible to use borohydrides, ascorbic acid, hydrazine, tannic acid, sugars and other compounds. For stabilization it is possible to employ various ligands, polymers, dendrimers and surfactants [217]. Selection of synthesis method depends on size, shape, charge and many other parameters of desired AuNPs.

Among non-aqueous AuNPs synthesis methods the Brust–Schiffrin method has been widely used. This technique allows to get nanoparticles with needed size and low polydispersity index. This synthesis is performed in toluene and $NaBH_4$ in presence of dodecanethiol, which is used as reducing agent [229]. For the use in biological systems AuNPs synthesized in non-aqueous media should be transferred to aqueous solutions. It can be seen as disadvantage, although AuNPs synthesized in non-aqueous solutions are distinguished by monodispersity. It can also be noted, that synthesis in non-aqueous solutions is often a difficult multi-stage process [230, 231].

Synthesis of AuNPs can be performed by photochemical methods. Reduction of $AuCl_4^-$ ions occur due to impact of UV-irradiation or sun light irradiation [232]. Besides, γ-irradiation [233] and microwave irradiation [234] can be used for synthesis. Formation of AuNPs is possible in ionic liquids, where they could play a role of reducing and stabilization agent simultaneously [235]. Sonochemical method allows to synthesize very small AuNPs. For elimination of size distribution problems, which are specific to sonochemical AuNPs formation, use of surfactants or other stabilization agents is required [217]. Furthermore, electrochemical methods have been adapted for synthesis of AuNPs for a long time [236]. Low cost, lower processing temperature and easy control of produced nanoparticles properties can be noted as advantages of this methods [237].

Biological synthesis is seen as green and eco-friendly method of AuNPs preparation [217]. The use of biologically-based methods allows to eliminate toxic and hazardous compounds from AuNPs synthesis solution and thereby reduce synthesis cost [238]. Besides, it is possible to achieve uniformity of nanoparticles. Synthesis can be performed by employment of microorganisms such as fungi, yeast and bacteria. In this regard, fungi are more suitable for large-scale production in comparison to other microorganisms. It is sufficient to get bacteria with required properties acquired by genetic manipulation [239-241]. Plant extracts can also be used for green AuNPs synthesis. During such synthesis Au precursor is mixed with plant extract. Reaction can be performed at room temperature in few minutes or few hours. Furthermore, there are a lot of plants whose extracts are suitable for AuNPs synthesis [242, 243]. Despite all advantages of biological AuNPs synthesis there are few scientific issues, which should be solved for more frequent use of such methods. Efficiency and time of synthesis primarily need further improvement. Furthermore, control of particles size and morphology should be also improved. These challenges can be effectively handled by understating of AuNPs synthesis process [244, 245].

1.7.2. Properties and applications of AuNPs

AuNPs as well as AgNPs due to such phenomenon as SPR possess unique optical properties. As a result, UV-Vis spectra of AuNPs colloidal solutions are characterized by specific plasmon band in the region of 500 to 600 nm. Plasmonic optical properties strongly depend on size and shape of AuNPs. For instance, in UV-Vis spectra of gold nanorods solutions there are two absorption bands that are related to diameter and length of nanorods [246], whereas extinction coefficient depends on the size of nanorods due to higher relative scattering efficiency of larger nanorods [247]. Change of nanoparticles diameter leads to alteration of wavelength of absorbance peak [248], wherein such phenomenon can be observed for nanoparticles with size higher than 2 nm. Changes of AuNPs in size by few nanometers can be easily detected

spectrophotometrically from absorbance peak shift. Therefore, such processes as aggregation or disaggregation can be easily detected and might be used for analytical purposes [249]. Kim *et al.* [250] developed a method for determination of small amounts of heavy metal in aqueous solutions. In this method AuNPs were capped by 11-mercaptoundecanoic acid. Due to coordination of metal ions by 11-mercaptoundecanoic acid, aggregation takes place and change in UV-Vis spectra was registered.

Change of AuNPs size can also be detected and considered as analytical signal. The group of Tian [251] developed a method for screening of lipase activity. Tween 80 in this work served as the reducing and stabilizing agent, but also as substrate for lipase. H_2O_2 formed during oxidation process of Tween 80 reduce $AuCl_4^-$ ions that leads to formation of AuNPs. Concentration of hydrogen peroxide depends on lipase activity. Therefore, enzyme activity can be defined by formation of AuNPs. Considering that H_2O_2 can reduce $AuCl_4^-$ ions into Au atoms, glucose oxidase and horseradish peroxidase can be used for enlargement of AuNPs [252, 253]. Slight change of determination method allows to detect concentration of enzyme inhibitors [254]. In another research enzymatic reaction, in contrast to previous examples, was monitored from decrease in absorbance and shift of SPR peak due to reduction of size of gold nanorods. Activity of acetylcholinesterase was determined by stopping or decreasing rate of enzymatic etching of gold nanorods in the presence of horseradish peroxidase [255].

Plasmonic properties of AuNPs also depend on temperature, pressure up to 1.2 GPa, electric charge and surrounding environment [256]. SPR depends on the dielectric constant of the non-absorbing surrounding medium, wherein various materials, which are adsorbed on AuNPs surface, can also have influence on plasmonic properties [249]. In this case, change in SPR may be related to alteration of the surrounding environment, variation of electronic density of states near the AuNPs Fermi level or change of effective size of AuNPs plasmonic metal core [256]. For instance, change in effective size takes place

when molecules with thiol groups adsorb on Au surface, resulting in reducing amount of effective ‘valence’ electrons [257].

AuNPs display fluorescence properties. AuNPs quench or enhance the fluorescence of fluorophore. Therefore, AuNPs can be used in design of metal-enhanced fluorescence sensors, for instance, for DNA and proteins detection [258]. AuNPs as well as AgNPs can enhance Raman scattering and are also employed in SERS sensing. Use of AuNPs allows to increase Raman signal 10^6 times. The main problems of SERS usage are fluorescence and reproducible enhancement factors. Even a weak fluorescence can disguise Raman signal and even minor changes in Au nanostructures can significantly influence the result of sensing and lead to SPR shift [259].

AuNPs are perfect candidates for catalysis. Gold as well as silver is inert in bulk form, wherein if Au is dispersed onto a support media, it possesses fantastic catalytic ability. The huge surface area has a significant role in catalytic properties of AuNPs [260]. Crystal structure, shape and dimensions are extremely important for selectivity and catalytic activity of Au nanostructures [261]. Unique properties make it possible to use AuNPs for electrochemical applications. AuNPs are not only good electronic signal transductors and display relatively high surface area to volume ratio, but also possess perfect biocompatibility and structural, electronic and catalytic properties. Thereby, AuNPs were used in design of biosensors, immunosensors, chemisensors and electrocatalyst [262-264].

Important features of AuNPs are chemical stability and relative simplicity of Au surface functionalization with organic and biological molecules. Chemisorption of molecules, which contain thiol group in their structure, is especially used for formation of self-assembled monolayer (SAM) onto Au surface. Sulfur during adsorption process forms covalent bonds with Au atoms. Structure of the sulfur - gold interface depends on AuNPs surface coverage [265]. The efficiency of chemisorption process can be controlled by changing time of adsorption and various parameters (pH, temperature, *etc*.). AuNPs are also great for bioconjugation with peptides, lipids and other organic

molecules [208]. AuNPs are commonly bound to biomolecules by non-covalent conjugation. Covalent conjugation (amine-carboxylate coupling) is normally performed between free biomolecules and SAM, which was pre-grafted onto Au surface by chemisorption of thiol groups [266].

As it was mentioned above colloidal gold was used in medicine from ancient times. Nowadays, AuNPs have become hopeful tools in several fields of medicine. During the past three decades AuNPs have been actively used in design of different sensors. AuNPs due to their unique properties improve characteristics of produced sensors. In some cases work of analytical systems such as SERS, metal-enhanced fluorescence and *etc*. are based on features, which are particular for Au nanostructures. Moreover, AuNPs can be employed in drug delivery, biomedical imaging and different types of therapy [267].

AuNPs can absorb photons and convert the collected energy into thermal. Therefore, gold nanostructures are suitable for photothermal therapies. Modification of AuNPs with molecules, which can specifically determine particular cells in organism, allows to localize AuNPs near to nests of these cells. Therapy performed in such manner allows to minimize negative effect to human health. Such type of therapy can be especially employed in cancer treatment [268].

In case of biomedical imaging AuNPs can be used as a contrast agent for X-ray computed tomography due to the fact that X-ray radiation of gold nanostructure is larger than widely used iodine. AuNPs also are suitable for employment in magnetic resonance imaging, ultrasound and optical imaging [269].

Especially useful characteristic of gold nanostructures applied for bioimaging is their ability to form strong bonds with various biomolecules, which can be selected depending on target in organism. Thus it becomes possible to visualize desired cells or tumors. [270]. Such ability is equally important for targeting drug delivery. Biomolecules adsorbed on AuNPs surface can serve as matrix for drugs and as part that recognizes, for instance, cancer cells [271, 272]. AuNPs as well as a few Au salts can be used as antiarthritic agents [267]. Au

nanomaterials are currently being used in food packing manufacturing as antimicrobial agents [260].

In most of the given examples of application it is important to evaluate not only the therapeutic effect, but also toxic actions of AuNPs. Cytotoxicity of AuNPs is related to few parameters: (i) size, (ii) coating materials, (iii) surface chemistry and (iv) biological target. Numerous studies have shown that smaller nanoparticles are more toxic for different type of cells [273]. Pan *et al*. [274] investigated cytotoxic effect of small AuNPs with a size of 0.8 - 15 nm. Particles with size of 1.4 nm possess the highest toxicity in four different cell lines, wherein viability of cells which were incubated with AuNPs was lower than viability of control group. Nanoparticles with size of 1.4 nm fit exactly to ensure that AuNPs will be easily attracted to DNA grooves due to the fact that Au is an electronegative metal. As a result DNA can be damaged [275], besides stress proteins can be overexpressed [276].

Large particles are detected by immune system fast enough and are delivered to the liver and to the spleen, whilst smaller particles can be excreted by kidney [273]. Small particles (15 nm) strongly accumulate in many tissues: blood, liver, lung, heart and kidney. Concentration of larger AuNPs (200 nm) was very low in blood, brain and spleen [277].

Charge of AuNPs is very important for toxicity. Cationic particles can be attracted to DNA, anionic AuNPs can get inside cells due to endocytotic pathways. Hydrophobicity is equally important parameter, but its role is not understood enough [273]. Proteins spontaneously adsorb on the surface of positively charged nanoparticles in the cellular media. Adsorbed layer of proteins is called corona. Shell of proteins is important for AuNPs stability and can help particles get into the cells [278]. Modification of AuNPs can allow to minimize negative effects. Polyethylene glycol due to biocompatibility is a good option for modification of AuNPs surface [279].

2. Materials and methods

2.1. Chemicals

Chemicals of analytical grade and deionized water were used, if not otherwise stated. Silver nitrate ($AgNO_3$), trisodium citrate dihydrate ($C_6H_5Na_3O_7 \times 2H_2O$), sodium borohydride ($NaBH_4$), sodium chloride (NaCl), sodium hydroxide (NaOH), hydrochloric acid (HCl), methanol (CH_3OH), dipotassium hydrogen phosphate (K_2HPO_4), disodium hydrogen phosphate (Na_2HPO_4), 1,6-hexanedithiol ($HS(CH_2)_6SH$) (1,6-HDT) and poly(allylamine hydrochloride) (PAH) of molar mass of 70 kDa were purchased from Sigma-Aldrich (Taufkirchen, Germany). Glucose oxidase from *Aspergillus niger* (EC 1.1.3.4, type VII, 208 U mg^{-1} and 215 U mg^{-1}) was obtained from Fluka (Buchs, Switzerland) and Carl Roth GmbH&Co (Karlsruhe, Germany). Ethanol (C_2H_5OH) was purchased from Vilniaus degtine (Vilnius, Lithuania). Sodium acetate trihydrate ($CH_3COONa \times 3H_2O$) and potassium chloride (KCl) were obtained from Reanal (Budapest, Hungary) and Lachema (Neratovice, Czech Republic), respectively. Aniline was purchased from Merck KGaA (Darmstadt, Germany). Tannic acid was obtained from Avantor Performance Materials Poland S.A. (Gliwice, Poland) and Carl Roth GmbH&Co (Karlsruhe, Germany). Aluminum oxide powder ((Al_2O_3), grain diameter 0.3 mm, Type N) was purchased from Electron Microscopy Sciences (Hatfield, USA). D-(+)-glucose and tetrachloroauric acid trihydrate ($HAuCl_4 \times 3H_2O$) were obtained from Carl Roth GmbH&Co (Karlsruhe, Germany).

The solution of glucose was prepared at least 24 h before usage in order to allow glucose to mutarotate and reach equilibrium between α and β forms.

2.2. Sample preparation

2.2.1. Preparation of polyaniline nanoparticles

Water soluble PANI could be prepared using a template guided enzymatic approach [280]. Aniline was filtered before the use through 5 cm column filled by Al_2O_3 powder to remove colored components. Polyaniline nanoparticles were prepared at room temperature in darkness in the solution of 0.05 mol L^{-1} sodium acetate (SA) buffer, pH 6.0, 0.05 mol L^{-1} of glucose, 0.50 mol L^{-1} of aniline and 0.75 mg mL^{-1} of GOx.

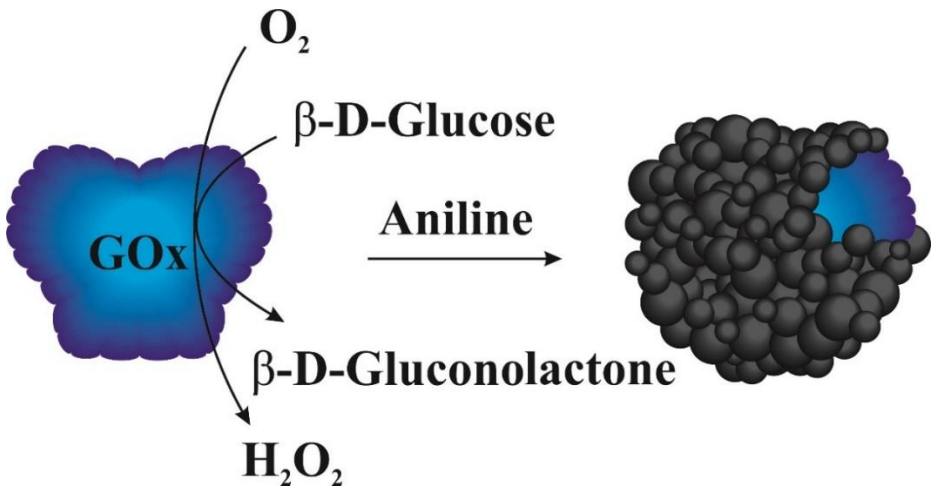

Fig. 8. Scheme of enzymatic synthesis of polyaniline nanoparticles.

In the presence of glucose and dissolved oxygen (Fig. 8) the β-D-glucose oxidase (GOx) generates hydrogen peroxide, which oxidizes the polymer chain, and β-D-gluconolactone that is hydrolyzed to gluconic acid.

2.2.1.1. The separation procedure of polyaniline nanoparticles

PANI nanoparticles after 21 h lasting synthesis at 20 ±2 °C were separated from the synthesis solution by centrifugation (5 min, 16.1×10^3 g). PANI nanoparticles were washed with selected washing solution. Suitability of (i) C_2H_5OH; (ii) 0.05 mol L^{-1} sodium acetate (SA) buffer, pH 6.0; (iii) 0.001 mol L^{-1} HCl or (iv) 1.0 mol L^{-1} HCl solutions for cleaning of PANI

nanoparticles was investigated. Washing procedure was repeated 3 times and PANI nanoparticles were collected by centrifugation. Then separated and washed PANI nanoparticles were resuspended in SA buffer and used for further investigations.

2.2.1.2. The optimization of PANI nanoparticle formation

The efficiency of PANI nanoparticles formation depends on the initial aniline and GOx concentrations in polymerization solution. The selection of optimal aniline concentration was performed by changing the aniline concentration from 0.10 to 0.90 mol L^{-1} in the polymerization solution consisting of 0.05 mol L^{-1} SA buffer, pH 6.0, 0.05 mol L^{-1} of glucose and 0.50 mg mL^{-1} of GOx during 21 h period. The optimization of GOx concentration was performed by changing GOx concentration from 0.125 to 0.75 mg mL^{-1} in the polymerization solution with 0.50 mol L^{-1} of aniline. The optimal duration of polymerization was studied changing the polymerization time from 1 to 331 h in 0.05 mol L^{-1} SA buffer, pH 6.0, 0.05 mol L^{-1} of glucose, 0.50 mol L^{-1} of aniline and 0.75 mg mL^{-1} of GOx. The separation and washing of PANI nanoparticles were carried out in the same way as it was described in the previous section. All experiments were performed at 20 ±2 °C. The influence of aniline and GOx concentrations, as well as polymerization duration was evaluated by UV-Vis spectroscopy.

2.2.2 Preparation of AgNPs and tannic acid monolayers

2.2.2.1. Preparation of colloidal suspensions

The silver nanoparticles suspension was obtained from silver nitrate by a chemical reduction method (Fig. 9). In the synthesis, 200 mL aqueous solution of silver nitrate (1 mol L^{-1}) was added dropwise into 400 mL of the mixture, which contained 580 mg of trisodium citrate and 64 mg of sodium borohydride. The process was carried out for 2 h at room temperature under continuous stirring. Afterwards, the excess of ions in yellow silver suspension was removed

by ultrafiltration method. The ultrafiltration procedure was continued until the conductivity of the effluent solution stabilized at 15 μS cm^{-1} [17].

The stock solution of tannic acid was prepared by dissolving of 100 mg of tannic acid in 100 mL of ultrapure water. Other solutions of tannic acid of a desired concentration were obtained by diluting the stock solution. In order to prevent an uncontrolled decomposition of tannic acid, the solutions were freshly prepared before each measurement.

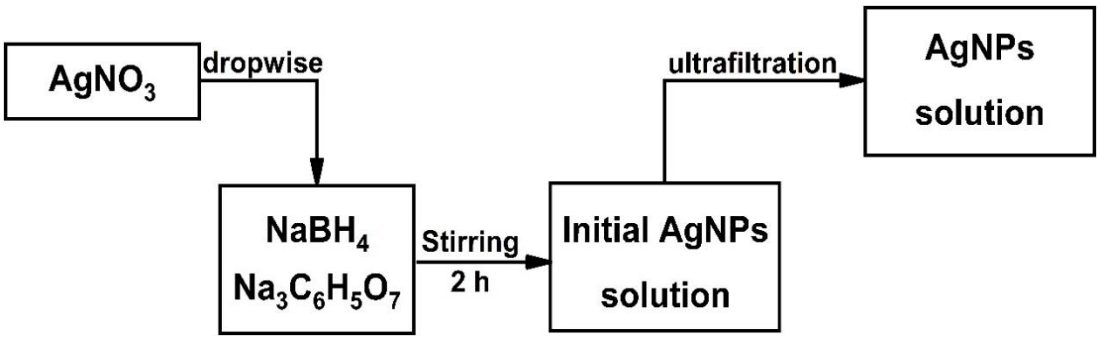

Fig. 9. Principle scheme of silver nanoparticles synthesis.

The mixtures of the silver nanoparticles and tannic acid of given concentrations were prepared using the stock solutions. pH and ionic strength of these suspensions were regulated by the addition of hydrochloric acid and sodium hydroxide using solutions of desired weight concentration.

The suspension of cationic polyelectrolyte was prepared by dissolving 10 mg of poly(allylamine hydrochloride) salt in 100 mL of ultrapure water. In order to obtain suspensions of lower concentration, the stock solution was diluted to an appropriate concentration before adsorption experiments.

2.2.2.2. Deposition of silver nanoparticles on PAH-covered mica

In the first step, PAH monolayers of a controlled coverage were produced on mica. Natural ruby mica sheets, obtained from Continental Trade, were used as substrate for particle deposition. The solid pieces of mica were freshly cleaved into thin fragments of desired area and used in each experiment without any additional pretreatment.

Accordingly, freshly cleaved mica sheets were placed into the PAH solution of the bulk concentration of 10 mg L^{-1} (I = 10^{-2} mol L^{-1} NaCl, pH 4.0). PAH molecules were allowed to adsorb under diffusion conditions over the time of 15 min. Afterwards, the mica sheets covered with a PAH monolayer were rinsed with ultrapure water and placed in thermostated diffusion cells containing a mixture of silver nanoparticles and tannic acid of desired concentration at fixed ionic strength of 10^{-2} mol L^{-1}. The deposition time was varied between 5 and 400 min. Finally, the obtained monolayers were rinsed, dried in air and characterized by scanning electron microscopy and atomic force microscopy imaging.

2.2.3. Biocatalytic enlargement of gold nanoparticles

2.2.3.1. Synthesis of AuNPs

AuNPs were synthesized reducing $AuCl_4^-$ anions by sodium citrate in the presence of tannic acid as an additional reductant (Fig. 10). 80 mL of 0.0125 % [w/v] of $HAuCl_4$ aqueous solution and a mixture of 20 mL consisting of sodium citrate (4 mL of 1% [w/v]) and tannic acid (0.025 mL of 1% [w/v]) in deionized water were prepared [218, 281].These solutions in deionized water were heated in an Erlenmeyer flasks up to 65 °C on a magnetic stirrer with electric heating.

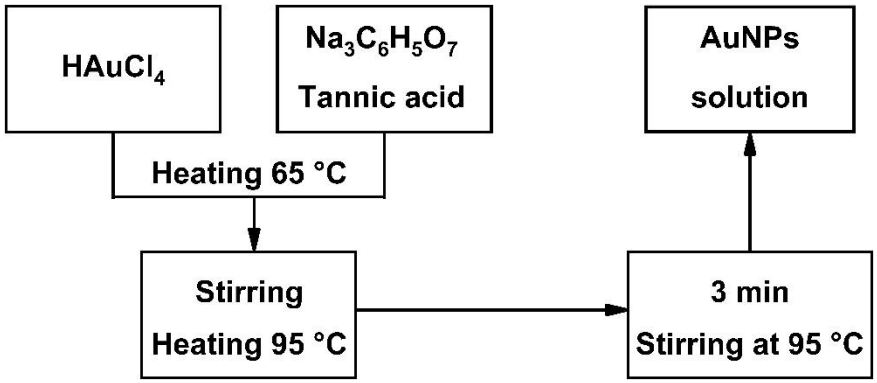

Fig. 10. Principle scheme of gold nanoparticles synthesis.

After preheating, solutions were mixed, heated up to 95 °C and kept at this temperature for 3 min to yield solution of nearly monodispersed AuNPs of 13.0 nm in diameter that was determined by AFM [282]. Solution of AuNPs was stored in dark glass flasks at +4 °C.

2.2.3.2. Biocatalytic enlargement of AuNPs seeds in the solution

Colloidal AuNPs seeds and 0.01 mol L^{-1} PBS solution were mixed at different ratios maintaining the same final concentration of GOx (25 μg mL^{-1}) and $HAuCl_4$ (0.976 mmol L^{-1}) (growing solution) in order to determine the optimal composition for the biocatalytical enlargement of AuNPs seeds (Fig. 11A). Six ratios of colloidal AuNPs seeds and growing solution (1:1, 2:3, 1:2, 1:3, 1:6 and 1:14) with 4×10^{-2} mol L^{-1} of glucose were analyzed at 20 °C temperature.

2.2.3.3. Preparation of Au SD surface for AuNPs immobilization

Surface plasmon resonance sensor disc with a planar Au layer (Au SD) were received from XanTec bioanalytics GmbH (Germany). A bare sensor disc surface was cleaned with 1 mol L^{-1} NaOH solution for 20 min and then with 1 mol L^{-1} HCl solution for 5 min. After the rinsing with deionized water and drying, the sensor disk was transferred to 1 mmol L^{-1} 1,6-HDT in methanol and stored for 24 h to form a self-assembled monolayer of the alkane dithiols. After the rinsing out the excess of alkane dithiols firstly with methanol and then with water, and drying the 1,6-HDT-modified sensor disc was used for AuNPs seeds immobilization.

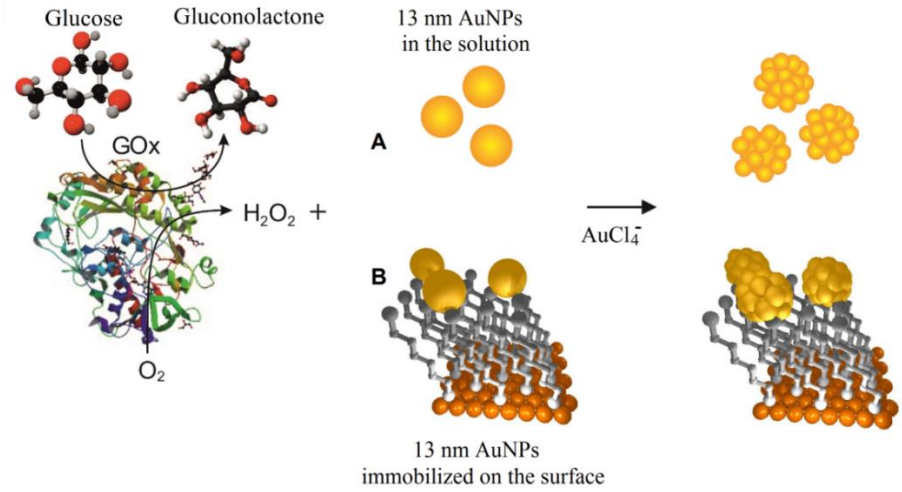

Fig. 11. Principle of the biocatalytic enlargement of gold nanoparticles in the growing solution (**A**) and immobilized on the 1,6-hexandithiol self-assembled monolayer modified sensor disc (**B**).

2.2.3.4. Biocatalytic enlargement of immobilized AuNPs seeds

Sensor disc functionalized with 1,6-HDT exposing thiol groups on the surface was placed into colloidal solution of AuNPs seeds for 20 min and then washed by water. The strong interaction between sulphur and gold atoms leads to the 13 nm AuNPs seeds immobilization on the surface. The enlargement of AuNPs seeds was performed in the growing solution for 60 and 90 min changing glucose concentration (Fig. 11B).

2.3. Instrumentation

2.3.1. UV-Vis spectrophotometry

The enzymatic ANI polymerization was evaluated by UV-Vis absorption spectroscopy. The absorbance of solutions was investigated in 300 - 700 nm wavelength range and it was used for the monitoring of PANI nanoparticle formation in the polymerization solution.

The appropriate ratio of AuNPs seeds and components needed for the biocatalytic enlargement of AuNPs seeds was determined spectrophotometrically. In both investigation UV-Vis absorption spectroscopy measurements were performed by UV-Vis spectrometer Lambda 25 (PerkinElmer, Shelton, USA). UV-Vis spectra were monitored in plastic disposable cuvettes of 1 cm optical path length.

UV-Vis spectra of silver and tannic acid suspensions in quartz cuvettes were recorded using the UV-1800 spectrometer (Shimadzu, Kyoto, Japan). Ultrapure water was used as the reference sample to take the ‘blank’ spectrum for all measurements. Additionally, the spectrophotometric measurements were used in order to determine the stability of silver nanoparticles under various pH values.

2.3.2. Atomic force microscopy and scanning electron microscopy

For the characterization of modified sensor disk surface and determination of AuNPs size the atomic force microscope BioScope II (Veeco, Santa Barbara,

USA) with TESP cantilevers (Veeco) operating in the tapping mode was used. On the basis of previous experiments, the enlargement was carried out at the optimal ratio of AuNPs seeds and growing solution.

The kinetics of AgNPs deposition on PAH monolayers were studied by AFM and SEM. AFM measurements were carried out using the Solver Pro instrument (NT-MDT, Tampa, USA) with the SMENA SFC050L scanning head (NT-MDT). The imaging was done in semi-contact mode using composite probes possessing a silicon body, polysilicon levers and high resolution silicon tips. The SEM investigations were carried out using the JEOL JSM-7500F Field Emission microscope at 15 kV. The number of particles per unit area of the substrate was determined from the AFM images or SEM micrographs using image-analysis software MultiScan Base. Typically, the number of particles was determined over 10 - 15 equally sized areas, which were randomly chosen over the PAH pre-covered mica sheets.

Morphology and the size of particles were determined using scanning electron microscope JEOL JSM-7500F working in transmission mode. Samples for this examination were prepared by dispersing a drop of the silver colloid on a copper grid which was covered by a carbon film.

2.3.3. Dynamic light scattering

Dynamic light scattering measurements were performed with Zetasizer Nano ZS (Malvern, Herrenberg, Germany) equipped with a 633 nm He-Ne laser and operating at 173º angle. The obtained data was analyzed with Dispersion Technology Software version 6.01 from Malvern. DLS investigations were evaluated and presented using SigmaPlot software.

DLS method is based on measurements of scattered light fluctuations. Then monochromatic light is scattered by particles in analyzed solution speckle pattern is visible on the screen. Speckle pattern consists of dark and bright areas. Bright areas belong to light scattered by particles. Due to Brownian motion particles are moving and changing their position during measurements so speckle pattern is changing in time. Fluctuation of intensity of scattering light is

recorded and DLS data is fitted with an autocorrelation function. As a result diffusion coefficient of particles is calculated. Larger particles are moving slower than small one [283-286]. The Stock-Einstein equation gives information about relationship between size and speed of a particle and establishes a connection between diffusion coefficient (D) and hydrodynamic radius (R_h) of particles:

$$D = \frac{k_B T}{6\pi\eta R_h} \quad (2)$$

where k_B is Boltzmann's constant, T is the absolute temperature and η is the viscosity of the solvent.

Samples of PANI nanoparticles for DLS measurements were performed by enzymatic polymerization of aniline in the solution consisting of 0.50 mol L^{-1} of aniline and 0.75 mg mL^{-1} of GOx for a defined period of time (from 21 to 163 h) at 20 ±2 °C. After synthesis PANI nanoparticles were washed with 0.05 mol L^{-1} SA buffer, pH 6.0, and collected by centrifugation (5 min, 16.1×10^3 g). Washing procedure was performed three times. After rinsing PANI nanoparticles were resuspended in SA buffer.

Also by DLS method was evaluated enlarged AuNPs hydrodynamic diameter after biocatalytic enlargement. Samples for DLS measurements were prepared by mixing of AuNPs seeds with solution containing components, which are required for the enlargement of AuNPs seeds at the ratio of 1:2. All samples were prepared in plastic cuvettes by consistent addition of components and gentle blending after each addition. The final growing solutions consisted out of 25 μg mL^{-1} GOx, 0.976 mmol L^{-1} $HAuCl_4$ and different concentration of glucose (4×10^{-2}, 4×10^{-3} and 4×10^{-4} mmol L^{-1}) dissolved in 0.01 mol L^{-1} PBS pH 6.0.

Diffusion coefficients and electrophoretic mobility of the silver nanoparticles as well as tannic acid molecules were measured by the DLS and microelectrophoresis, respectively, using the Zetasizer Nano ZS instrument.

2.3.4. Cyclic voltammetry

Enzymatic polymerization of aniline (duration of synthesis 112 h) and washing procedure of PANI nanoparticles were performed in the same way as for DLS measurements. Cyclic voltammograms were registered using a computerized potentiostat PGSTAT 30/Autolab (EcoChemie, Utrecht, Netherlands) with GPES 4.9 software in cyclic voltammetry mode at scan rate of 0.10 V s^{-1}. A conventional three-electrode system comprising of modified graphite rod as a working electrode, platinum wire as a counter electrode and $Ag/AgCl_{(3\ mol\ L^{-1}\ KCl)}$ (Metrohm, Herisau, Switzerland) as a reference electrode was used in cyclic voltammetry based measurements. Graphite rod was cut and polished on fine emery paper. After this PANI nanoparticles were deposited on the surface of electrode. Then modified electrode was covered with a polycarbonate membrane with a pore size of 3 μm, which was received from Merck Millipore (Carrigtwohill, Ireland), in order to avoid the detachment of PANI nanoparticles from the surface of electrode. Cyclic voltammogram was performed in 1 mol L^{-1} HCl electrolyte solution at 20 ±2 °C. The electrode potential was swept from -0.20 to +1.20 V *vs* $Ag/AgCl_{(3\ mol\ L^{-1}\ KCl)}$.

2.3.5. Measurement of AgNPs concentration

Silver particle concentration in the suspensions was determined using a high-precision densitometer DMA5000M (Anton Paar, Ostfildern, Germany) according to the procedure described previously [287].

The kinetics of AgNPs adsorption is dependent on the bulk concentration of AgNPs colloidal suspension. Moreover, for calculation of coverage it is necessary to know AgNPs concentration. The stock solution of AgNPs was prepared by ultrafiltration method using a stirred membrane filtration cell model 8400 (Millipore, Guyancourt, France). Further densities of AgNPs stock solution and supernatant solution were measured using densitometer. Bulk concentration of AgNPs colloidal solution (w) was calculated from the formula [288]:

$$w = \frac{\rho_p(\rho_s - \rho_e)}{\rho_s(\rho_p - \rho_e)} \quad \textbf{(3)}$$

where ρ_s is the density of the stock AgNPs colloidal suspension, ρ_e is the density of the supernatant solution and ρ_p = 13.49 g cm^{-3} is specific density of silver.

2.3.6. Streaming potential measurements

The adsorption processes of tannic acid at PAH monolayers were studied using streaming potential measurements according to the previously described procedure [289, 290].

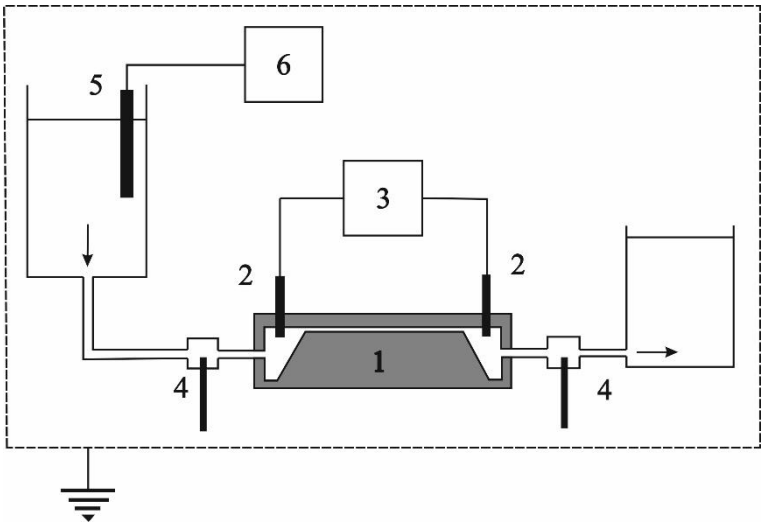

Fig. 12. Schematic view of apparatus, which was used for streaming potential measurements: (**1**) cell (**2**) Ag/AgCl electrodes (**3**) electrometer (**4**) electrodes for cell resistance measurements (**5**) conductivity cell (**6**) conductometer. Adapted from [291].

Streaming potential measurements were performed using homemade cell (Fig. 12) consisting of two Teflon blocks. In one of them, rectangular form inlet and outlet were done. Between the blocks two mica sheets separated by a Teflon gasket (250 μm) were placed. Blocks were put to the pressing machine and as a result a channel (2b × 2c × L = 0.025 × 0.33 × 6.0 cm) was formed between mica sheets separated by Teflon spacer. During the measurements electrolyte was streamed through the cell. Streaming potential appears due to constant pressure gradient of electrolyte. Two Ag/AgCl electrodes, which were in direct contact with inlet and outlet, were used for streaming potential measurements. Apparatus was placed to the Faraday cage to avoid effect of any electromagnetic fields [291, 292].

3. Results and discussion

3.1. Evaluation of enzymatic formation of polyaniline nanoparticles

In this section synthesis of PANI nanoparticles by polymerization/oligomerization of aniline monomers using hydrogen peroxide, which was formed during GOx catalyzed enzymatic reaction, is discussed. During this process GOx could be capsulated within formed PANI nanoparticles. The optimal conditions for enzymatic formation of PANI nanoparticles were determined.

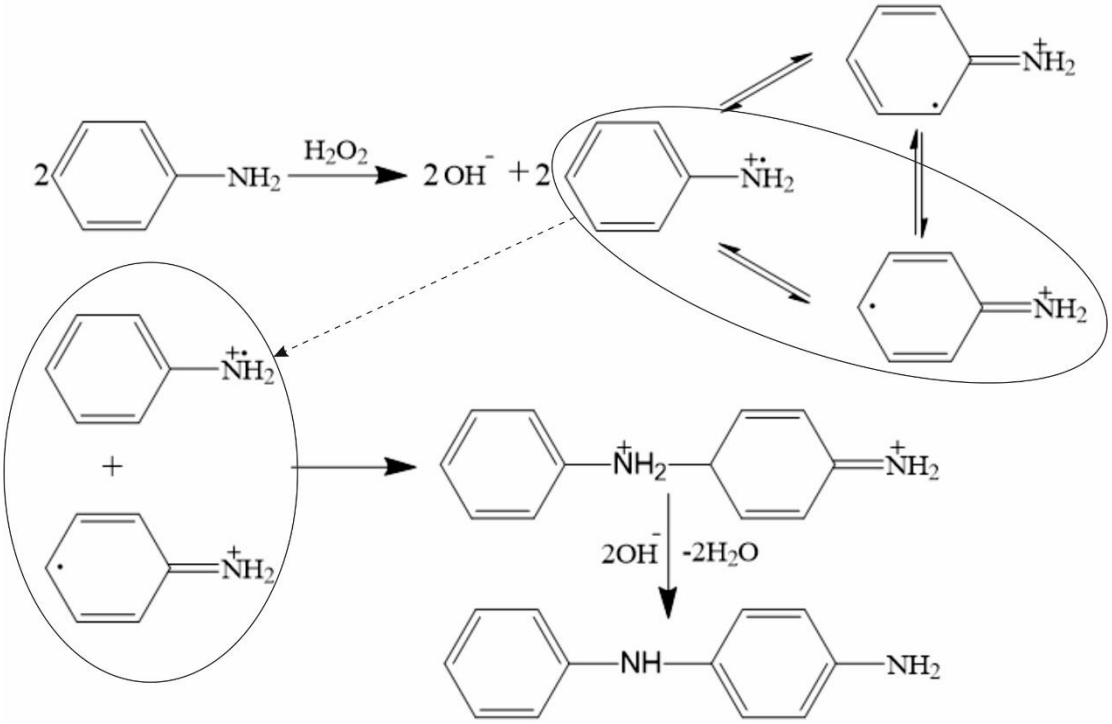

Fig. 13. Schematic representation of polyaniline formation initiated by hydrogen peroxide formed during enzymatic reaction.

The process of enzymatic polymerization/oligomerization is based on a mechanism where monomer of aniline is attacked by a radical cation, leading directly to the aniline reaction with the oxidized oligomer [67, 140]. The main steps of enzymatic polymerization and PANI nanoparticle formation are illustrated in Fig. 13. H_2O_2 was produced during catalytic reaction of glucose

oxidase creating conditions for the aniline polymerization. According Liu *et al*. [133] results, the optimal pH for the catalytic activity (the oxidation of polyaniline in the complex begins) has been observed at pH about 6.0, when aniline oligomers with different structures are formed in aqueous solution [106, 131]. Such oligomers contain orto- and para-coupled units with cyclic phenazine fragments [106].

The synthesis of polyaniline depends on the reaction conditions (solution pH, the type of oxidant, the nature of the acid protonating, the aniline and the concentration of reactants). The selected washing solution, the procedure of the separation and the purification of synthesized PANI nanoparticles from the reaction components have got significant influence on further investigations [293]. In order to select suitable washing solution synthesized PANI nanoparticles were centrifuged and washed with (i) C_2H_5OH; (ii) 0.05 mol L^{-1} SA buffer, pH 6.0; (iii) 0.001 mol L^{-1} HCl or (iv) 1.0 mol L^{-1} HCl. Washing/centrifugation procedure was repeated 3 times. The degree of successful separation and purification of PANI nanoparticles was evaluated by UV-Vis spectroscopy. Spectra of resuspended PANI nanoparticles and washing solution were compared. No absorbance peaks were observed using 0.05 mol L^{-1} SA buffer, pH 6.0, and these results confirmed that the selected washing solution and purification procedure of PANI nanoparticles are appropriate. It should be mentioned that investigated C_2H_5OH, 0.001 and 1.0 mol L^{-1} HCl solutions dissolved polymer in the first stage of the purification. Synthesized, washed and resuspended in SA buffer, pH 6.0, PANI nanoparticles were used in our further investigation.

Successful enzymatic polymerization/oligomerization of polymers depends on such factors like the concentration of monomer and glucose oxidase and the duration of polymerization [133, 140]. It was demonstrated in previous studies that higher oxidant concentration has influence on the higher yield of polymer [294]. In order to improve PANI formation the influence of aniline concentration on the absorbance was evaluated. To achieve the best conditions, aniline monomer concentration in 0.05 mol L^{-1} SA buffer, pH 6.0, with

0.05 mol L^{-1} glucose, 0.50 mg mL^{-1} GOx was changed from 0.10 to 0.90 mol L^{-1}. Fig. 14A illustrates that registered absorbance of polymerization solution using 0.05 mol L^{-1} of glucose increased by increasing concentration of aniline and it was the highest at 0.5 mol L^{-1} of aniline. The absorbance of synthesis solution containing 0.50 mol L^{-1} of aniline increased 21.5 times if compared with the absorbance registered in the presence 0.10 mol L^{-1} of aniline.

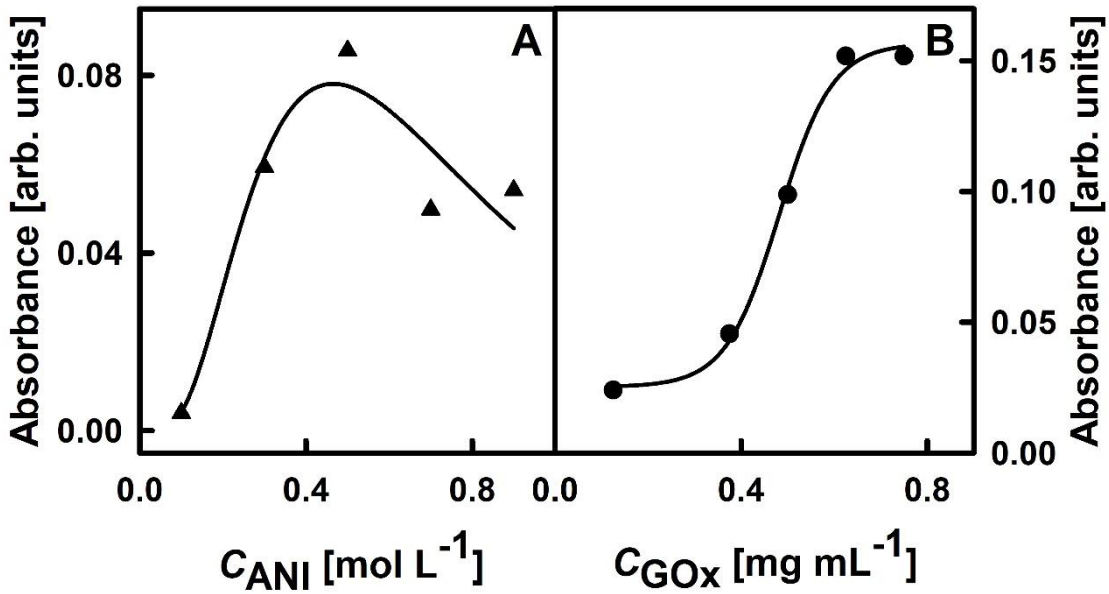

Fig. 14. The effect of aniline (A) and glucose oxidase (B) concentration in the polymerization solution on the registered absorbance in the presence 0.05 mol L^{-1} of glucose. (Polymerization solution: A – 0.05 mol L^{-1} SA buffer, pH 6.0, with 0.05 mol L^{-1} glucose, 0.50 mg mL^{-1} glucose oxidase; B – 0.05 mol L^{-1} SA buffer, pH 6.0, with 0.05 mol L^{-1} glucose, 0.50 mol L^{-1} aniline; polymerization time 21 h. The absorbance was measured in 0.05 mol L^{-1} SA buffer, pH 6.0.)

The most significant amount of aniline monomers is oxidized by oxidant during the early stage of the polymerization and oligomers of high molecular weight are formed [140]. The polymerization is faster at higher (up to 0.5 mol L^{-1}) aniline concentration [133, 294], but further increasing of aniline concentration negatively influenced the polyaniline nanoparticles formation. Thus, 0.5 mol L^{-1} of aniline was selected as the optimal concentration of monomers.

In the next set of experiments spectrometric measurements were performed in order to determine the effect of GOx concentration on the PANI formation.

Experiment was performed at 0.50 mol L^{-1} of aniline and GOx concentration varying from 0.125 to 0.75 mg mL^{-1}. The influence of GOx concentration on the registered absorbance is presented in Fig. 14B. The registered absorbance significantly increased by increasing GOx concentration in the polymerization solution up to 0.75 mg mL^{-1}. Absorbance of PANI nanoparticles, which were prepared using 0.75 mg mL^{-1} of GOx, increased by 6.33 times if compared with the absorbance obtained by PANI nanoparticles prepared using 0.125 mg mL^{-1} of GOx. Thus, the 0.75 mg mL^{-1} of GOx was selected as optimal concentration for PANI nanoparticles formation. The similar effect of aniline and GOx concentration on PANI formation has been reported by other authors who have investigated enzymatic polymerization of aniline [140].

Polymerization time is one of the most important factors for the synthesis of polymers. Thus, the influence of polymerization time on the absorbance during enzymatic polymerization/oligomerization of aniline was evaluated. Enzymatic polymerization of PANI nanoparticles was performed from 1 to 331 h. Initially polymerization solutions were colorless and no absorption peaks were present in the visible part of UV-Vis spectra (Fig. 15A). After some time of polymerization solutions turned to yellowish color. In the early stage of aniline oxidative polymerization intermediate form of PANI was formed [69, 106, 107, 140, 295] and two absorbance peaks at λ = 325 nm and λ = 434 nm were registered. Sapurina and Stejskal proposed that at initial stage of aniline polymerization the most probable structure is cyclic aniline dimer (5,10-dihydrophenazine) with the absorbance at 380 nm [106]. During the oxidation of 5,10-dihydrophenazine phenazylium radical cation was formed, which absorbs at λ = 420 nm [106]. The increase of absorbance peak at 434 nm after longer period of synthesis is characteristic for PANI nanoparticles formation. It means that the starting units of the chain of PANI nanoparticles were formed. It was in an agreement with higher concentration of hydrogen peroxide produced during GOx catalyzed enzymatic reaction [132, 140, 296] initiated formation of multiple PANI branched structure during polaron band transition [295, 297, 298]. Another peak of the absorbance at 325 nm is due to

π→π* transition of the benzenoid ring and is attributed to formation of linear polyaniline structure [295, 298-300]. These peaks indicate that conducting form of enzymatically synthesized polyaniline is similar to obtained by chemical and electrochemical methods [298, 301] and are associated with the stabilization of the composite in the emeraldine form [299], which has got a lower oxidation potential than protonated monomer and is oxidized preferentially [106].

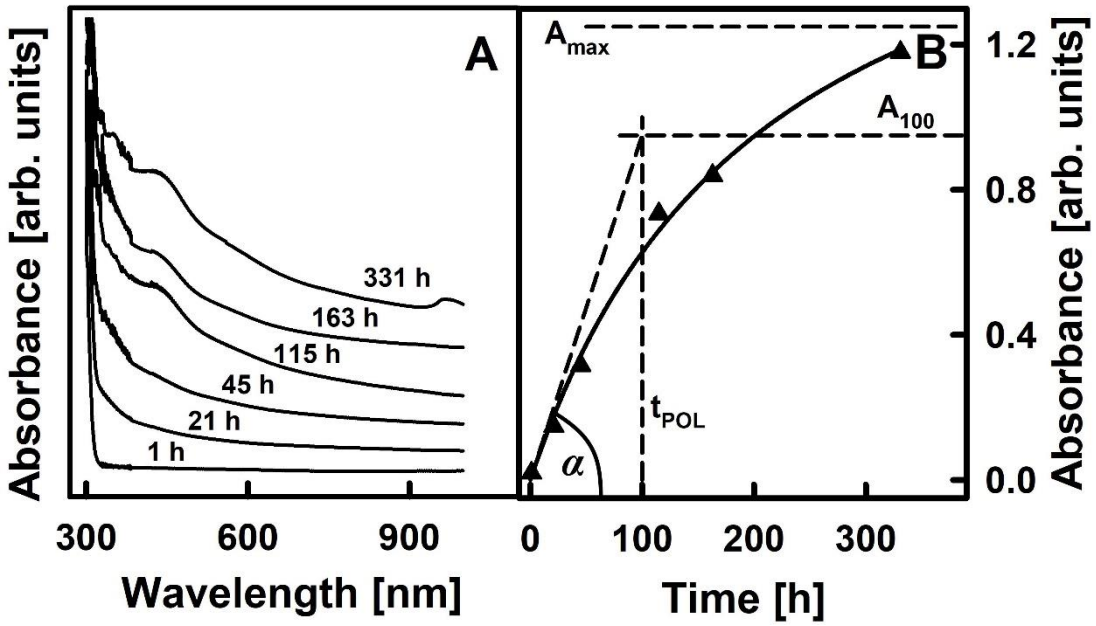

Fig. 15. Spectra of enzymatic polymerization/oligomerization of aniline (A) and the influence of polymerization time on the absorbance at 434 nm (B) in the presence of 0.05 mol L^{-1} glucose. (Polymerization solution: 0.05 mol L^{-1} SA buffer, pH 6.0, with 0.05 mol L^{-1} glucose, 0.50 mol L^{-1} aniline and 0.75 mg mL^{-1} glucose oxidase. The absorbance was measured in 0.05 mol L^{-1} SA buffer, pH 6.0.)

Figure 15B shows that the registered absorbance at 434 nm increased with the time of polymerization and was the highest after 331 h of PANI nanoparticles synthesis. Absorbance registered after 331 h of enzymatic synthesis of PANI increased by 62.4 times in comparison to the absorbance registered after 1 h. However 331 h of polymerization is inconvenient and too long, so it is recommended to perform polymerization up to 115 h. Although the absorbance after 115 h of enzymatic synthesis was 1.60 times lower in comparison with absorbance registered after 331 h of synthesis. Initial aniline conversion into polymer rate (*V*), which corresponds to *tga* in Fig. 15B can be calculated using

estimated/approximated optical absorbance (approximately 1.25 (a.u.)) of PANI nanoparticle solution formed if 100% of aniline present in initial 0.50 mol L^{-1} aniline monomer solution would be converted into PANI (Fig. 15B). Then initial aniline polymerization rate (*V*) is equal:

$$\mathbf{V = (tg\alpha) = \frac{A_{100} \times C_{ANI}}{A_{max} \times t_{Pol}} = \frac{0.95 \times 0.50}{1.25 \times 100} = 0.0038\ mol\ L^{-1}h^{-1}}$$

The size of PANI nanoparticles formed after certain period of time was evaluated using DLS method. Results presented in Fig. 16 illustrate that the size of polymeric nanoparticles increased by increasing time of the polymerization. PANI nanoparticles size was 15.8 nm after 21 h of enzymatic synthesis, while size of nanoparticles increased up to 142 nm after 163 h of the polymerization. It could be predicted that after 163 h of enzymatic polymerization the aggregates of PANI nanoparticles were formed. As it is present in fig. 16A the formation of smaller PANI nanoparticles (115 nm) allows to use shorter (115 h) polymerization time.

In order to confirm the electroactive nature of the PANI obtained by GOx catalyzed polymerization, cyclic voltammograms were recorded. Figure 17 illustrates the cyclic voltammogram of electrode modified with enzymatically synthesized PANI nanoparticles in the range between -0.20 and +1.20 V *vs* $Ag/AgCl_{(3\ mol\ L^{-1}\ KCl)}$.

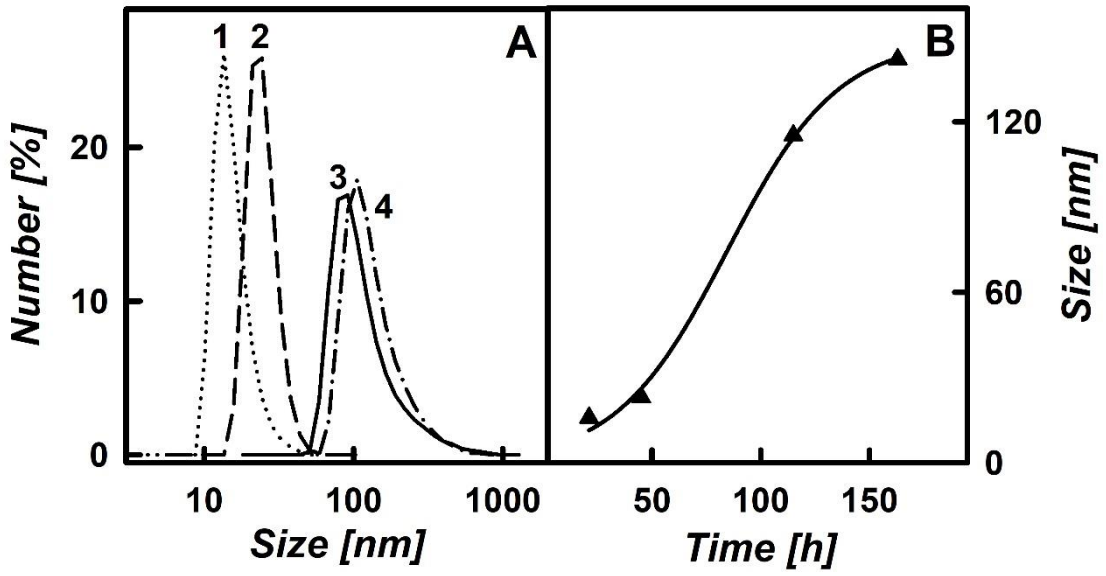

Fig. 16. The distribution of PANI nanoparticles size after certain period of enzymatic polymerization/oligomerization determined using DLS (A) and the dependence of PANI nanoparticles size on the time of synthesis (B). (Polymerization solution: 0.05 mol L^{-1} SA buffer, pH 6.0, with 0.05 mol L^{-1} glucose, 0.50 mol L^{-1} aniline and 0.75 mg mL^{-1} glucose oxidase. DLS signal was measured in 0.05 mol L^{-1} SA buffer, pH 6.0. A: 1, 2, 3 and 4 curves – 21, 45, 115 and 163 h of polymerization.)

The cyclic voltammogram of polyaniline showed two oxidation waves with peaks at +0.51 and +0.68 V, which are similar to that obtained in acidic medium in previously reported papers [73, 133, 296]. The first peak at +0.51 V is not distinctly resolved, but it is reversible. The peak is slightly shifted towards lower potential in comparison to that reported for PANI nanoparticles, which were synthesized enzymatically by glucose oxidase at pH 6.0 [296] or by horseradish peroxidase at pH 4.1 [302]. It can be related to the formation of branched or cross-linked structures of the polyaniline backbone [296]. It corresponds to the transformation of leucoemeraldine to emeraldine salt [73]. The second PANI oxidation peak, which is observed at +0.68 V, is well defined and reversible too. The observed peak could be explained as a radical cationic polaron state and a cationic bipolaron state, and it is associated with the formation of p-benzoquinone and hydroquinone as side products [73]. The

enzymatic polymerization/oligomerization of aniline is strongly depended on pH, and this pH-dependence is related to the differences of peaks in cyclic voltammograms of PANI, which was formed in aqueous solution of pH 4.0 - 4.3, reported by other authors [132, 297, 302].

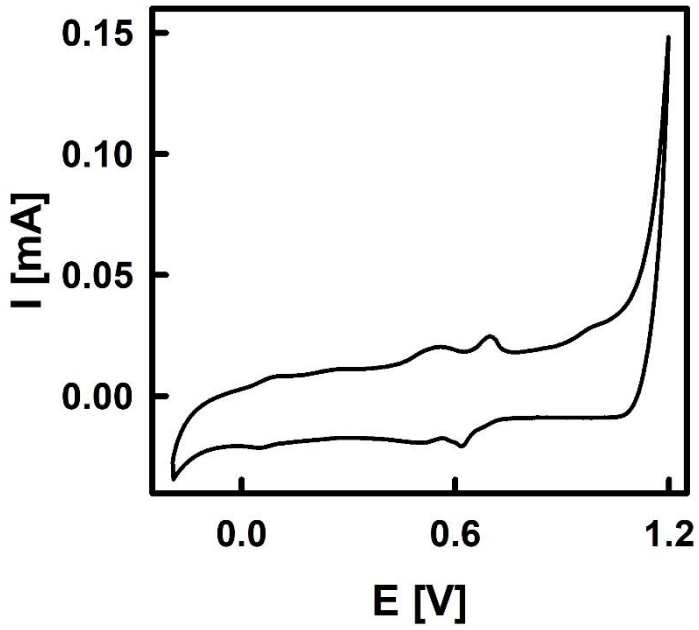

Fig. 17. The cyclic voltammogram of electrode modified with enzymatically synthesized polyaniline nanoparticles. (Cyclic voltammogram was registered in 1 mol L^{-1} HCl, v = 0.10 V s^{-1})

Recently PANI based nano and micro scale particles have attracted much attention through their broad range of applications [303]. The formation, separation and purification of PANI nanoparticles make these particles particularly suitable for the attachment of proteins and other biologically active materials. Nanocomposite structure of polyaniline with gold [303], Fe_3O_4 [304] nanoparticles could be used as an excellent matrix for electrocatalysis and enzyme immobilization in biosensors and micro-fabrications because of their novel properties [305].

Conclusions of 3.1. section

PANI nanoparticles were synthesized by enzymatic polymerization / oligomerization of aniline monomers during enzymatic reaction of glucose oxidase. The concentration of aniline, GOx and the

polymerization time showed a significant influence on PANI nanoparticle formation. It was determined that for the efficient formation of PANI nanoparticles solution containing 0.50 mol L^{-1} of aniline and 0.75 mg mL^{-1} of glucose oxidase is optimal. DLS-based measurements showed that size of PANI nanoparticles increased by increasing duration of polymerization. Optimal duration of enzymatic PANI formation was 115 h. Enzymatically synthesized polyaniline was characterized by two oxidation waves with peaks at +0.51 and +0.68 V. Formed PANI nanoparticles were pure from surfactants and interfering species what increases the applicability of synthesized polymeric nanoparticles for various biomedical applications.

3.2. Deposition of AgNPs from suspensions containing tannic acid

Silver nanoparticles, due to their well pronounced biocidal properties [306, 307], are often used for surface modification of polymers [308], fibers [309, 310], implants and surgical tools [311, 312]. Deposition of AgNPs on various surfaces, leading to the formation of monolayers and films, is often carried out in order to obtain functional materials, which are applied in catalysis [313], microelectronics [314], diagnostics [315] and spectroscopic methods [316].

In response to these wide range of practical applications, many experimental studies have been devoted to AgNPs monolayer formation at various solid substrates such as glass, quartz, silicon and ITO surfaces [317-320]. In most of these works, attention was focused on determining the morphology of the AgNPs monolayers using AFM and SEM imaging [321-324]. However, the suspensions used in these studies were often poorly defined in respect to chemical composition, the presence of contaminants and particle concentration. This prohibits a quantitative analysis of the experimental kinetic results and makes it difficult to draw valid conclusions about particle deposition mechanisms. This contamination issue may become important when AgNPs suspensions are synthesized in the presence of tannic acid. These suspensions exhibit unusually high activity against the antibiotic resistant bacteria

strains [325]. It has been shown in a recent publication [326], that tannic acid appears in the form of nanoparticles having a shape of oblate spheroids and the hydrodynamic diameter of 1.63 nm. Because of a negative charge and high diffusion coefficient, tannic acid molecules (nanoparticles) may adsorb on polycation-modified substrates, which blocks AgNPs deposition and prevents the formation of dense monolayers. This effect may profoundly decrease the antibacterial activity of silver suspensions because of tannic acid attachment to bacteria's membranes. Despite a vital significance this issue has not been studied before in the literature.

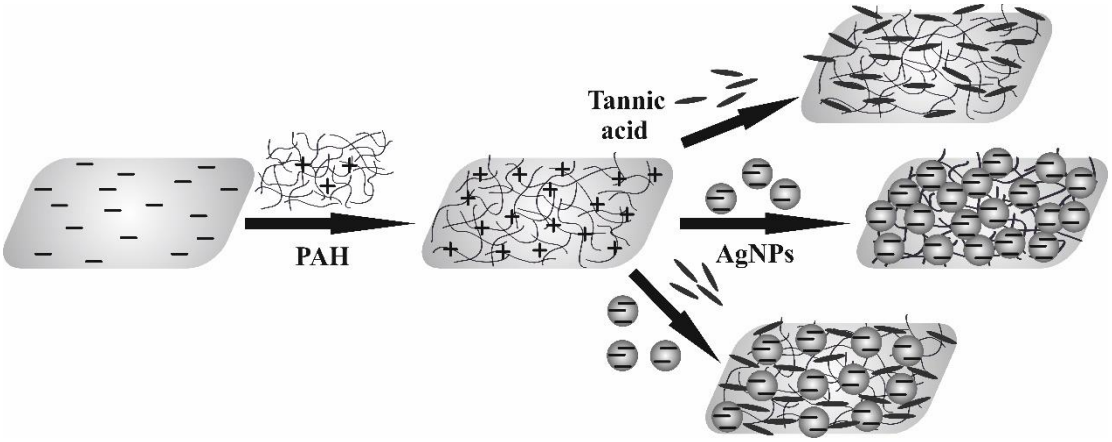

Fig. 18. Schematic representation of AgNPs and tannic acid adsorption on PAH covered mica.

Therefore, the main goal of this work was the systematical study the kinetics of AgNPs deposition in the presence of controlled amounts of tannic acid and in the absence of this reagent (Fig. 18), whose coverage can be precisely controlled by the streaming potential measurements. On the other hand, the coverage of silver particles is uniquely evaluated by a direct SEM and AFM imaging. This allows one to quantitatively determine the kinetics of particle deposition interpreted in terms of the random sequential adsorption model (RSA).

Tannic acid and AgNPs suspensions under various pHs and ionic strengths was determined that is a prerequisite for a quantitative interpretation of particle deposition experiments.

Tannic acid belongs to a group of tannic acids which are widely distributed in plants [327, 328]. The molecule consists of a hepta- to octa-galloyl-β-D-glucose in which, on average, two to three additional galloyl groups are esterified in depside form to a preexisting β-1,2,3,4,6-pentagalloyl-D-glucose core (Fig. 19) [327]. Due to the specific chemical structure, this compound is often used in the preparation of noble metal nanoparticle suspension [329, 330]. However, as shown in previous works [290, 331] at elevated temperature and under basic conditions, tannic acid is unstable and it slowly hydrolyses what results in the release of gallic acid and other organic derivatives.

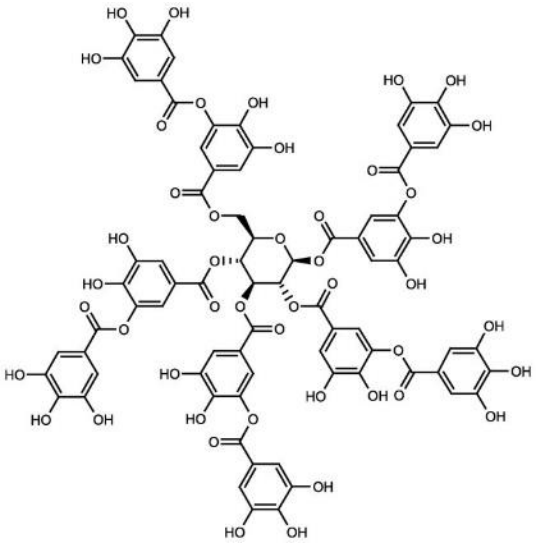

Fig. 19. Chemical structure of tannic acid.

In the previous work [290] it was shown that the hydrodynamic diameter of tannic acid remains practically constant at pH range 3.0–5.0, assuming an average value of 1.63 nm, regardless of the ionic strength. On the other hand, the electrophoretic mobility of tannic acid molecules and the zeta potential calculated from the Henry's equation, depend on both pH and ionic strength. Thus, at pH 3.5 the electrophoretic mobility varies between −0.54 and −0.42 μm cm V^{-1} s^{-1} and zeta potential from −12 to −9.2 mV for ionic strength 3.3×10^{-3} mol L^{-1} and 10^{-2} mol L^{-1}. However, at pH 5.5 the mobility and the zeta potential assume much lower values of −3.1 and −1.6 μm cm V^{-1} s^{-1} and −58 and −30 mV for ionic strength 3.3×10^{-3} mol L^{-1} and 10^{-2} mol L^{-1}, respectively.

Therefore, at pH 3.5 the average number of electrokinetic charges (calculated by using the Stokes-Lorenz equation) is close to −0.5 (see Table 2). At pH 5.5, the number of electrokinetic charges varies between −2.9 and −1.4 for ionic strength of 10^{-4} and 10^{-2} mol L^{-1}. The higher values of surface charge at pH 5.5 indicate that the dissociation degree of tannic acid increases with the increase of pH. As a consequence, more charged phenolate groups are formed in tannic acid molecules.

Table 2. Physicochemical properties of the silver nanoparticles and tannic acid.

Quantity [unit]	**Silver nanoparticles**	**Tannic acid molecules**	**Remarks**
Specific density [g cm^{-3}]	10.49*	1.61**	from Refs. *[332] *[290]
Molecular mass [Da]	----	1701	manufacturer data
Molecular volume, v_1 [nm^3]	---	1.75	from Ref. [290]
Plasmon absorption maximum [nm]	393	214 and 271	determined in this work
Particle size [nm]	15 ±3		from TEM measurements
Diffusion coefficient [cm^2 s^{-1}]	3.07×10^{-7} $\pm 0.10 \times 10^{-7}$	2.93×10^{-6} $\pm 0.06 \times 10^{-6}$	determined in this work using DLS method for T=298 K, pH 4.0, I=0.01 mol L^{-1} NaCl
Hydrodynamic diameter [nm]	16 ±8	1.63 ±0.15	determined in this work using DLS method for T=298 K, pH 3.5-5.5, I=0.01 mol L^{-1} NaCl
Geometrical cross-section area [nm^2]	206	2.40	calculated from geometry
Electrophoretic mobility μ_e [μm cm V^{-1} s^{-1}]	−2.53	−1.22 ±0.06	determined in this work, for T=298 K, pH 4.5 I=10^{-2} mol L^{-1} NaCl
Zeta potential ζ [mV]	−56	−23	determined in this work, for T=298 K, pH 4.5 I=10^{-2} mol L^{-1} NaCl
Number of elementary charge N_c	−22	−1.05	determined in this work, for T=298 K, pH 4.5 I=10^{-2} mol L^{-1} NaCl
Two-dimensional electrokinetic charge densities σ [e nm^{-2}]	−0.0316	−0.438	determined in this work, for T=298 K, pH 4.5 I=10^{-2} mol L^{-1} NaCl

These results suggest that in order to avoid an uncontrolled hydrolysis of tannic acid the deposition experiments should be carried out at pH values

below 5.0. In the next stage, the physicochemical characteristics of AgNPs and their suspensions were carried out. The weight concentration of AgNPs suspension was determined precisely according to the procedure described previously [287]. The morphology of the silver particles and their size distribution were determined using the micrographs obtained from TEM. The particles were spherical and fairly monodisperse. Therefore, the size of a single particle was defined as an average of the two maximal diameters perpendicular to each other and from the surface area of a particles using MultiScan Base software. Based on the data presented in Fig. 20. It was found that the average size of the nanoparticles was 15 ±3 nm (see Table 2).

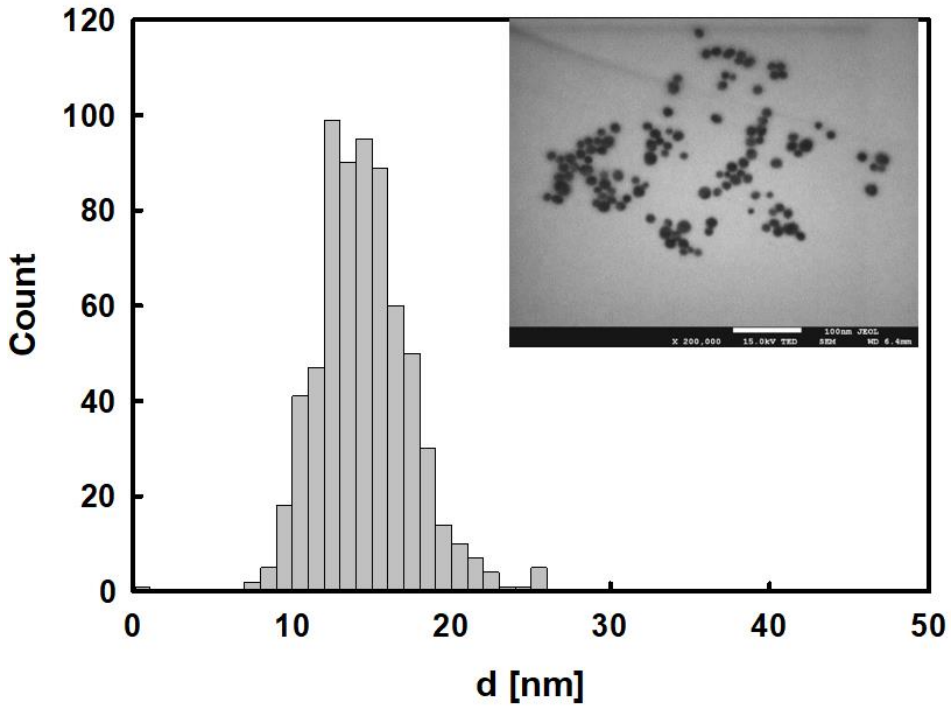

Fig. 20. The histogram of the size distribution of the silver nanoparticles determined from TEM micrographs.

Additionally, the DLS was used to determine the hydrodynamic diameter of the AgNPs at various pH. Firstly, the diffusion coefficients were measured by DLS and the hydrodynamic diameters were calculated using the Stokes–Einstein relationship (Eq. 2) [287]. The results obtained at ionic strength 10^{-2} mol L^{-1} NaCl and the pH range 3.0–9.5 are presented in Fig. 21. As can be noticed, at the pH range 4.0–8.0, the hydrodynamic diameter remains practically constant

and equals to 15 nm. A significant increase in the nanoparticle size is observed only at pH below 4.0, what indicates some instability of the AgNPs suspension.

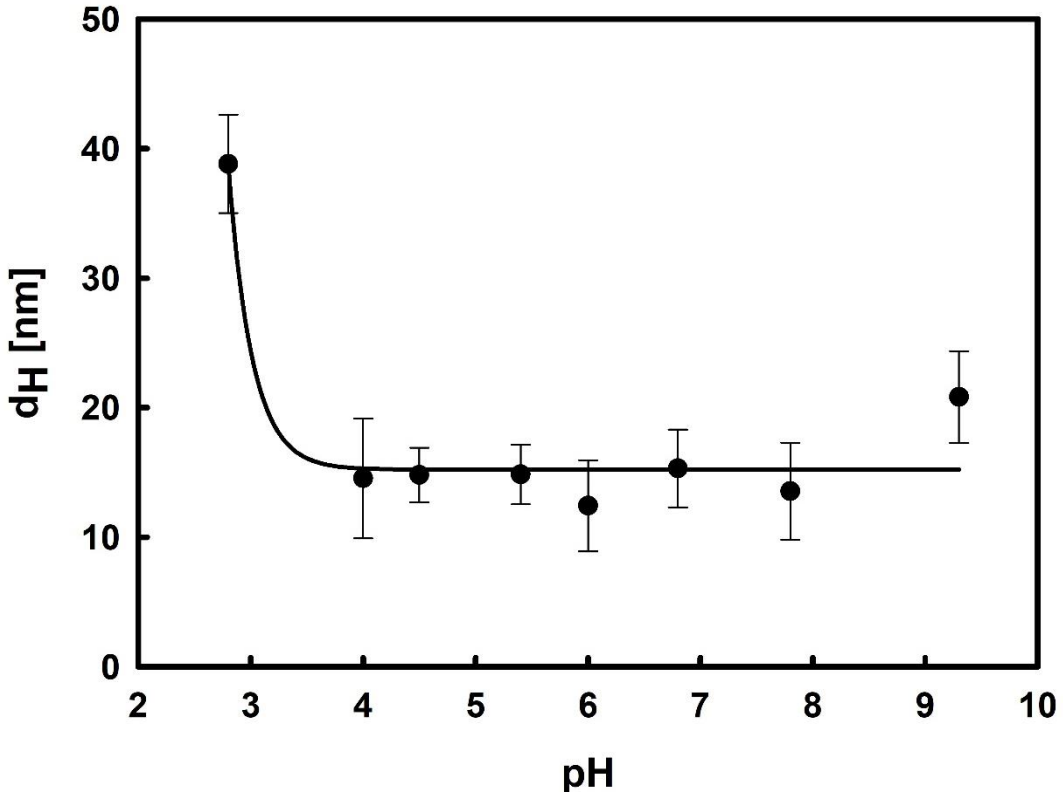

Fig. 21. The dependence of the hydrodynamic diameter of silver nanoparticles on pH. Experimental conditions: the concentration of the silver suspensions 50 mg L^{-1}, I = 10^{-2} mol L^{-1} NaCl, and T = of 298 K. The solid line represents nonlinear fit of experimental data.

Moreover, the measurements of electrophoretic mobility (μ_e) of the AgNPs at controlled pH conditions were carried out at constant value of ionic strength. When the electrophoretic mobility of the AgNPs was determined, the zeta potential of nanoparticles was calculated using the Henry's equation analogously as it was done for tannic acid nanoparticles [290]. As can be observed in Fig. 22, the zeta potential of the AgNPs remains negative for the entire range of pH indicating that the particles acquired a net negative electrokinetic charge. Moreover, with the increase of pH, the zeta potential attains more negative values and equals −49 mV at pH 3.5 and −61 mV at pH 9.0.

For the sake of convenience, the physicochemical parameters pertinent to tannic acid and the silver particle suspensions are collected in Table 2. It can be

deduced from the above presented experimental results that both tannic acid and silver nanoparticle suspensions are stable at pH range 3.5–5.0.

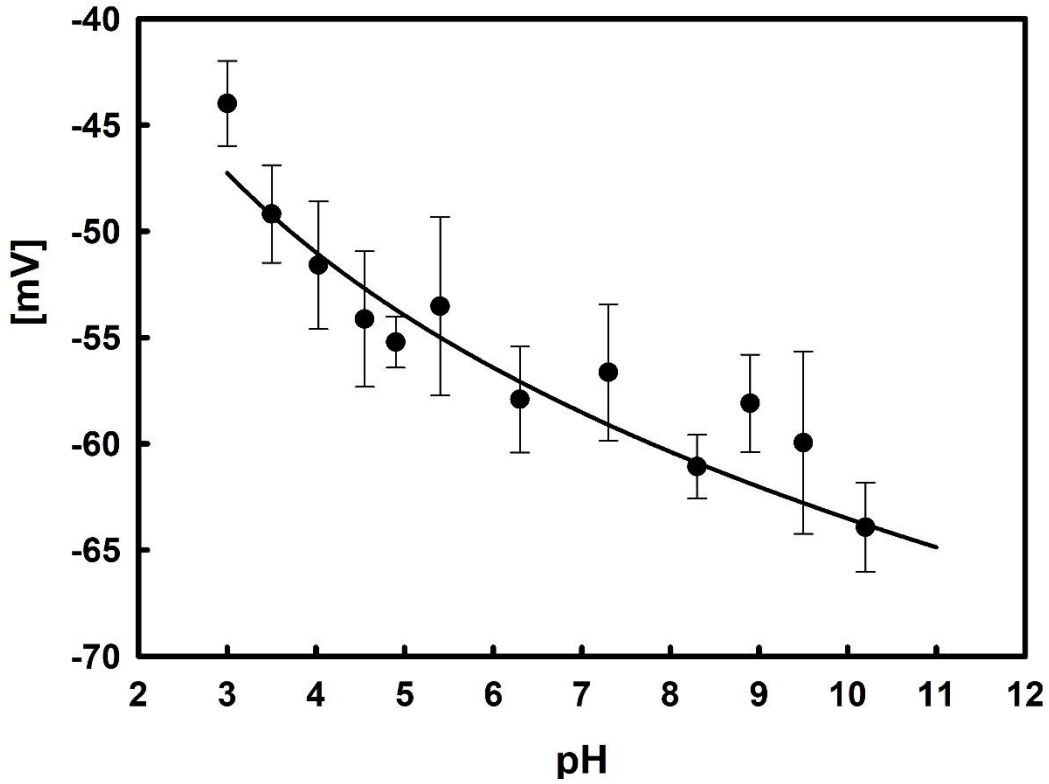

Fig. 22. The dependence of the zeta potential of the silver nanoparticles on pH at ionic strength of 10^{-2} mol L^{-1} NaCl. Measurement conditions: the concentration of the silver suspensions was 50 mg L^{-1}, T = 298 K. The solid line represents nonlinear fit of experimental data.

Additionally, the series of UV-Vis spectroscopy experiments were performed in order to evaluate the stability of the tannic acid and silver nanoparticle mixtures. The spectra obtained for native suspensions and the mixture consisting 15 mg L^{-1} of silver particles and 25 mg L^{-1} tannic acid are presented in Fig. 23. It can be seen that the characteristic absorption maximum of the pure silver suspension appears at 393 nm. In the case of tannic acid, the absorption spectrum exhibits two peaks at 214 and 271 nm that are in agreement with previously reported results [333, 334].

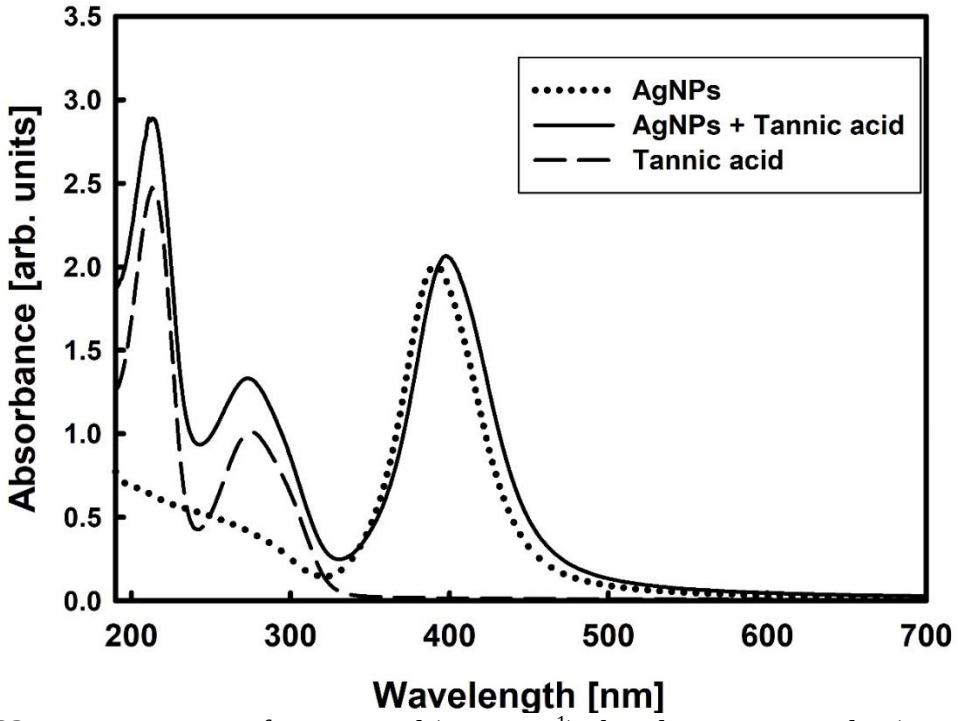

Fig. 23. UV-Vis spectra of: tannic acid (25 mg L^{-1}), the silver nanoparticles (15 mg L^{-1}) and the mixtures of silver nanoparticles and tannic acid with the same concentrations recordered at ionic strength of 10^{-2} mol L^{-1} NaCl and pH 4.5.

The position of the peaks remains practically unchanged in the case of the mixtures and their absorbance is additive. This indicates that tannic acid did not induce the aggregation of the silver particles. In order to confirm this conclusion, the spectra of the tannic acid/silver particle mixtures having various composition were recorded as a function of time. It was revealed in these experiments that the mixtures remain stable over the time period of 24 h at pH range 3.5–5.0.

3.2.2. Adsorption of tannic acid and AgNPs on PAH monolayers

Adsorption of tannic acid molecules on PAH monolayers was studied using the streaming potential measurments according to the procedure described by Ocwieja *et al.* [290]. It consisted of the following steps. Firstly, the zeta potential of bare mica was determined in pure electrolyte of the concentration 10^{-2} mol L^{-1}. Afterwards, PAH monolayer was adsorbed in situ in the streaming potential cell from the PAH suspension of the bulk concentration of 10 mg L^{-1} at the same ionic strength over the time of 15 min. After a complete formation

of the PAH monolayer, the cell was flushed with the pure electrolyte solution and the streaming potential of the PAH monolayers was measured. The zeta potential of the monolayer was calculated from the Smoluchowski's equation as previously described [335]. It varied between 49 mV at pH 4.0 and 58 mV at pH 5.0. In the next step, tannic acid molecules were adsorbed over the time of 15 min on the PAH monolayer under diffusion-controlled conditions from the solutions in which the bulk concentration of PAH varied between 1 and 250 mg L^{-1}. After the formation of tannic acid/PAH bilayers, the cell was flushed with pure electrolyte and the streaming potential was measured again. In this way the dependence of the zeta potential of the bilayer (ζ) on the tannic acid bulk concentration (c_{bt}) was determined. Additionally, in order to increase the precision of these measurements, the PAH/tannic acid bilayers on mica were externally adsorbed in a diffusion cell over a controlled period of time. Afterwards, the wet mica sheets bearing the bilayers were assembled into the electrokinetic cell and the streaming potential was measured.

The primary data obtained in these experiments are shown in Fig. 24 as the dependence of the zeta potential of the PAH/tannic acid bilayer on the bulk concentration, which varied between 0 and 250 mg L^{-1}. As one can observe, the adsorption of tannic acid causes an abrupt decrease in the zeta potential of the PAH-covered mica that leads to the inversion of its sign for the bulk tannic acid concentration of 30 mg L^{-1}. Interestingly, the zeta potential assumes negative values for higher bulk concentration range and finally attains the limiting value of -23 mV, which is close to the tannic acid bulk zeta potential at pH 4.5. This behavior indicates that negatively charged tannic acid molecules continue to adsorb at surfaces bearing negative mean-field zeta potential. Analogous phenomenon was previously observed in the case of silver particle adsorption on PAH-covered mica [289] and protein adsorption on mica [336, 337]. This anomalous adsorption, indicating the limitation of the mean-field theory in the nanoscale, was explained in terms of heterogeneous charge distribution within the particle monolayers.

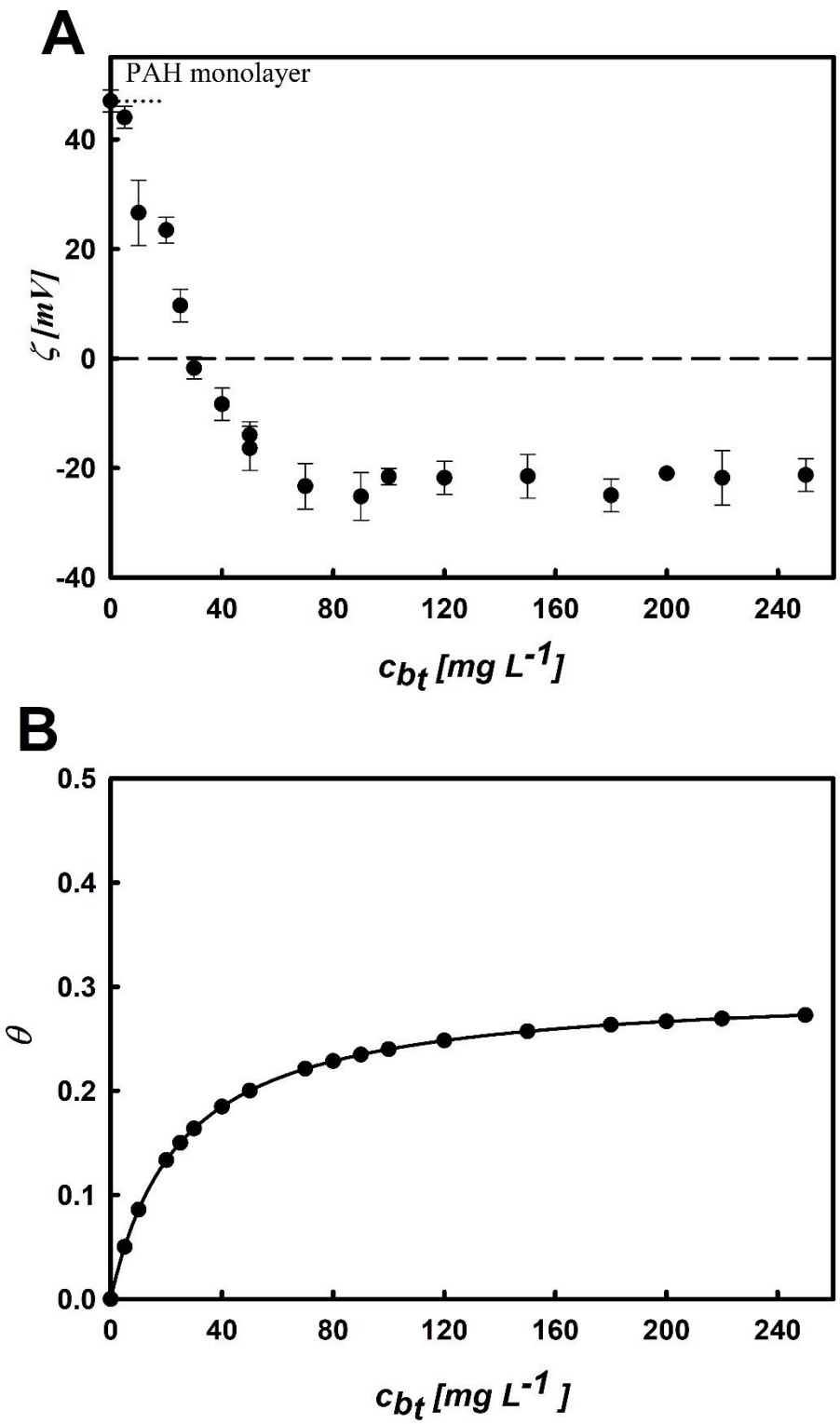

Fig. 24. (A) The dependence of the zeta potential of PAH monolayer on the bulk concentration of tannic acid. The adsorption conditions: I = 10^{-2} mol L^{-1} NaCl, pH 4.0-5.0, T = 298 K, the monolayer formation time 15 min. **(B)** The tannic acid adsorption isotherm on the PAH monolayer determined from Eq. (7) (I = 10^{-2} mol L^{-1} NaCl, pH 4.0-5.0, T = 298 K). The solid line denotes the theoretical results calculated from the Langmuir model, i.e, $\theta = \theta_{mx}\frac{K_a c_{b_t}}{1+K_a c_{b_t}}$, where θ_{mx} = 0.30 and K_a = 0.04 L mg^{-1}.

It is useful for the interpretation of tannic acid/silver nanoparticle mixture deposition kinetics to convert the zeta potential *vs* the bulk concentration dependence, shown in Fig. 24A, into the coverage *vs* the bulk concentration dependence that corresponds to an adsorption isotherm. Given the oblate spheroid shape of the tannic acid molecule-resembling a disk, and its small size that facilitates the penetration into the polyelectrolyte monolayer, one can expect that the Gouy-Chapmann (GC) patchy adsorption model can be adequate. It was previously shown that this model works well in the case of protein adsorption at polymeric carrier particle in the limit of lower ionic strength [338, 339]. Accordingly, because the charge additivity is assumed in the GC model, one can express the net charge of the PAH/tannic acid bilayer by the simple relationship:

$$\sigma = \sigma_0 + NN_c e = \sigma_0 + \theta\sigma_t \qquad (\mathbf{4})$$

where N is the surface concentration of tannic acid molecules, e is the elementary charge, $\theta = N S_g$ is the coverage of tannic acid, S_g is the geometrical cross-section area of tannic acid, σ_t is the electrokinetic charge density of tannic acid and σ_0 is the electrokinetic charge density of the PAH monolayer on mica calculated from the dependence valid for 1:1 electrolyte:

$$\sigma_0 = 2\left(2\varepsilon kTn\right)^{\frac{1}{2}} \sinh\left(\frac{e\zeta_i}{2kT}\right) \qquad (\mathbf{5})$$

where ε is the permittivity of water, k is the Boltzmann constant, T is the absolute temperature, ζ is the zeta potential of the PAH monolayer and $n = 6.023\text{x}10^{20}\, I$ (where I is the number concentration of cations in the bulk).

Considering that the net charge is connected with the tannic acid/PAH bilayer zeta potential through the relationship:

$$\sigma = \sigma_0 + \theta\sigma_t = 2\left(2\varepsilon kTn\right)^{\frac{1}{2}} \sinh\left(\frac{e\zeta}{2kT}\right) \qquad (\mathbf{6})$$

One can calculate the tannic acid coverage from the dependence:

$$\theta = -\frac{\sigma_0}{\sigma_t}\left[1-\frac{\sinh\left(\frac{e\zeta}{2kT}\right)}{\sinh\left(\frac{e\zeta_i}{2kT}\right)}\right] \quad (7)$$

It should be noted that no adjustable parameters are used in Eq. (7).

The tannic acid coverage *vs* the bulk concentration relationship calculated from Eq. (7) is shown in Fig. 24B. As can be noticed, the tannic acid coverage increases proportionally to the bulk concentration assuming the value of 0.05 for c_{b_t} = 5 mg L^{-1} and 0.09 for c_{b_t} = 10 mg L^{-1}. The charge inversion occurs at tannic acid coverage of 0.18 and that limiting coverage approached in to the limit of the high tannic acid concentration of 250 mg L^{-1} is 0.26. It is also interesting to note that the experimental data can be adequately reflected by the Langmuir model:

$$\theta = \theta_{mx}\frac{K_a c_{b_t}}{1+K_a c_{b_t}} \quad (8)$$

where θ_{mx} = 0.30 and K_a = 0.04 L mg^{-1}.

Knowing the maximum coverage of tannic acid as a function of its bulk concentration one can theoretically predict the characteristic time of the monolayer formation. Under the diffusion-controlled transport conditions, the adsorption time can be calculated from the dependence [287]:

$$t_{ch} = \frac{\pi}{4}\frac{\theta^2}{Dn_b^2 S_g^2} \quad (9)$$

where $n_{b_t} = 10^{-6} c_{b_t} A_v / M_w$ is the number concentration of tannic acid and A_v is the Avogadro's constant number.

For c_{b_t} = 10 mg L^{-1} using the diffusion coefficient of 2.93 × 10^{-6} cm^{-2} s^{-1} (Table 2), one can calculate from Eq. (9) that t_{ch} = 0.24 s. Analogously, for c_{b_t} = 250 mg L^{-1} one obtains t_{ch} = 0.004 s. As can be noticed, these monolayer

formation times are considerably shorter than the adsorption time of 900 s (15 min) used in experiments that ensures a full equilibration of tannic acid monolayers. Also, because of such short transition time, the adsorption of tannic acid proceeds much faster than the deposition of silver nanoparticles that is expected to significantly affect the kinetics of this process.

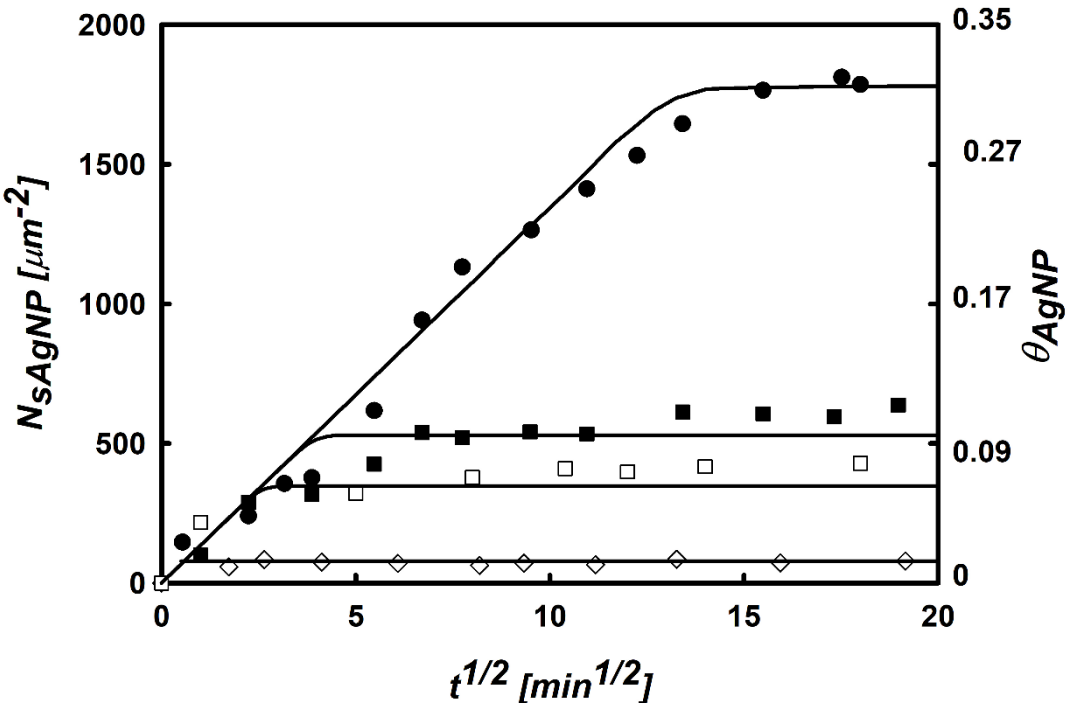

Fig. 25. Kinetics of silver nanoparticles deposition on mica modified by the PAH monolayers determined for various tannic acid concentration: (●) 0 mg L^{-1}, (■) 5 mg L^{-1}, (□) 10 mg L^{-1} and (◊) 250 mg L^{-1}. The other experimental conditions: the concentration of silver nanoparticles is 50 mg L^{-1}, I = 10^{-2} mol L^{-1} NaCl, pH 4.0-5.0 and T = 298 K. The solid lines denotes the theoretical results calculated from the random sequential model (RSA).

In order to examine this competitive adsorption, the experiments were performed in which the silver/tannic acid mixtures of increasing tannic acid concentration were studied. The silver particles coverage was quantitatively determined according to the above described AFM and SEM monolayer imaging. Typical results obtained for the tannic acid concentration of 5, 10 and 250 mg L^{-1} are plotted in Fig. 25. For comparison, the reference results obtained for the pure silver particle suspension having the concentration of 50 mg L^{-1} are also presented in Fig. 25 (filled dots). As can be observed, for the pure silver particle suspension the time of monolayer formation is about 200 min, exceeding

by orders of magnitude the above estimated time of tannic acid monolayer formation. The maximum coverage of the particle attained for such a long time is 0.28. The addition of tannic acid at the level of 5 mg L^{-1} that corresponds to a 3×10^{-6} mol L^{-1} solution drastically reduces the maximum coverage of the silver particles that in this case is 0.09.

It can be seen in Fig. 25 that this trend is continued with increasing tannic acid concentration. As a result, for tannic acid concentration above 10 mg L^{-1} the silver particle deposition becomes negligible. For the sake of convenience, the maximum coverage of silver particles determined for various tannic acid bulk concentration in the mixture is collected in Table 3.

Also, it is worth mentioning, that the experimental data shown in Fig. 25 are adequately reflected by theoretical results derived from numerical solution of the governing mass transfer equation (the solid lines in Fig. 25). The surface blocking function used as the boundary condition for this equation is calculated using the random sequential adsorption model. The details of this theoretical approach and the modelling procedure are discussed in Refs. [11, 326, 340].

Table 3. The maximum coverage of the silver particle monolayer *vs* the bulk concentration of tannic acid in the mixture ($I = 10^{-2}$ mol L^{-1} NaCl, pH 4.0-5.0 and T = 298 K).

Concentration of tannic acid *vs* concentration of silver nanoparticles [mg L^{-1}: mg L^{-1}]	N_s [μm^{-2}]	θ_{AgNPs}
0:50	1598	0.282
5:50	548	0.096
10:50	356	0.063
25:50	187	0.033
50:50	190	0.034
100:50	149	0.026
250:50	140	0.025
500:50	135	0.024

Hence, these results unequivocally show that the presence of low molecular weight component at low bulk concentration range can significantly reduce the attachment efficiency of silver particle to polymer-modified surfaces. This effect is illustrated in Fig. 26 where the dependence of the maximum

coverage of the silver particles, which has attained in the long time, is plotted against the bulk concentration of tannic acid and the coverage calculated from the adsorption isotherm. It should be mentioned that the experimental data qualitatively agree with theoretical predictions presented in Ref. [341].

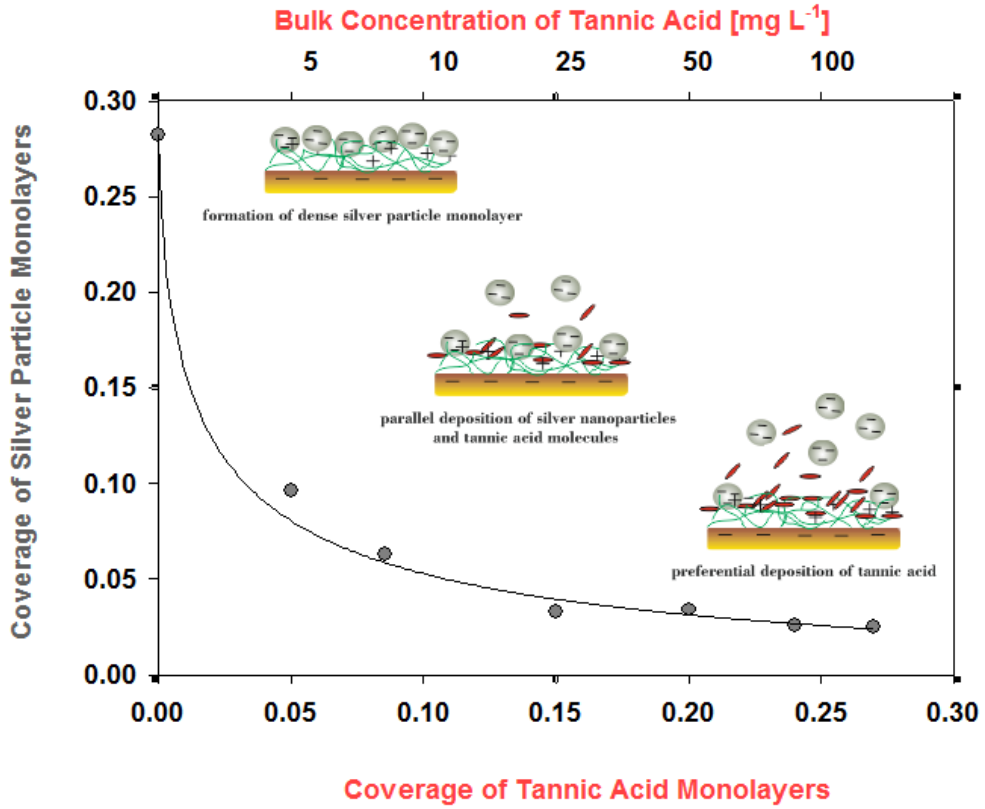

Fig. 26. The dependence of the maximum coverage of silver particles on the bulk concentration of tannic acid (upper horizontal axis) and the equilibrium surface coverage of tannic acid derived from the adsorption isotherm (lower horizontal axis). ($I = 10^{-2}$ mol L^{-1} NaCl, pH 4.0-5.0 and T = 298 K). The solid line shows a non-linear fit of experimental data.

These results were obtained using the Monte-Carlo RSA modelling for particle deposition on surfaces pre-covered with spherical particles of smaller size. The maximum coverage of larger particles was calculated as the function of smaller particle coverage for various size ratios denoted by λ. For $\lambda = 10$, which corresponds to the silver particle/tannic acid hydrodynamic ratio, was also analyzed. In this case, an abrupt decrease in the larger particle coverage is theoretically predicted. Accordingly, the maximal coverage is expected to vanish for the smaller particle coverage larger than 0.1. This agrees with the experimental data shown in Fig. 26, although the decrease in the silver particle

coverage with the tannic acid coverage is more abrupt than theoretically predicted. The deviation is probably due to the electrostatic repulsion between tannic acid and deposition silver particles that increases the surface blocking effects. In the theoretical modelling, performed in Ref. [341], the electrostatic interactions were neglected.

Conclusions of 3.2. section

The adsorption isotherm of tannic acid on PAH-covered mica can be conveniently determined using the streaming potential measurements. Using this isotherm one can quantitatively analyze the kinetics of silver particle deposition from mixtures containing a controlled amount of tannic acid that was determined using the SEM method.

These kinetic results showed unequivocally that the presence of tannic acid at low bulk concentration in the range of 10^{-6} to 10^{-5} mol L^{-1} significantly reduces the attachment efficiency of silver particle to the polymer modified surfaces. This effect was theoretically interpreted using the random sequential adsorption model. The experimental results confirmed also that by quantitative determination of the kinetics of the silver particle deposition in the model system of mica/PAH monolayer, one can precisely estimate the suspension purity and its ability to form dense monolayers on solid substrates.

3.3. Investigation of biocatalytic enlargement of AuNPs seeds

In our study 13 nm AuNPs were synthesized and were used as seeds for the biocatalytic enlargement of nanoparticles. GOx in the presence of oxygen catalyzed oxidation of glucose to gluconolactone and H_2O_2, followed by the reduction of $AuCl_4^-$ on the surface of AuNPs seeds by the H_2O_2.

This reduction is attractive due to the location of catalytic centers on the surface of AuNPs and the dependence of AuNPs size on the concentration of glucose in the growing solution. Biocatalytically enlarged AuNPs can be monitored in the solution and on the surface after AuNPs seeds immobilization using different optical methods and surface scanning probe microscopy.

3.3.1. Biocatalytic enlargement of AuNPs seeds in the solution

Firstly, the optimal ratio of AuNPs seeds and components required for the growing of nanoparticles could be determined in order to successfully perform the biocatalytic enlargement of AuNPs seeds. Six ratios of colloidal AuNPs seeds and growing solution (1:1, 2:3, 1:2, 1:3, 1:6 and 1:14) keeping the same final concentration of GOx (25 μg mL^{-1}) and $HAuCl_4$ (0.976 mmol L^{-1}) with 4×10^{-2} mol L^{-1} of glucose were analyzed spectrophotometrically immediately after mixing and after 60 and 90 min. Initial λ_{max} value of 13 nm AuNPs was 520 nm, while after mixing with growing solution it shifted to 533 nm. UV-Vis absorption spectra, which were registered after 60 min of AuNPs seeds incubation in growing solution, showed that the λ_{max} value was shifted to 554 nm. The increase of plasmon absorbance and a shift to longer wavelengths are occurring due to enlargement of AuNPs seeds. Our investigations showed that the maximal shift of plasmon absorbance during the time was achieved using colloidal AuNPs seeds and growing solutions mixed at ratio equal to 1:2 (Table 4). At this ratio the most AuNPs seeds were applied for the biocatalytic enlargement and it resulted in the higher difference of plasmon absorbance after 60 and 90 min of synthesis. The same ratio was used in all further experiments. The importance of Au^{3+}/Au^0 (seeds) ratio was shown during the enlargement of AuNPs seeds (10 nm) by γ-irradiation [233].

Table 4. The values of absorbance maximum of AuNPs in growing solution after selected periods of incubation at 20 °C.

	0 min, $A_{533\ nm}$	**60 min, A_{max}**	**90 min, A_{max}**	**$\Delta A_{60\ min}$**	**$\Delta A_{90\ min}$**
1:1	0.625	1.190	1.336	0.565	0.711
2:3	0.508	1.127	1.299	0.619	0.791
1:2	0.437	1.099	1.304	**0.662**	**0.867**
1:3	0.390	1.021	1.179	0.631	0.789
1:6	0.186	0.591	0.839	0.405	0.653
1:14	0.125	0.527	0.877	0.402	0.752

Biocatalytic enlargement of AuNPs seeds in the growing solution was followed spectrophotometrically while changing glucose concentration from 0 to 2.0 mol L^{-1}. As it is visible from the UV–Vis spectra registered after 60 min. (Fig. 27A), increasing glucose concentration increases the amount of reducing agent produced during enzymatic reaction, which leads to the faster enlargement of AuNPs seeds. Fig. 27B shows the calibration curves, which provide the hyperbolic dependence of plasmon absorbance on the glucose concentration in the evaluated concentration interval after 60 and 90 min of synthesis.

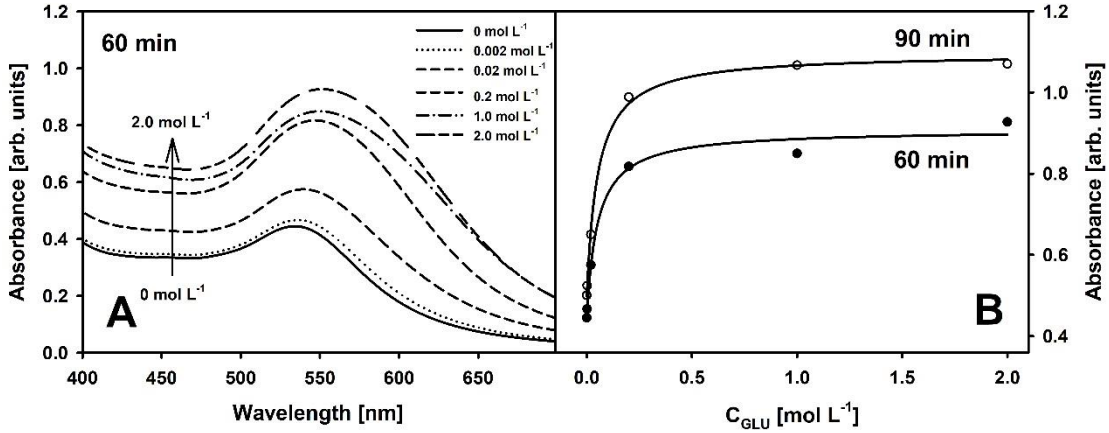

Fig. 27. UV-Vis spectra (**A**) and dependences of plasmon absorbance (**B**) on the concentration of glucose in the mixture of AuNPs seeds and growing solution (1:2). **A** – UV-Vis spectra after 60 min of biocatalytic growth of AuNPs seeds. **B** – plasmon absorbance depending on concentration of glucose in the growing solution after the selected period of incubation.

However, the linear dependence was observed using glucose concentration lower than 0.02 mol L^{-1}. Obtained calibration curves revealed that the increase of glucose concentration from 0.2 to 2.0 mol L^{-1} has not significant effect on the intensity of plasmon absorbance of AuNPs seeds, which were incubated for tested intervals of time. Thus, for the further investigations three glucose concentrations were selected: 4×10^{-4} mol L^{-1}, 4×10^{-3} mol L^{-1} and 4×10^{-2} mol L^{-1}, and the growth of AuNPs seeds was performed for 60 and 90 min at 20 ˚C. The correlation between enlarged AuNPs solution plasmon absorbance and glucose was observed by other authors after 10 min in the growing solution additionally containing cetyltrimethylammonium chloride as surfactant at 30 ˚C [342]. Besides, other enzymes, such as different oxidases,

hydrolases, hydrolytic proteins, or NAD(P)H dependent enzymes can be used as biocatalyst for the enlargement of AuNPs and for the development of optical and electrochemical sensors dedicated for the determination of corresponding substrates [343]. Additionally it was shown that upon the inhibition of enzymes the growth of AuNPs seeds was terminated [344].

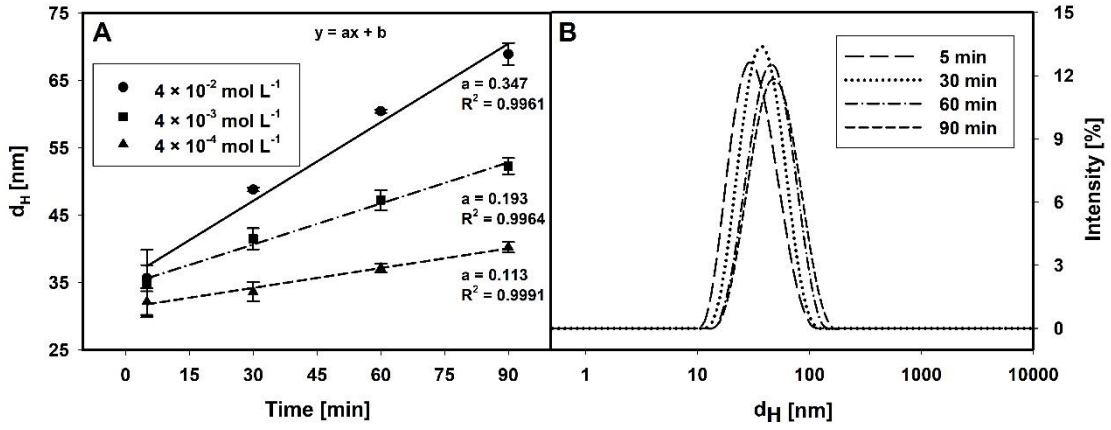

Fig. 28. (**A**) Dependence of enlarged AuNPs hydrodynamic diameter on the duration of AuNPs seeds biocatalytic enlargement at different concentrations of glucose. (**B**) The distribution of enlarged AuNPs hydrodynamic diameter after different durations of enlargement in solution containing 4×10^{-3} mol L^{-1} of glucose.

In order to determine the size of enlarged AuNPs after biocatalytic enlargement, DLS and AFM measurements were performed. DLS is a powerful technique for the determination of hydrodynamic diameter of particles. This method successfully was applied for the evaluation of kinetics of AuNPs synthesis and growth at different temperatures [345]. Using a mixture of colloidal AuNPs seeds and growing solutions at ratio of 1:2 (keeping the same final concentration of GOx and $HAuCl_4$ as for UV–Vis spectra registration) and changing concentration of glucose, changes of AuNPs size were determined by DLS. The obtained results showed that hydrodynamic diameter of enlarged AuNPs depended on the glucose concentration in the solution and on the duration of synthesis (Fig. 28). Enlarged AuNPs of 37.2 nm hydrodynamic diameter were obtained after 60 min of biocatalytic enlargement using the smallest concentration of glucose (4×10^{-4} mol L^{-1}), while 47.2 nm and 60.4 nm AuNPs were obtained using 4×10^{-3} mol L^{-1} and 4×10^{-2} mol L^{-1} of glucose, respectively. After 90 min lasting enlargement of AuNPs seeds, they became of

40.3 nm, 52.3 nm and 68.9 nm in diameter, respectively. The distribution of enlarged AuNPs hydrodynamic diameter after different durations of enlargement in solution containing 4×10^{-3} mol L^{-1} of glucose is presented in Fig. 28B. It is obvious that during enzymatic enlargement the size of enlarged AuNPs depends on the concentration of glucose in the solution and on the duration of the enlargement. Using glucose concentration in the range from 4×10^{-4} mol L^{-1} to 4×10^{-2} mol L^{-1} hydrodynamic diameter of enlarged AuNPs linearly depends on the duration of biocatalytic processes. Additionally, from the slope of lines presented in Fig. 28A it is visible, that process of AuNPs seeds enlargement was the most rapid using the highest concentration of glucose (4×10^{-2} mol L^{-1}). However, it should be mentioned that after 5 min lasting enlargement of AuNPs seeds in solutions containing GOx, $HAuCl_4$ and glucose, relatively large nanoparticles were detected. If 4×10^{-4} mol L^{-1} concentration of glucose was used enlarged AuNPs of 29–34 nm diameter were formed. It might be due to adsorption of GOx on the surface of gold nanoparticles at the initial step of AuNPs seeds enlargement followed by relatively fast increase of particles size at the initial step of this process.

3.3.2. Modification of Au SD surface by self-assembled monolayer

A bare Au SD surface after cleaning was modified with 1,6-HDT in order to prepare the surface suitable for the immobilization of AuNPs seeds. Due to chemisorption of thiol functional group present at one end of 1,6-HDT the planar gold surface was modified with self-assembled monolayer containing free thiol functional groups directed outward from the planar gold surface. These functional groups were used for AuNPs seeds immobilization on the Au sensor disc and for their further biocatalytic enlargement.

The surface of Au SD before and after each step of modification was analyzed by AFM (Fig. 29). Obtained data showed that after 24 h of Au SD incubation in the 1,6-HDT solution the SAM (Fig. 29 2A-C) was formed and this SAM increased the size of planar gold structures on sensor disk and slightly

reduced the surface roughness (Fig. 29 1A-C). After the incubation of modified sensor disc in the solution of 13 nm AuNPs seeds for 20 min and washing, the structures of 10-14 nm were observed on the surface (Fig. 29 3A-C).

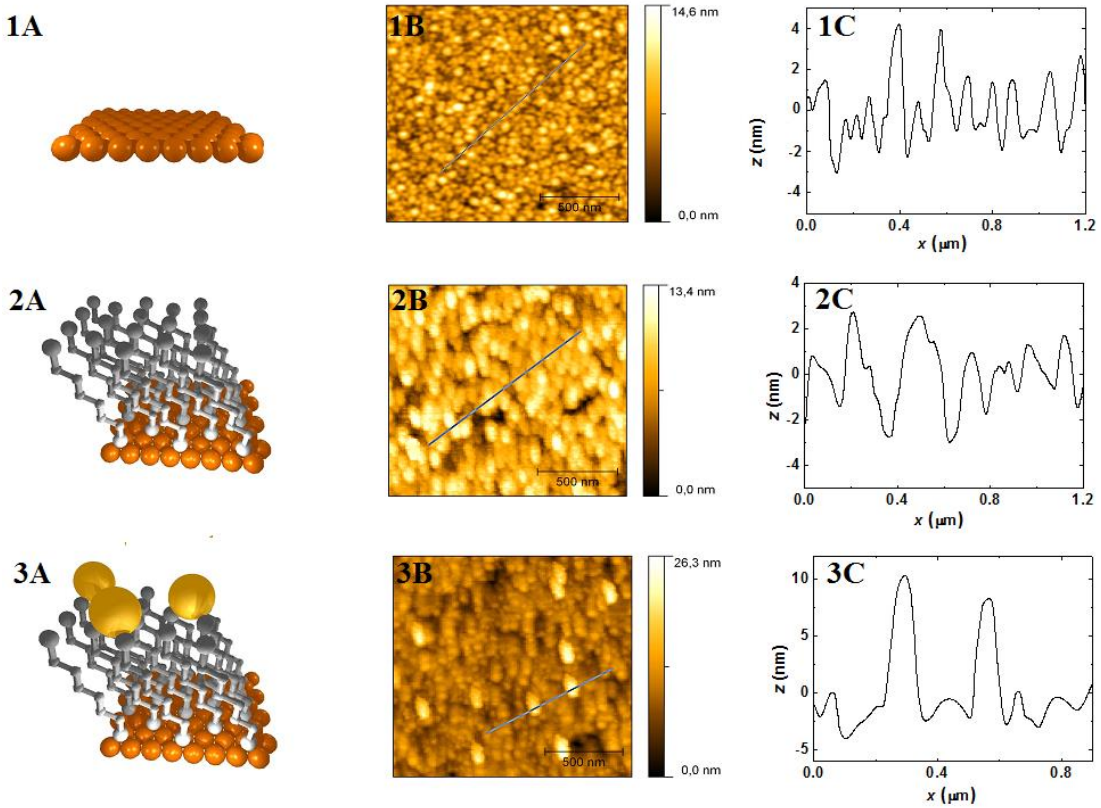

Fig. 29. The most important steps of sensor disc modification (**A**), 2D AFM images of modified surfaces (**B**) and the cross-section of substrate topography marked AFM image (**C**). 1 A-C – a planar gold layer of Au SD; 2 A-C – 1,6-HDT modified Au SD surface; 3 A-C – 1,6-HDT and AuNPs modified Au SD surface.

The strong interaction between sulphur and gold atoms led to the successful surface modification with AuNPs seeds, which were regularly distributed on the surface. Summarizing the obtained results it could be concluded, that AuNPs seeds were successfully immobilized on the 1,6-HDT self-assembled monolayer modified sensor disc. In the same way surfaces modified by AuNPs seeds were used for the further study in order to observe the biocatalytic enlargement of AuNPs seeds, which were immobilized on the sensor disc surface.

3.3.3. Biocatalytic enlargement of AuNPs seeds immobilized on the surface modified with self-assembled monolayer

In order to confirm the biocatalytic enlargement of AuNPs seeds determined using optical methods, AFM-based evaluation was performed. All tested samples were prepared identically as it was presented in previous section using the same 1,6-hexanedithiol self-assembled monolayer and the same initial concentrations of AuNPs seeds. The biocatalytical enlargement of AuNPs seeds immobilized on the surface was performed using three different concentrations of glucose (4×10^{-4} mol L^{-1}, 4×10^{-3} mol L^{-1} and 4×10^{-2} mol L^{-1}) for the determined period of time (60 or 90 min). As it is presented in Fig. 11B, the enlargement of immobilized AuNPs seeds in the solution with $HAuCl_4$ was based on the GOx catalysed enzymatic reaction, which occurred in the presence of dissolved oxygen and added known concentration of glucose. The concentration of produced H_2O_2 is an important factor for the reduction rate of $AuCl_4^-$ ions on the surface of AuNPs seeds and, therefore, on the growth rate of AuNPs. Otherwise, the size of AuNPs after biocatalytic enlargement depends on the concentration of glucose. As it is visible from AFM images, increasing concentration of glucose increased the height of nanostructures formed on SAM and enlarged AuNPs modified sensor disc surfaces. Additionally from the AFM images obtained after 60 and 90 min lasting enlargement it is obvious that the efficiency of biocatalytic enlargement of AuNPs depends on the duration of this process at initial glucose concentrations. Thus, the biocatalytic enlargement of AuNPs seeds, which were initially immobilized on formed SAM layer, in the growing solution containing 4×10^{-2}, 4×10^{-3} or 4×10^{-4} mol L^{-1} of glucose after 60 min leads to the formation of 70−90 nm (with the highest number of 80 nm nanoparticles) (Fig. 30 1A), 50−70 nm (with the highest number of 61 nm nanoparticles) (Fig. 30 2A) or 35−55 nm (with the highest number of 45 nm nanoparticles) (Fig. 30 3A) height AuNPs, while after 90 min the size of formed AuNPs at the same glucose concentrations increased up to 150–180 nm (with the highest number of 168 nm nanoparticles) (Fig. 30 2A), 60–90 nm (with the

highest number of 80 nm nanoparticles) (Fig. 30 2B) or 50−70 nm (with the highest number of 60 nm nanoparticles) (Fig. 30 3B) respectively.

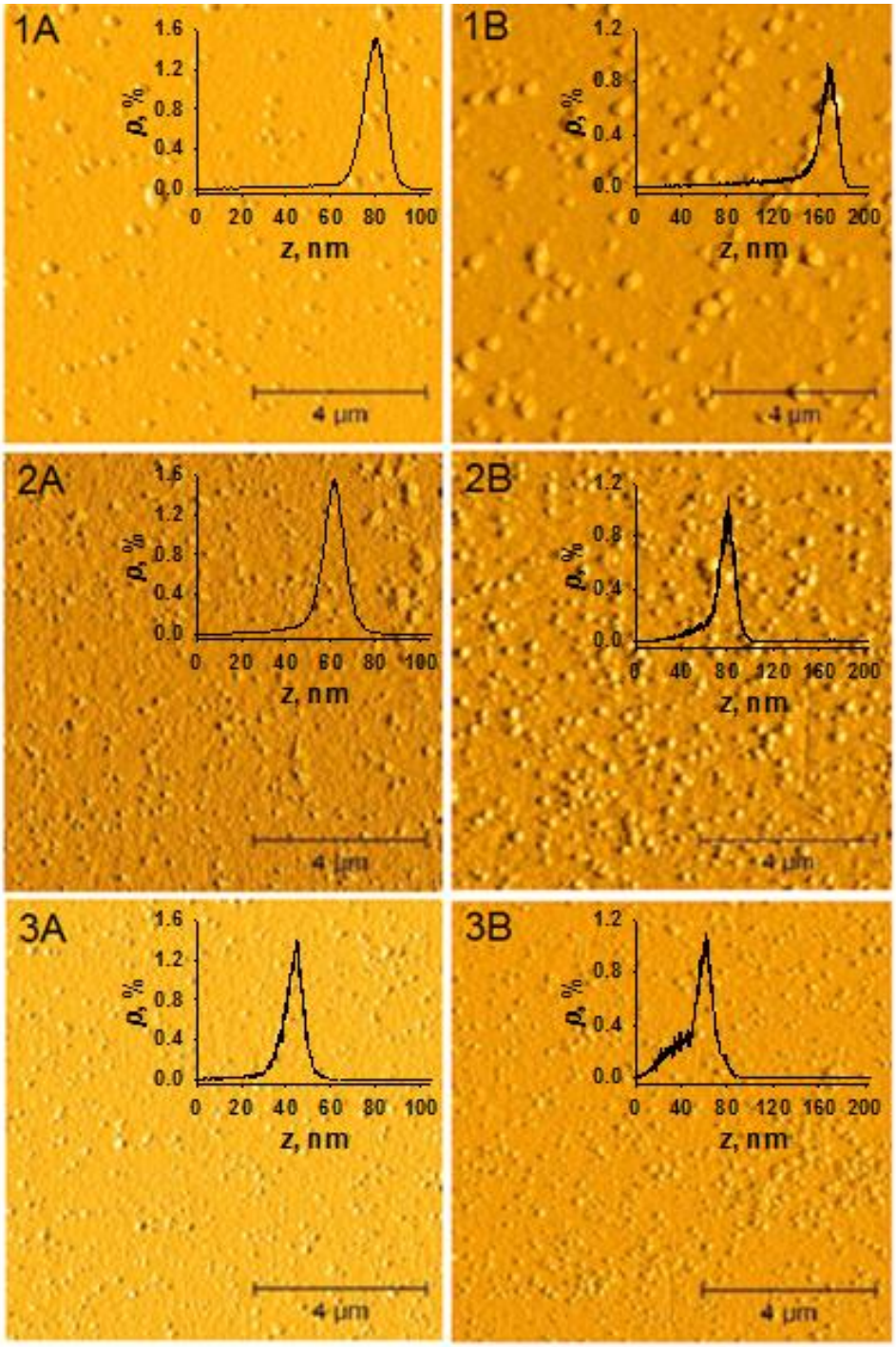

Fig 30. AFM images and height distribution histograms of biocatalytically enlarged AuNPs immobilized on the Au SD pre-modified with 1,6-HDT self-assembled monolayer. The enlargement of AuNPs seeds was performed at different initial concentrations of glucose and different durations of biocatalytic enlargement. Concentrations of glucose: 4×10^{-2} mol L^{-1} (**1A, B**), 4×10^{-3} mol L^{-1} (**2A, B**) and 4×10^{-4} mol L^{-1} (**3A, B**); duration of synthesis: 60 min (**A**) and 90 min (**B**).

It can be assumed that at glucose concentrations ranging from 4×10^{-4} to 4×10^{-2} mol L^{-1} the biocatalytic enlargement of AuNPs should be performed for the different period of time in order to obtain the enlarged AuNPs of same diameter. Therefore, lower glucose concentrations also could be useful if the duration of biocatalytic enlargement would be extended. Some other authors have shown the accuracy and applicability of AFM-based method for the evaluation of kinetics of AuNPs synthesis and growth using classical Turkevich citrate synthesis method at different temperatures [345]. The biocatalytic enlargement of AuNPs immobilized on the glass support after the salinization through amino functional groups was employed in the design of optical biosensor [342].

Comparing the size of enlarged AuNPs, which was determined by DLS and AFM, it is obvious that the determined size of AuNPs was slightly different. These differences in the observations could be explained by the different initial concentration of AuNPs seeds in the solution and surface concentration of AuNPs seeds immobilized on the sensor disc initially used for the biocatalytic enlargement at the same concentration of other chemicals applied for this reaction. In the solution where DLS measurements were performed the concentration of AuNPs seeds was higher in comparison to surface concentration of AuNPs seeds deposited on SAM-modified gold surface of sensor disc.

Conclusions of 3.3. section

The biocatalytic enlargement of AuNPs using optimal concentration of components was studied by three different methods – UV-Vis spectroscopy, DLS and AFM methods. The dependence of nanoparticle growth on the glucose concentration was evaluated changing initial glucose concentrations and the duration of biocatalytic enlargement. It was shown that plasmon absorbance, hydrodynamic diameter and height of enlarged AuNPs change depending on the concentration of glucose in the solution after the same duration of enlargement procedure. Therefore, the enlargement of AuNPs could be applied in the development of glucose biosensors based on UV–Vis spectroscopy, DLS and

AFM. It could be expected that such environmentally friendly synthesis method of different size AuNPs can be used for some other bioanalytical, nanotechnological or biomedical applications.

General conclusions

1. It was determined that 0.5 mol L^{-1} of aniline and 0.75 mg mL^{-1} of glucose oxidase concentrations and 115 h duration of enzymatic polymerization are the optimal conditions for PANI nanoparticles formation. The initial rate of PANI nanoparticles formation was equal to 0.0038 mol $L^{-1}h^{-1}$. The size of PANI nanoparticles after 115 h lasting polymerization was 115 nm.

2. Solutions of tannic acid and colloidal solution of silver nanoparticles are stable at pH range from 3.5 to 5.0.

3. The maximal coverage of silver nanoparticles monolayer on PAH-modified mica deposited from colloidal solution without any tannic acid was 0.28, while at the 3×10^{-5} mol L^{-1} concentration of tannic acid AgNPs coverage abruptly decreased up to 0.03.

4. Plasmon absorbance of enlarged AuNPs linearly depends on glucose concentration in the range from 2×10^{-3} to 0.02 mol L^{-1}.

5. The hydrodynamic diameter of AuNP after 60 min of biocatalytic enlargement was 37.2 nm, 47.2 nm and 60.4 nm, while after 90 min it was 40.3 nm, 52.3 nm and 68.9 nm using 4×10^{-4}, 4×10^{-3} and 4×10^{-2} mol L^{-1} concentrations of glucose in the solution, respectively. Furthermore, the rate of AuNPs seeds enlargement increases increasing initial concentration of glucose in the solution.

6. The height of enlarged AuNP after 60 min of biocatalytic enlargement was 35 – 55 nm, 50 – 70 nm and 70 – 90 nm, while after 90 min it increased up to 50 – 70 nm, 60 – 90 nm and 150 – 180 nm in growing solution containing 4×10^{-4}, 4×10^{-3} and 4×10^{-2} mol L^{-1} of glucose, respectively.

Validation of the results

List of author's publications summarized in the dissertation:

1. M. Ocwieja, **A. Popov**, Z. Adamczyk, M. Morga, A. Ramanaviciene, A. Ramanavicius, Deposition of silver nanoparticles from suspensions containing tannic acid, Colloids and Surfaces A: Physicochemical and Engineering Aspects 2015, (477) 70-76.
2. A. Ramanaviciene, J. Voronovic, **A. Popov**, R. Drevinskas, A. Kausaite-Minkstimiene, A. Ramanavicius, Investigation of biocatalytic enlargement of gold nanoparticles using dynamic light scattering and atomic force microscopy, Colloids and Surfaces A: Physicochemical and Engineering Aspects 2016, (510) 183-189.
3. N. German, **A. Popov**, A. Ramanaviciene, A. Ramanavicius, Evaluation of enzymatic formation of polyaniline nanoparticles, Polymer 2017, (115) 211-216.

List of Conferences, where the results of the dissertation were presented:

1. **A. Popov**, M. Ocwieja, Z. Adamczyk, A. Ramanaviciene, A. Ramanavicius, Physicochemical Characteristics of Charge Stabilized Silver Sols, Ecobalt 2014, Riga, Latvia , 8-10 October 2014.
2. A. Ramanaviciene, J. Voronovic, **A. Popov**, R. Drevinskas, A. Ramanavicius, Investigation of biocatalytic growth of gold nanoparticles using atomic force microscopy and dynamic light scattering, 29th Conference of the European Colloids and Interface Society „ECIS 2015", 6-11 September 2014, Bordeaux, France.
3. **A. Popov**, J. Voronovic, A. Ramanaviciene, The Investigation of Biocatalytic Growth of Gold Nanoparticles, EuroNanoForum2015, Riga, Latvia, 10-12 June 2015.
4. **A. Popov**, M. Ocwieja, Z. Adamczyk, M. Morga, A. Ramanavicius, A. Ramanaviciene, Deposition of silver nanoparticles from suspensions containing tannic acid, 9th Nanoconference Advance in Bioelectrochemistry and Nanomaterials, Vilnius, Lithuania, 20-22 October, 2016.

Publications not included in the thesis

1. L. Mikoliunaite, R. Kubiliute, **A. Popov**, J. Voronovic, S. Sakirzanovas, A. Ramanaviciene, A. Ramanavicius, Development of gold nanoparticle-polypyrrole nanocomposites. Chemija, 2014, 25(2) 63-69.
2. A. Garbaras, L. Mikoliunaite, **A. Popov**, A. Ramanaviciene, V. Remeikis, A. Ramanavicius. Isotope method for the determination of stoichiometry between compounds forming polypyrrole and glucose oxidase composite. Physical Chemistry Chemical Physics 2015, 17(3) 2252-8.

Curriculum Vitae

Name, Surname Anton Popov
E-mail anton.popov87@gmail.com
Date of birth 1987 08 27

EDUCATION

2013 – 2017 Vilnius University, Faculty of Chemistry and Geosciences, PhD student of Chemistry.

2011 – 2013 Vilnius University, Faculty of Chemistry, Master of Chemistry.

2006 – 2011 Vilnius Gediminas Technical University, Faculty of Fundamental Sciences, Department of Chemistry and Bioengineering, Bachelor of bioengineering.

CURRENT RESEARCH AND ACADEMIC POSITIONS

2017 06 01 – present Vilnius University, Faculty of Chemistry and Geosciences, Institute of Chemistry, junior researcher.

PROFESSIONAL TRAINING

1. Intensive summer school „EUCHEME 2013”, 2013 07 30 – 08 12, Camerino University (Italy);
2. Research fellowship, 2014 02 01 – 2014 04 31, J. Haber Institute of Catalysis and Surface Chemistry, Polish Academy of Sciences, Cracow (Poland)
3. Research fellowship, 2016 09 16 – 2016 12 16, J. Haber Institute of Catalysis and Surface Chemistry, Polish Academy of Sciences, Cracow (Poland)

Acknowledgments

I would like to express my deepest gratitude to my supervisor prof. dr. Almira Ramanavičienė for her guidance, support and numerous discussions during my PhD studies.

I am sincerely grateful to all Vilnius University, Faculty of Chemistry and geoscience staff members for the provided possibility to study a doctoral degree.

My warmest thanks are directed to prof. dr. Zbigniew Adamczyk from J. Haber Institute of Catalysis and Surface Chemistry for giving me the opportunity to work in his laboratory. I wish to thank all my colleagues from my internship in Cracow and especially dr. Magdalena Oćwieja for their wonderful collaboration.

I would like to offer my special thanks to all members of Center of Nanotechnology and Material Science "NanoTechnas", especially to prof. dr. Arūnas Ramanavičius, dr. Lina Mikoliūnaitė, dr. Jaroslav Voronovič, dr. Viktor Mažeiko, dr. Asta Makaravičiūtė and student Benediktas Brasiūnas. You supported me greatly and were always willing to help.

I thank my family members and friends for their love and support. I do not know how to thank you all enough for providing me with the opportunity to be where I am today.

Most importantly, I wish to thank my loving and supportive wife, Julia. You are always there for me.

References

1. Goodwin, J.W., 2004, John Wiley & Sons, Ltd. p. 1-26.
2. Norde, W., Materials Today, 2003. **6**(10): p. 47.
3. Myers, D., 2002, John Wiley & Sons, Inc. p. 1-7.
4. Vincent, B., 2009, Blackwell Publishing Ltd. p. 1-13.
5. Dautzenberg, H., Acta Polymerica, 1983. **34**(11-12): p. 761-761.
6. Zsigmondy, R. 1917: John Wiley & Sons.
7. Schmid, G., 2007, Wiley-VCH Verlag GmbH. p. 1-4.
8. Dugyala, V.R., S.V. Daware, and M.G. Basavaraj, Soft Matter, 2013. **9**(29): p. 6711-6725.
9. Haegel, M.J.S.F.-H. 1994: Steinkopff-Verlag Heidelberg.
10. Hornyak, G.L., et al., Micron, 1998. **29**(2): p. 183-190.
11. Adamczyk, Z., Current Opinion in Colloid & Interface Science, 2012. **17**(3): p. 173-186.
12. Nili, H. and N.G. Green, 2016, Springer Netherlands: Dordrecht. p. 1-10.
13. Liang, Y., et al., Advances in colloid and interface science, 2007. **134**: p. 151-166.
14. Hamaker, H.C., Physica, 1937. **4**(10): p. 1058-1072.
15. Dzyaloshinskii, I.E., E.M. Lifshitz, and L.P. Pitaevskii, Advances in Physics, 1961. **10**(38): p. 165-209.
16. Jiang, K. and P. Pinchuk, Nanotechnology, 2016. **27**(34): p. 345710.
17. Morgan, H. and N. Green, Hertfordshire, England: Research Studies Press LTD. **324**.
18. Tadros, T., 2013, Springer Berlin Heidelberg: Berlin, Heidelberg. p. 363-363.
19. Cosgrove, T. 2010: John Wiley & Sons.
20. Israelachvili, J.N., 2011, Academic Press: San Diego. p. 341-380.
21. Singh, A.K., 2016, Academic Press: Boston. p. 343-450.
22. Tareste, D., et al., Langmuir, 2007. **23**(6): p. 3225-3229.
23. Liang, Y., et al., Advances in Colloid and Interface Science, 2007. **134**(Supplement C): p. 151-166.
24. Bhattacharjee, S., Journal of Controlled Release, 2016. **235**(Supplement C): p. 337-351.
25. Grasso, D., et al., Reviews in Environmental Science and Biotechnology, 2002. **1**(1): p. 17-38.
26. Eastman, J., 2009, Blackwell Publishing Ltd. p. 36-49.
27. Kontogeorgis, G.M. and S. Kiil, 2016, John Wiley & Sons, Ltd. p. 211-242.
28. Hunter, R.J., 1981, Academic Press. p. 219-257.
29. Hunter, R.J., 1981, Academic Press. p. 305-344.
30. Schwuger, M.J. and F.-H. Haegel. 1994: Springer.
31. Kontogeorgis, G.M. and S. Kiil, 2016, John Wiley & Sons, Ltd. p. 96-120.
32. Goodwin, J.W., 2004, John Wiley & Sons, Ltd. p. 195-239.

33. Schmitt, T.M. 2001: CRC Press.
34. Raffa, P., et al., Chemical Reviews, 2015. **115**(16): p. 8504-8563.
35. Semenov, A. and A. Shvets, Soft matter, 2015. **11**(45): p. 8863-8878.
36. Goodwin, J.W., 2004, John Wiley & Sons, Ltd. p. 153-176.
37. Oćwieja, M., et al., Journal of Colloid and Interface Science, 2017. **501**(Supplement C): p. 192-201.
38. Molina-Bolívar, J.A. and J.L. Ortega-Vinuesa, Langmuir, 1999. **15**(8): p. 2644-2653.
39. Moore, T.L., et al., Chemical Society Reviews, 2015. **44**(17): p. 6287-6305.
40. Daniels, E.S., E.D. Sudol, and M.S. El-Aasser, 2001, American Chemical Society. p. 1-12.
41. Hetemi, D. and J. Pinson, Chemical Society Reviews, 2017. **46**(19): p. 5701-5713.
42. Yang, L. and P. Alexandridis, Current Opinion in Colloid & Interface Science, 2000. **5**(1): p. 132-143.
43. Uppalapati, D., et al., Biomaterials, 2016. **111**(Supplement C): p. 149-162.
44. Khatoon, H. and S. Ahmad, Journal of Industrial and Engineering Chemistry, 2017. **53**(Supplement C): p. 1-22.
45. Shirakawa, H., et al., Journal of the Chemical Society, Chemical Communications, 1977(16): p. 578-580.
46. Zhao, F., et al., Accounts of Chemical Research, 2017. **50**(7): p. 1734-1743.
47. Inzelt, G., Journal of Solid State Electrochemistry, 2017. **21**(7): p. 1965-1975.
48. Wolfart, F., et al., Journal of Solid State Electrochemistry, 2017. **21**(9): p. 2489-2515.
49. Rasmussen, S.C., Substantia, 2017. **1**(2).
50. Sultana, S., et al., IET Nanobiotechnology, 2017. **11**, 835-842.
51. Matindoust, S., et al., Journal of Materials Science: Materials in Electronics, 2017. **28**(11): p. 7760-7768.
52. Wu, Y., et al., Acta Biomaterialia, 2016. **33**(Supplement C): p. 122-130.
53. Wang, H., J. Lin, and Z.X. Shen, Journal of Science: Advanced Materials and Devices, 2016. **1**(3): p. 225-255.
54. Pud, A., et al., Progress in Polymer Science, 2003. **28**(12): p. 1701-1753.
55. Ito, S., et al., Synthetic Metals, 1998. **96**(2): p. 161-163.
56. Keyhanpour, A., S.M. Seyed Mohaghegh, and A. Jamshidi, Iranian Polymer Journal, 2012. **21**(5): p. 307-315.
57. Massoumi, B. and R. Mohammadi, Polymer Science Series B, 2013. **55**(11): p. 593-600.
58. Cao, Y., et al., Polymer, 1989. **30**(12): p. 2305-2311.
59. Jun, L., et al., Journal of Wuhan University of Technology-Mater. Sci. Ed., 2003. **18**(3): p. 53-55.
60. Bankar, P.K., S.S. Patil, and M.A. More, AIP Conference Proceedings, 2015. **1665**(1): p. 050078.

61. Yang, L., et al., Journal of Applied Polymer Science, 2017. **134**(47): p. 45547.
62. Gu, H., et al., Journal of Applied Polymer Science, 2013. **130**(4): p. 2238-2244.
63. Oueiny, C., S. Berlioz, and F.-X. Perrin, Progress in Polymer Science, 2014. **39**(4): p. 707-748.
64. Runge, F., Annalen der Physik, 1834. **107**(5): p. 65-78.
65. Fritsche, J., Advanced Synthesis & Catalysis, 1840. **20**(1): p. 453-459.
66. 2008, Springer Berlin Heidelberg: Berlin, Heidelberg. p. 1-6.
67. Freund, M.S. and B.A. Deore, 2007, John Wiley & Sons, Ltd. p. 75-155.
68. Heinze, J., B.A. Frontana-Uribe, and S. Ludwigs, Chemical Reviews, 2010. **110**(8): p. 4724-4771.
69. Gospodinova, N. and L. Terlemezyan, Progress in Polymer Science, 1998. **23**(8): p. 1443-1484.
70. Eftekhari, A., L. Li, and Y. Yang, Journal of Power Sources, 2017. **347**(Supplement C): p. 86-107.
71. Freund, M.S. and B.A. Deore, 2007, John Wiley & Sons, Ltd. p. 156-218.
72. Özden, M., E. Ekinci, and A.E. Karagözler, Turkish Journal of Chemistry, 1999. **23**(1): p. 89-98.
73. Crowley, K., et al., Chemical Papers, 2013. **67**(8): p. 771-780.
74. Bakker, E. and Y. Qin, Analytical Chemistry, 2006. **78**(12): p. 3965-3984.
75. Lindfors, T. and A. Ivaska, Analytica Chimica Acta, 2000. **404**(1): p. 101-110.
76. Karyakin, A.A., et al., Analytical Chemistry, 1999. **71**(13): p. 2534-2540.
77. A. Karyakin, A., et al., Analytical Communications, 1999. **36**(4): p. 153-156.
78. Mano, N., et al., Journal of the American Chemical Society, 2007. **129**(22): p. 7006-7007.
79. Ates, M., Journal of Adhesion Science and Technology, 2016. **30**(14): p. 1510-1536.
80. Abu-Thabit, N.Y., Journal of Chemical Education, 2016. **93**(9): p. 1606-1611.
81. Huang, J. and R.B. Kaner, Angewandte Chemie, 2004. **116**(43): p. 5941-5945.
82. Sen, T., S. Mishra, and N.G. Shimpi, RSC Advances, 2016. **6**(48): p. 42196-42222.
83. Baker, C.O., et al., Chemical Society Reviews, 2017. **46**(5): p. 1510-1525.
84. Masters, J.G., et al., Synthetic Metals, 1991. **41**(1): p. 715-718.
85. Lee, K., et al., Nature, 2006. **441**(7089): p. 65-68.
86. Molapo, K.M., et al., International Journal of Electrochemical Science, 2012. **7**(12): p. 11859-11875.
87. Stejskal, J., et al., Synthetic Metals, 1999. **105**(3): p. 195-202.
88. Bhadra, S., et al., Progress in Polymer Science, 2009. **34**(8): p. 783-810.
89. Gvozdenović, M.M., et al., 2011, InTech.

90. Tang, S.-J., et al., Journal of Physics D: Applied Physics, 2013. **46**(50): p. 505301.
91. Kaitsuka, Y. and H. Goto, Polymers, 2016. **8**(2): p. 34.
92. Huang, W.S. and A.G. MacDiarmid, Polymer, 1993. **34**(9): p. 1833-1845.
93. D'Aprano, G., M. Leclerc, and G. Zotti, Synthetic Metals, 1996. **82**(1): p. 59-61.
94. Trchová, M., et al., Chemical Papers, 2012. **66**(5): p. 415-445.
95. Stejskal, J. and R. Gilbert, Pure and Applied Chemistry, 2002. **74**(5): p. 857-867.
96. Sariciftci, N.S., A.J. Heeger, and Y. Cao, Physical Review B, 1994. **49**(9): p. 5988-5992.
97. Scully, M., M.C. Petty, and A.P. Monkman, Synthetic Metals, 1993. **55**(1): p. 183-187.
98. Sun, Y., A.G. MacDiarmid, and A.J. Epstein, Journal of the Chemical Society, Chemical Communications, 1990(7): p. 529-531.
99. Bazito, F.F., et al., Physical Chemistry Chemical Physics, 2008. **10**(10): p. 1457-1462.
100. D'Aprano, G., M. Leclerc, and G. Zotti, Macromolecules, 1992. **25**(8): p. 2145-2150.
101. Valentová, H. and J. Stejskal, Synthetic Metals, 2010. **160**(7): p. 832-834.
102. Peikertová, P., et al., Chemical Papers, 2017. **71**(2): p. 379-385.
103. Hillman, A.R., M.A. Mohamoud, and I. Efimov, Analytical Chemistry, 2011. **83**(14): p. 5696-5707.
104. Brožová, L., et al., Polymer Degradation and Stability, 2008. **93**(3): p. 592-600.
105. Kulkarni, V.G., L.D. Campbell, and W.R. Mathew, Synthetic Metals, 1989. **30**(3): p. 321-325.
106. Sapurina, I.Y. and J. Stejskal, Russian Journal of General Chemistry, 2012. **82**(2): p. 256-275.
107. Li, Y., et al., Chemical Papers, 2013. **67**(8): p. 876-890.
108. Boeva, Z.A. and V.G. Sergeyev, Polymer Science Series C, 2014. **56**(1): p. 144-153.
109. Kumar, A., et al., Nanotechnology, 2010. **21**(17): p. 175102.
110. Humpolicek, P., et al., Synthetic Metals, 2012. **162**(7): p. 722-727.
111. Sun, K.-H., et al., Scientific reports, 2016. **6**.
112. Humpolicek, P., et al., RSC Advances, 2015. **5**(84): p. 68796-68805.
113. Bayer, C.L., I.J. Trenchard, and N.A. Peppas, Journal of Biomaterials Science, Polymer Edition, 2010. **21**(5): p. 623-634.
114. Saikia, J.P., et al., Colloids and Surfaces B: Biointerfaces, 2010. **81**(1): p. 158-164.
115. Prabhakar, P.K., et al., Colloids and Surfaces B: Biointerfaces, 2011. **86**(1): p. 146-153.
116. Tan, J., et al., Journal of Materials Science, 2018. **53**(1): p. 447-455.
117. Yslas, E.I., et al., Materials Science and Engineering: C, 2015. **51**(Supplement C): p. 51-56.

118. Qazi, T.H., R. Rai, and A.R. Boccaccini, Biomaterials, 2014. **35**(33): p. 9068-9086.
119. Sapurina, I. and J. Stejskal, Polymer International, 2008. **57**(12): p. 1295-1325.
120. Ćirić-Marjanović, G., Synthetic Metals, 2013. **177**(Supplement C): p. 1-47.
121. Wallace, G.G., et al. 2008: CRC press.
122. Genies, E.M. and C. Tsintavis, Journal of Electroanalytical Chemistry and Interfacial Electrochemistry, 1985. **195**(1): p. 109-128.
123. McClelland, R.A., et al., Journal of the American Chemical Society, 1996. **118**(20): p. 4794-4803.
124. Stejskal, J., et al., 2002, John Wiley & Sons, Inc.
125. Stejskal, J., et al., Encyclopedia of Polymer Science and Technology, 2015.
126. Chowdhury, D., A. Paul, and A. Chattopadhyay, The Journal of Physical Chemistry B, 2002. **106**(17): p. 4343-4347.
127. Yang, C.-H., et al., Polymer, 2007. **48**(11): p. 3237-3247.
128. Jing, X., et al., Journal of Polymer Science Part A: Polymer Chemistry, 2006. **44**(2): p. 1014-1019.
129. Nastase, C., et al., Composites Part A: Applied Science and Manufacturing, 2005. **36**(4): p. 481-485.
130. Sassolas, A., L.J. Blum, and B.D. Leca-Bouvier, Biotechnology Advances, 2012. **30**(3): p. 489-511.
131. I.Yu. Sapurina, M.A.S. New Polymers for Special Applications, ed. A.D.S.G. (Ed.). 2012.
132. Nabid, M.R., Z. Zamiraei, and R. Sedghi, Iranian Polymer Journal (English Edition), 2010. **19**(9): p. 699-706.
133. Liu, W., et al., Journal of the American Chemical Society, 1999. **121**(1): p. 71-78.
134. Nagarajan, R., et al., Macromolecules, 2000. **33**(26): p. 9542-9547.
135. Cruz-Silva, R., et al., Polymer, 2006. **47**(5): p. 1563-1568.
136. Zemel, H. and J.F. Quinn, *Enzymatic synthesis of polyaniline*. 1995, Google Patents.
137. de Salas, F., et al., PloS one, 2016. **11**(10): p. e0164958.
138. Aizawa, M., et al., Journal of Biotechnology, 1990. **14**(3): p. 301-309.
139. Longoria, A., R. Tinoco, and R. Vázquez-Duhalt, Chemosphere, 2008. **72**(3): p. 485-490.
140. Kausaite, A., A. Ramanaviciene, and A. Ramanavicius, Polymer, 2009. **50**(8): p. 1846-1851.
141. Cruz-Silva, R., P. Roman, and J. Romero, Biocatalysis in polymer chemistry, 2010: p. 187-210.
142. Pradeep, T. and Anshup, Thin Solid Films, 2009. **517**(24): p. 6441-6478.
143. Lai-Kwan, C. and H.-T. Chang. 2012: Crc Press.
144. Zhang, Y., et al., Chinese Science Bulletin, 2012. **57**(2): p. 238-246.
145. Conde, J., G. Doria, and P. Baptista, Journal of drug delivery, 2011. **2012**.

146. Pareek, V., et al., Advanced Science, Engineering and Medicine, 2017. **9**(7): p. 527-544.
147. Sheng, W., Q. Yang, and J. Weng, Current Organic Chemistry, 2011. **15**(21): p. 3692-3705.
148. Dauthal, P. and M. Mukhopadhyay, Industrial & Engineering Chemistry Research, 2016. **55**(36): p. 9557-9577.
149. Alexander, J.W., Surgical infections, 2009. **10**(3): p. 289-292.
150. Mijnendonckx, K., et al., BioMetals, 2013. **26**(4): p. 609-621.
151. Lansdown, A.B., 2006, Karger Publishers. p. 17-34.
152. White, R.J., British Journal of Nursing, 2001. **10**(Sup4): p. S3-S8.
153. Klasen, H.J., Burns, 2000. **26**(2): p. 131-138.
154. Sreeprasad, T.S. and T. Pradeep, 2013, Springer. p. 303-388.
155. Nowack, B., H.F. Krug, and M. Height, Environmental Science & Technology, 2011. **45**(4): p. 1177-1183.
156. Singh, R., et al., Applied microbiology and biotechnology, 2015. **99**(11): p. 4579-4593.
157. Pacioni, N.L., et al., 2015, Springer International Publishing: Cham. p. 13-46.
158. García-Barrasa, J., J.M. López-de-Luzuriaga, and M. Monge, Central European journal of chemistry, 2011. **9**(1): p. 7-19.
159. Lee, P. and D. Meisel, The Journal of Physical Chemistry, 1982. **86**(17): p. 3391-3395.
160. Pillai, Z.S. and P.V. Kamat, The Journal of Physical Chemistry B, 2004. **108**(3): p. 945-951.
161. Henglein, A. and M. Giersig, The Journal of Physical Chemistry B, 1999. **103**(44): p. 9533-9539.
162. Creighton, J.A., C.G. Blatchford, and M.G. Albrecht, Journal of the Chemical Society, Faraday Transactions 2: Molecular and Chemical Physics, 1979. **75**: p. 790-798.
163. Polte, J., et al., ACS Nano, 2012. **6**(7): p. 5791-5802.
164. Sun, Y., Chemical Society Reviews, 2013. **42**(7): p. 2497-2511.
165. Liu, H., et al., Biotechnology and bioprocess engineering, 2016. **21**(1): p. 1-18.
166. Swathy, B., IOSR J Pharm, 2014. **4**: p. 38-44.
167. León-Silva, S., F. Fernández-Luqueño, and F. López-Valdez, Water, Air, & Soil Pollution, 2016. **227**(9): p. 306.
168. Abdelghany, T.M., et al., BioNanoScience, 2017.
169. Mashwani, Z.-u.-R., et al., Applied Microbiology and Biotechnology, 2015. **99**(23): p. 9923-9934.
170. Cao, W., et al., Journal of applied physics, 2011. **109**(3): p. 034310.
171. Jeong, S.H., et al., Particle & Particle Systems Characterization, 2015. **32**(2): p. 164-175.
172. Lee, K.-C., et al., Surface and Coatings Technology, 2008. **202**(22): p. 5339-5342.
173. Baek, S.-W., et al., Scientific reports, 2013. **3**.

174. Sakir, M., et al., ACS applied materials & interfaces, 2017. **9**(45): p. 39795-39803.
175. Neutens, P., et al., Nature Photonics, 2009. **3**(5): p. 283-286.
176. Raj, D.R., S. Prasanth, and C. Sudarsanakumar, Plasmonics, 2017. **12**(4): p. 1227-1234.
177. Martin-Moreno, L., Nature Physics, 2009. **5**: p. 457.
178. Qian, X.M. and S.M. Nie, Chemical Society Reviews, 2008. **37**(5): p. 912-920.
179. Kunzmann, A., et al., Biochimica et Biophysica Acta (BBA) - General Subjects, 2011. **1810**(3): p. 361-373.
180. Liu, J. and G. Jiang. 2015: Springer.
181. Kim, S.H., et al., Journal of Alloys and Compounds, 2007. **433**(1): p. 261-264.
182. Navaladian, S., et al., Nanotechnology, 2008. **19**(4): p. 045603.
183. Patil, G.P., et al., in *AIP Conference Proceedings*. 2017. AIP Publishing.
184. Park, K., D. Seo, and J. Lee, Colloids and Surfaces A: Physicochemical and Engineering Aspects, 2008. **313-314**(Supplement C): p. 351-354.
185. Lin, J.C. and C.Y. Wang, Materials Chemistry and Physics, 1996. **45**(2): p. 136-144.
186. Yu, S.-j., Y.-g. Yin, and J.-f. Liu, Environmental Science: Processes & Impacts, 2013. **15**(1): p. 78-92.
187. Wang, M., et al., RSC Advances, 2017. **7**(20): p. 12144-12149.
188. Tolaymat, T.M., et al., Science of The Total Environment, 2010. **408**(5): p. 999-1006.
189. Le Ouay, B. and F. Stellacci, Nano Today, 2015. **10**(3): p. 339-354.
190. Akbarzadeh, A., et al., Toxin Reviews, 2016. **35**(3-4): p. 180-186.
191. Li, W.-R., et al., Applied Microbiology and Biotechnology, 2010. **85**(4): p. 1115-1122.
192. Alarcon, E.I., M. Griffith, and K.I. Udekwu. 2015: Springer.
193. Durán, N., et al., Nanomedicine: Nanotechnology, Biology and Medicine, 2016. **12**(3): p. 789-799.
194. Dakal, T.C., et al., Frontiers in microbiology, 2016. **7**.
195. Zhang, X.-F., et al., International journal of molecular sciences, 2016. **17**(9): p. 1534.
196. Xiu, Z.-M., J. Ma, and P.J. Alvarez, Environmental science & technology, 2011. **45**(20): p. 9003-9008.
197. Brennan, S.A., et al., Bone & Joint Journal, 2015. **97-B**(5): p. 582-589.
198. Bik, E.M., et al., The ISME journal, 2010. **4**(8): p. 962-974.
199. Dewhirst, F.E., et al., Journal of bacteriology, 2010. **192**(19): p. 5002-5017.
200. Corrêa, J.M., et al., International journal of biomaterials, 2015. **2015**.
201. Wei, L., et al., Drug Discovery Today, 2015. **20**(5): p. 595-601.
202. Ahmed, K.B.A., T. Raman, and A. Veerappan, Materials Science and Engineering: C, 2016. **68**(Supplement C): p. 939-947.

203. Mishra, S. and H. Singh, Applied microbiology and biotechnology, 2015. **99**(3): p. 1097-1107.
204. Murr, L.E., 2015, Springer International Publishing: Cham. p. 3-9.
205. Donaldson, J.A., Gold Bulletin, 1980. **13**(4): p. 160-165.
206. Davies, G. 2010: University of Wales Press.
207. Pricker, S.P., Gold bulletin, 1996. **29**(2): p. 53-60.
208. Daniel, M.-C. and D. Astruc, Chemical reviews, 2004. **104**(1): p. 293-346.
209. Krukemeyer, M., et al., Journal of Nanomedicine & Nanotechnology, 2015. **6**(6): p. 1.
210. Sciau, P., 2012, InTech.
211. Giljohann, D.A., et al., Angewandte Chemie International Edition, 2010. **49**(19): p. 3280-3294.
212. Thompson, D., Gold Bulletin, 2007. **40**(4): p. 267-269.
213. Mingos, D.M.P., 2014, Springer. p. 1-47.
214. Sharma, V., K. Park, and M. Srinivasarao, Materials Science and Engineering: R: Reports, 2009. **65**(1): p. 1-38.
215. Turkevich, J., P.C. Stevenson, and J. Hillier, Discussions of the Faraday Society, 1951. **11**: p. 55-75.
216. Frens, G., Nature, 1973. **241**(105): p. 20-22.
217. Herizchi, R., et al., Artificial Cells, Nanomedicine, and Biotechnology, 2016. **44**(2): p. 596-602.
218. Ramanaviciene, A., et al., Sensors and Actuators B: Chemical, 2009. **137**(2): p. 483-489.
219. Kimling, J., et al., The Journal of Physical Chemistry B, 2006. **110**(32): p. 15700-15707.
220. Frens, G., Nature Physical Science, 1973. **241**: p. 20.
221. Polte, J., CrystEngComm, 2015. **17**(36): p. 6809-6830.
222. Sugimoto, T., Journal of Colloid and Interface Science, 2007. **309**(1): p. 106-118.
223. Ji, X., et al., Journal of the American Chemical Society, 2007. **129**(45): p. 13939-13948.
224. Wuithschick, M., et al., ACS Nano, 2015. **9**(7): p. 7052-7071.
225. Thanh, N.T.K., N. Maclean, and S. Mahiddine, Chemical Reviews, 2014. **114**(15): p. 7610-7630.
226. Polte, J., et al., Journal of the American Chemical Society, 2010. **132**(4): p. 1296-1301.
227. Park, J.-W. and J.S. Shumaker-Parry, Journal of the American Chemical Society, 2014. **136**(5): p. 1907-1921.
228. Teobaldi, G. and F. Zerbetto, The Journal of Physical Chemistry C, 2007. **111**(37): p. 13879-13885.
229. Brust, M., et al., Journal of the Chemical Society, Chemical Communications, 1994(7): p. 801-802.
230. Sperling, R.A. and W.J. Parak, Philosophical Transactions of the Royal Society of London A: Mathematical, Physical and Engineering Sciences, 2010. **368**(1915): p. 1333-1383.

231. López-Millán, A., et al., Applied Sciences, 2017. **7**(3): p. 273.
232. Ganeshkumar, M., et al., Materials Research Bulletin, 2012. **47**(9): p. 2113-2119.
233. Duy, N.N., et al., Colloids and Surfaces A: Physicochemical and Engineering Aspects, 2013. **436**: p. 633-638.
234. Augustine, A.K., V.P.N. Nampoori, and M. Kailasnath, Optik - International Journal for Light and Electron Optics, 2014. **125**(22): p. 6696-6699.
235. Kim, K.-S., et al., Journal of Materials Chemistry, 2006. **16**(14): p. 1315-1317.
236. Reetz, M.T. and W. Helbig, Journal of the American Chemical Society, 1994. **116**(16): p. 7401-7402.
237. Ma, H., et al., ChemPhysChem, 2004. **5**(1): p. 68-75.
238. Benedec, D., et al., International Journal of Nanomedicine, 2018. **13**: p. 1041.
239. Thakkar, K.N., S.S. Mhatre, and R.Y. Parikh, Nanomedicine: Nanotechnology, Biology and Medicine, 2010. **6**(2): p. 257-262.
240. Molnár, Z., et al., Scientific Reports, 2018. **8**(1): p. 3943.
241. Sengani, M., A.M. Grumezescu, and V.D. Rajeswari, OpenNano, 2017. **2**: p. 37-46.
242. Tiloke, C. and A.A. Chuturgoon, 2017, Springer. p. 269-291.
243. Nadeem, M., et al., Green Chemistry Letters and Reviews, 2017. **10**(4): p. 216-227.
244. Hulkoti, N.I. and T.C. Taranath, Colloids and Surfaces B: Biointerfaces, 2014. **121**: p. 474-483.
245. Singh, P., et al., Trends in Biotechnology, 2016. **34**(7): p. 588-599.
246. Nehl, C.L. and J.H. Hafner, Journal of Materials Chemistry, 2008. **18**(21): p. 2415-2419.
247. Lohse, S.E. and C.J. Murphy, Chemistry of Materials, 2013. **25**(8): p. 1250-1261.
248. Haiss, W., et al., Analytical Chemistry, 2007. **79**(11): p. 4215-4221.
249. Krajczewski, J., K. Kołątaj, and A. Kudelski, RSC Advances, 2017. **7**(28): p. 17559-17576.
250. Kim, Y., R.C. Johnson, and J.T. Hupp, Nano Letters, 2001. **1**(4): p. 165-167.
251. Tang, Y., et al., Nanoscale, 2015. **7**(14): p. 6039-6044.
252. Shang, L., et al., Biosensors and Bioelectronics, 2008. **23**(7): p. 1180-1184.
253. Zayats, M., et al., Nano Letters, 2005. **5**(1): p. 21-25.
254. Parashar, A., et al., New Journal of Chemistry, 2017. **41**(24): p. 15079-15086.
255. Saa, L., et al., ACS Applied Materials & Interfaces, 2016. **8**(17): p. 11139-11146.
256. Vincenzo, A., et al., Journal of Physics: Condensed Matter, 2017. **29**(20): p. 203002.
257. Malola, S., et al., ACS Nano, 2013. **7**(11): p. 10263-10270.

258. Zhang, Y., et al., Materials, 2014. **7**(7): p. 5169-5201.
259. Bantz, K.C., et al., Physical Chemistry Chemical Physics, 2011. **13**(24): p. 11551-11567.
260. Majdalawieh, A., et al., Journal of nanoscience and nanotechnology, 2014. **14**(7): p. 4757-4780.
261. Priecel, P., et al., Chinese Journal of Catalysis, 2016. **37**(10): p. 1619-1650.
262. Guo, S. and E. Wang, Analytica Chimica Acta, 2007. **598**(2): p. 181-192.
263. Ramanavicius, A., N. German, and A. Ramanaviciene, Journal of The Electrochemical Society, 2017. **164**(4): p. G45-G49.
264. German, N., et al., Colloids and Surfaces A: Physicochemical and Engineering Aspects, 2012. **413**: p. 224-230.
265. Pensa, E., et al., Accounts of chemical research, 2012. **45**(8): p. 1183-1192.
266. Yeh, Y.-C., B. Creran, and V.M. Rotello, Nanoscale, 2012. **4**(6): p. 1871-1880.
267. Hornos Carneiro, M.F. and F. Barbosa Jr, Journal of Toxicology and Environmental Health, Part B, 2016. **19**(3-4): p. 129-148.
268. Panahi, Y., et al., Drug research, 2017. **67**(02): p. 77-87.
269. Wang, T., et al., Nano Life, 2015. **5**(03): p. 1542007.
270. Arvizo, R., R. Bhattacharya, and P. Mukherjee, Expert opinion on drug delivery, 2010. **7**(6): p. 753-763.
271. Yang, J., et al., Advanced Materials, 2009. **21**(43): p. 4339-4342.
272. Topete, A., et al., ACS Nano, 2014. **8**(3): p. 2725-2738.
273. Fratoddi, I., et al., Nano Research, 2015. **8**(6): p. 1771-1799.
274. Pan, Y., et al., Small, 2007. **3**(11): p. 1941-1949.
275. Rivera Gil, P., et al., Pharmacological Research, 2010. **62**(2): p. 115-125.
276. Pompa, P.P., et al., Nano Research, 2011. **4**(4): p. 405-413.
277. Sonavane, G., K. Tomoda, and K. Makino, Colloids and Surfaces B: Biointerfaces, 2008. **66**(2): p. 274-280.
278. Lynch, I. and K.A. Dawson, Nano Today, 2008. **3**(1): p. 40-47.
279. Simpson, C.A., et al., Nanomedicine: Nanotechnology, Biology and Medicine, 2013. **9**(2): p. 257-263.
280. Freund, M.S. and B.A. Deore, 2007, John Wiley & Sons, Ltd. p. 1-74.
281. Mühlpfordt, H., Experientia, 1982. **38**(9): p. 1127-1128.
282. Romaskevic, T., et al., Macromolecular Chemistry and Physics, 2011. **212**(21): p. 2291-2299.
283. Lorber, B., et al., Biochemistry and Molecular Biology Education, 2012. **40**(6): p. 372-382.
284. Zakharov, P. and F. Scheffold, 2009, Springer Berlin Heidelberg: Berlin, Heidelberg. p. 433-467.
285. Li, Y., V. Lubchenko, and P.G. Vekilov, Review of Scientific Instruments, 2011. **82**(5): p. 053106.
286. Chu, B., 1991, Academic Press. p. 13-61.
287. Oćwieja, M., Z. Adamczyk, and K. Kubiak, Journal of Colloid and Interface Science, 2012. **376**(1): p. 1-11.

288. Adamczyk, Z., B. Jachimska, and M. Kolasińska, Journal of Colloid and Interface Science, 2004. **273**(2): p. 668-674.
289. Oćwieja, M., M. Morga, and Z. Adamczyk, Journal of Nanoparticle Research, 2013. **15**(3): p. 1460.
290. Oćwieja, M., Z. Adamczyk, and M. Morga, Journal of Colloid and Interface Science, 2015. **438**: p. 249-258.
291. Zembala, M., Z. Adamczyk, and P. Warszyski, Colloids and Surfaces A: Physicochemical and Engineering Aspects, 2001. **195**(1): p. 3-15.
292. Zembala, M. and Z. Adamczyk, Langmuir, 2000. **16**(4): p. 1593-1601.
293. Vikki, T., et al., Macromolecules, 1996. **29**(8): p. 2945-2953.
294. Kim, D., et al., Macromolecules, 2002. **35**(13): p. 5314-5316.
295. Albuquerque, J.E., et al., Synthetic Metals, 2000. **113**(1): p. 19-22.
296. Kausaite-Minkstimiene, A., et al., Sensors and Actuators B: Chemical, 2011. **158**(1): p. 278-285.
297. Roy, S., et al., Biomacromolecules, 2002. **3**(5): p. 937-941.
298. Yin, W. and E. Ruckenstein, Macromolecules, 2000. **33**(4): p. 1129-1131.
299. Khan, R., et al., Advances in Chemical Engineering and Science, 2011. **01**: p. 4.
300. Gaikwad, P.D., et al., Bulletin of Materials Science, 2006. **29**(4): p. 417-420.
301. Olinga, T.E., et al., Macromolecules, 2000. **33**(6): p. 2107-2113.
302. Rumbau, V., et al., Enzyme and Microbial Technology, 2007. **40**(5): p. 1412-1421.
303. Xian, Y., et al., Biosensors and Bioelectronics, 2006. **21**(10): p. 1996-2000.
304. Liu, Z., et al., Small, 2008. **4**(4): p. 462-466.
305. Wei, D. and A. Ivaska, Chemia Analityczna, 2006. **51**(6): p. 839-852.
306. Nair, L.S. and C.T. Laurencin, Journal of Biomedical Nanotechnology, 2007. **3**(4): p. 301-316.
307. Eckhardt, S., et al., Chemical Reviews, 2013. **113**(7): p. 4708-4754.
308. Ilana, P., et al., Nanotechnology, 2008. **19**(24): p. 245705.
309. Jin, W.-J., et al., Synthetic Metals, 2007. **157**(10): p. 454-459.
310. Zhang, F., et al., Fibers and Polymers, 2009. **10**(4): p. 496-501.
311. Prabhu, S. and E.K. Poulose, International Nano Letters, 2012. **2**(1): p. 32.
312. Roe, D., et al., Journal of Antimicrobial Chemotherapy, 2008. **61**(4): p. 869-876.
313. Isse, A.A., et al., Electrochemistry Communications, 2006. **8**(11): p. 1707-1712.
314. Zhao, D., et al., Microelectronic Engineering, 2012. **96**: p. 71-75.
315. Liu, C.-H., et al., Analytical Chemistry, 2006. **78**(11): p. 3738-3744.
316. Stamplecoskie, K.G., et al., The Journal of Physical Chemistry C, 2011. **115**(5): p. 1403-1409.
317. Bright, R.M., M.D. Musick, and M.J. Natan, Langmuir, 1998. **14**(20): p. 5695-5701.

318. Malynych, S., H. Robuck, and G. Chumanov, Nano Letters, 2001. **1**(11): p. 647-649.
319. Huo, S.-J., et al., The Journal of Physical Chemistry B, 2006. **110**(51): p. 25721-25728.
320. Chapman, R. and P. Mulvaney, Chemical Physics Letters, 2001. **349**(5): p. 358-362.
321. Zhao, S., et al., Materials Letters, 2006. **60**(9): p. 1215-1218.
322. Bar, G., et al., Langmuir, 1996. **12**(5): p. 1172-1179.
323. Flores, C.Y., et al., Journal of Colloid and Interface Science, 2010. **350**(2): p. 402-408.
324. Dubas, S.T., P. Kumlangdudsana, and P. Potiyaraj, Colloids and Surfaces A: Physicochemical and Engineering Aspects, 2006. **289**(1): p. 105-109.
325. Kujda, M., et al., Journal of Nanoscience and Nanotechnology, 2015. **15**(5): p. 3574-3583.
326. Oćwieja, M., et al., Advances in Colloid and Interface Science, 2015. **222**: p. 530-563.
327. Hemingway, R.W. and P.E. Laks. Vol. 59. 2012: Springer Science & Business Media.
328. Kraus, T.E.C., R.A. Dahlgren, and R.J. Zasoski, Plant and Soil, 2003. **256**(1): p. 41-66.
329. Dadosh, T., Materials Letters, 2009. **63**(26): p. 2236-2238.
330. Dutta, A. and S.K. Dolui, Applied Surface Science, 2011. **257**(15): p. 6889-6896.
331. Kim, T.J., et al., Food Chemistry, 2010. **118**(3): p. 740-746.
332. Fuertes, M.C., et al., Small, 2009. **5**(2): p. 272-280.
333. Sivaraman, S.K., et al., Current Science, 2009. **97**(7): p. 1055-1059.
334. Shutava, T., et al., Macromolecules, 2005. **38**(7): p. 2850-2858.
335. Morga, M. and Z. Adamczyk, Journal of Colloid and Interface Science, 2013. **407**: p. 196-204.
336. Wasilewska, M. and Z. Adamczyk, Langmuir, 2011. **27**(2): p. 686-696.
337. Dąbkowska, M. and Z. Adamczyk, Journal of Colloid and Interface Science, 2012. **366**(1): p. 105-113.
338. Kujda, M., et al., Colloids and Surfaces B: Biointerfaces, 2013. **112**: p. 165-170.
339. Adamczyk, Z., et al., Langmuir, 2012. **28**(1): p. 474-485.
340. Adamczyk, Z., Journal of Colloid and Interface Science, 2000. **229**(2): p. 477-489.
341. Adamczyk, Z. and P. Weroński, The Journal of Chemical Physics, 1998. **108**(23): p. 9851-9858.
342. Zayats, M., et al., Nano Letters, 2005. **5**(1): p. 21-25.
343. Willner, I., R. Baron, and B. Willner, Advanced Materials, 2006. **18**(9): p. 1109-1120.
344. Pavlov, V., Y. Xiao, and I. Willner, Nano Letters, 2005. **5**(4): p. 649-653.
345. Georgiev, P., et al., Colloids and Surfaces A: Physicochemical and Engineering Aspects, 2013. **434**: p. 154-163.